PONTIFÍCIA UNIVERSIDADE CATÓLICA DO PARANÁ

ESCOLA DE MEDICINA

PROGRAMA DE PÓS-GRADUAÇÃO EM CIÊNCIAS DA SAÚDE

ALTERAÇÕES ANATOMOPATOLÓGICAS PLACENTÁRIAS E SUA ASSOCIAÇÃO COM A INTENSIDADE DOS SINTOMAS DE COVID-19 EM GESTANTES

Aluno: Patricia Zadorosnei Rebutini

Orientadora: Profa. Dra. Lúcia de Noronha

Curitiba, abril/2022

PONTIFÍCIA UNIVERSIDADE CATÓLICA DO PARANÁ

ESCOLA DE MEDICINA

PROGRAMA DE PÓS-GRADUAÇÃO EM CIÊNCIAS DA SAÚDE

ALTERAÇÕES ANATOMOPATOLÓGICAS PLACENTÁRIAS E SUA ASSOCIAÇÃO COM A INTENSIDADE DOS SINTOMAS DE COVID-19 EM GESTANTES

Tese apresentada ao Programa de Pós-Graduação em Ciências da Saúde como requisito parcial para obtenção do título de Doutor em Ciências da Saúde.

Orientadora: Profa. Dra. Lúcia de Noronha

Curitiba, abril/2022

Dados da Catalogação na Publicação
Pontifícia Universidade Católica do Paraná
Sistema Integrado de Bibliotecas – SIBI/PUCPR
Biblioteca Central
Pamela Travassos de Freitas – CRB 9 /1960

R293a
2022

Rebutini, Patricia Zadorosnei
Alterações anatomopatológicas placentárias e sua associação com a intensidade dos sintomas de covid-19 em gestantes / Patricia Zadorosnei Rebutini ; orientadora: Lúcia de Noronha. – 2022.
[108] f. : il. ; 30 cm

Tese (doutorado) – Pontifícia Universidade Católica do Paraná, Curitiba, 2022
Bibliografia: f. 64-74

1. Ciência da saúde. 2. COVID-19. 3. SARS-CoV-2. 4. Transmissão vertical de doenças infecciosas. 5. Placenta. 6. Histopatologia. I. Noronha, Lúcia de. II. Pontifícia Universidade Católica do Paraná. Programa de Pós-Graduação em Ciências da Saúde. III. Título.

CDD 22. ed. – 610

ATA DA SESSÃO PUBLICA DE EXAME DE TESE DO PROGRAMA DE PÓS-GRADUAÇÃO EM CIÊNCIAS DA SAÚDE EM NÍVEL DE DOUTORADO DA PONTIFICIA UNIVERSIDADE CATÓLICA DO PARANÁ.

Aos **07 dias do mês de abril de 2022 às 13:30,** realizou-se a sessão aberta de Defesa de Tese **"Alterações anatomopatológicas placentárias e sua associação com a intensidade dos sintomas de COVID-19 em gestantes"** apresentado por **Patricia Zadorosnei Rebutini** para obtenção do título de Doutor; Área de concentração: Pesquisa Médica Translacional.

A banca examinadora foi composta pelos seguintes membros:

MEMBROS DA BANCA	ASSINATURA
Profa. Dra. Lucia de Noronha - Presidente	
Profa. Dra. Andrea Novais Moreno Amaral (PUCPR)	
Profa. Dra. Marina Luise Viola de Azevedo (PUCPR)	
Profa. Dra. Ana Paula Percicote (UFPR)	
Prof. Dr. Cleber Machado De Souza (UFPR)	

De acordo com as normas regimentais a Banca Examinadora deliberou sobre os conceitos a serem distribuídos e que foram os seguintes:

Profa. Dra. Lucia de Noronha	Conceito: Aprovada
Profa. Dra. Andrea Novais Moreno Amaral	Conceito: Aprovada
Profa. Dra. Marina Luise Viola de Azevedo	Conceito: Aprovada
Profa. Dra. Ana Paula Percicote	Conceito: Aprovada
Prof. Dr. Cleber Machado De Souza	Conceito: Aprovada

Parecer Final: Aprovada

Observações da Banca Examinadora:

Profa. Dra. Lucia de Noronha
Presidente da Banca Examinadora

Profa. Dra. Cristina Pellegrino Baena
Coordenadora do PPGCS-PUCPR

A tese foi redigida seguindo a normatização estabelecida pela ABNT e as normas para elaboração de dissertações e teses do Programa de Pós-Graduação em Ciências da Saúde da PUCPR. Este trabalho foi realizado nas instalações do Laboratório de Patologia Experimental da Escola de Medicina da PUCPR, em colaboração com o Laboratório de Imuno-histoquímica do Serviço de Anatomia Patológica do Complexo Hospital de Clínicas da UFPR e do Laboratório de Biologia Molecular do Instituto de Pesquisa Pelé Pequeno Príncipe. Declaramos que não há conflito de interesse na realização da presente tese.

Dedico esta obra aos meus pais,

Antonio e Estela, e à minha avó, Sofia.

AGRADECIMENTOS

A Deus, pela minha vida, ao Senhor Jesus Cristo, pela minha salvação, e ao Espírito Santo, pela consolação.

Aos meus pais, Antonio e Estela, à minha avó, Sofia, e à minha irmã, Vanessa, pela compreensão e incentivo.

Ao meu esposo, Raphael, tanto pelo amor, carinho e encorajamento, quanto pela paciência e parceria nos momentos mais difíceis.

À minha orientadora, Profa. Dra. Lúcia de Noronha, pela oportunidade, confiança e orientação, assim como pela amizade construída desde o início da minha formação como médica residente em Anatomia Patológica.

À equipe do Laboratório de Patologia Experimental da PUCPR, Seigo Nagashima, Ana Paula Camargo Martins e Caroline Busatta Vaz de Paula, pela acolhida calorosa e pela colaboração diligente e generosa em todas as etapas desse trabalho.

À médica residente Emanuele Therezinha Schueda Stonoga, aos alunos Júlio César Honório Dagostini e Elisa Carolina Hlatchuk, a Maurício de Oliveira e Katiucia Thiara Fantinel Picolli, assim como aos pesquisadores, professores e colegas do PPGCS, do Complexo Hospital de Clínicas da UFPR, do Hospital Nossa Senhora das Graças e do Instituto de Pesquisa Pelé Pequeno Príncipe que contribuíram significativamente para a realização deste projeto.

À PUCPR, à CAPES, ao CNPq e ao Banco Regional de Desenvolvimento do Extremo Sul (BRDE), pelo suporte acadêmico, técnico e financeiro, sem o qual este projeto não se tornaria realidade.

“O temor do SENHOR é o princípio da sabedoria...”

Salmo 111:10a

RESUMO

Desde o início da pandemia, apenas alguns artigos descreveram as características morfológicas e morfométricas das placentas de gestantes infectadas pelo SARS-CoV-2. Foram relatadas alterações como baixo peso placentário, aceleração da maturação vilosa, vasculopatia decidual, infartos, trombose de vasos fetais e intervilosite crônica histiocitária. **Objetivo:** Analisar as alterações morfológicas e morfométricas de placentas de mulheres grávidas infectadas pelo SARS-CoV-2 (grupo COVID-19) em comparação com as placentas de mulheres grávidas não infectadas, pareadas pela idade materna e comorbidades, além da idade gestacional do parto (grupo controle), correlacionando os achados com dados clínicos. **Método:** As pacientes do grupo COVID-19 e do grupo controle foram pareadas por idade materna, idade gestacional e comorbidades. A análise morfológica das placentas foi realizada com base nos critérios propostos pelo Consenso de Amsterdam. A avaliação morfométrica incluiu a aferição do diâmetro e perímetro de vilosidades terciárias, contagem do número de brotos e nós, assim como a quantificação de fibrina vilosa e deposição de colágeno intraviloso I e III por *sirius red*. Além disso, as células de Hofbauer destacadas por imuno-histoquímica com marcador CD68 foram contadas. **Resultados:** As mulheres sintomáticas do grupo COVID-19 foram mais propensas a ter pelo menos uma comorbidade, evoluir para trabalho de parto prematuro e morte infantil, e ter teste para SARS-CoV-2 positivo em seus conceptos. Em comparação com o grupo controle, as placentas do grupo COVID-19 exibiram mais frequentemente alterações decorrentes de má perfusão vascular materna e fetal. No grupo COVID-19, as placentas de mulheres sintomáticas foram mais propensas a apresentar intervilosite crônica histiocitária. A análise morfométrica não demonstrou diferenças significativas entre os grupos. Apenas a deposição de fibrina vilosa pode ser mais acentuada no grupo COVID-19 ($p = 0{,}08$). O número de células de Hofbauer/vilosidades avaliadas pela imuno-histoquímica para CD68 não mostrou diferença entre os dois grupos. **Conclusão**: Mulheres grávidas com sintomas de infecção por SARS-CoV-2, particularmente com sintomas intensos, foram mais propensas a exibir um efeito fetal adverso (parto prematuro ou morte) com transmissão perinatal do vírus, assim como achados histopatológicos ligeiramente mais frequentes de má perfusão vascular materna e fetal, e intervilosite crônica histiocitária. As alterações morfométricas e imuno-histoquímicas encontradas nas placentas do grupo COVID-19 não parecem ser diferentes daquelas observadas no grupo controle, quando a idade materna, idade gestacional e comorbidades são pareadas.

Palavras-chave: SARS-CoV-2, COVID-19, transmissão vertical, placenta, análise morfométrica, histopatologia placentária.

ABSTRACT

Since the beginning of the pandemic, few papers describe the placenta's morphological and morphometrical features in SARS-CoV-2–positive pregnant women. Alterations, such as low placental weight, accelerated villous maturation, decidual vasculopathy, infarcts, thrombosis of fetal placental vessels, and chronic histiocytic intervillositis, have been described. **Objective:** To analyze the placental morphological and morphometric changes of pregnant women infected with SARS-CoV-2 (COVID-19 group) in comparison with the placentas of non-infected pregnant women, matched for maternal age and comorbidities, besides gestational age of delivery (Control group), and its correlation with clinical data. **Method:** The patients in the COVID-19 and the Control group were matched for maternal age, gestational age, and comorbidities. The morphological analysis of placentas was performed using Amsterdam Placental Workshop Group Consensus Statement. The quantitative morphometric evaluation included perimeter diameter and number of tertiary villi, number of sprouts and knots, evaluation of deposition of villous fibrin, and deposition of intra-villous collagen I and III by Sirius Red. Additionally, Hofbauer cells were counted within villi by immunohistochemistry with CD68 marker. **Results:** Symptomatic women in the COVID-19 group were more likely to have at least one comorbidity, to evolve to preterm labor and infant death, and to have positive SARS-CoV-2 RNA testing in their concepts. Compared to controls, placentas in the COVID-19 group were more likely to show features of maternal and fetal vascular malperfusion. In the COVID-19 group, placentas of symptomatic women were more likely to show chronic histiocytic intervillositis. No significant results were found after morphometric analysis. Only the deposition of villous fibrin could be more accentuated in the COVID-19 group ($p = 0.08$). The number of Hofbauer cells/villous evaluated with CD68 immunohistochemistry did not show a difference between both groups. **Conclusion:** Pregnant women with symptomatic SARS-CoV-2 infection, particularly with the severe course, were more likely to exhibit an adverse fetal outcome, perinatal transmission of the virus and slightly more frequent histopathologic findings of maternal and fetal vascular malperfusion, and chronic histiocytic intervillositis. The morphometric and immunohistochemical changes found in the placentas of the COVID-19 group do not seem to be different from those observed in the Control group, as far as maternal age, gestational age, and comorbidities are paired.

Keywords: SARS-CoV-2, COVID-19, vertical transmission, placenta, morphometric analysis, placental histopathology.

RESUMO POPULAR

A placenta é o órgão gerado durante a gravidez que une o feto à parede do útero materno, permitindo que o bebê receba os nutrientes necessários para o seu desenvolvimento, e a eliminação de resíduos metabólicos. Uma placenta saudável, portanto, é crucial para uma gestação saudável. As grávidas com COVID-19 podem ter o órgão prejudicado, o que gera reflexos nos fetos, como nascimento prematuro e até mesmo morte intrauterina. O objetivo deste trabalho foi determinar o tipo de alteração que as placentas dessas mulheres apresentavam, e correlacionar essas alterações com o estado de saúde das gestantes e dos bebês, em uma tentativa de, no futuro, prever as consequências da COVID-19 materna para os fetos. Para isso, foram estudadas as placentas de mães com diagnóstico do novo coronavírus durante a gestação, tanto com quadros moderados a graves, que precisaram ser internadas por conta da doença, quanto mulheres com quadro leve de COVID-19, que permaneceram em casa e compareceram ao hospital somente para o parto. O estudo foi realizado no Hospital de Clínicas e no Hospital Nossa Senhora das Graças, com consentimento das pacientes e aprovado pelo comitê de ética das instituições. Observou-se que as grávidas que desenvolveram quadros moderados e graves da doença apresentaram lesões vasculares e inflamatórias na placenta, o que pode prejudicar o pleno desenvolvimento do feto. Nesse sentido, foram verificadas consequências para os bebês, como morte intrauterina, óbito logo após o nascimento e nascimentos prematuros. Alguns recém-nascidos foram infectados com o vírus. As pacientes com forma leve da doença, porém, deram à luz a bebês saudáveis e suas placentas não apresentaram lesões decorrentes da infeção pelo SARS-CoV-2.

LISTA DE FIGURAS

LISTA DE TABELAS

SUMÁRIO

1 INTRODUÇÃO

Após pouco mais de dois anos do reconhecimento da doença causada pelo *Severe Acute Respiratory distress Syndrome Coronavirus 2* (SARS-CoV-2), esse novo vírus deu origem a uma pandemia com mais de 430 milhões de casos confirmados e mais de 5,9 milhões de mortes em todo o mundo até fevereiro de 2022 (1). No Brasil, segundo dados da Organização Mundial da Saúde, houve mais de 28 milhões de casos confirmados e mais de 640 mil mortes atribuídas à *Coronavirus disease 19* (COVID-19) no mesmo período (2). A princípio, casos graves e óbitos foram descritos em idosos com comorbidades, mas logo emergiram relatos de jovens acometidos pela doença, com evolução clínica semelhante (3, 4).

Já nas fases iniciais da pandemia, suspeitou-se que o SARS-CoV-2 pudesse ser transmitido para o concepto durante a gestação (5–8). Paralelamente à sua disseminação mundial, relatos de eventos adversos na gravidez surgiram na literatura, tais como parto prematuro, aborto espontâneo, morte fetal intrauterina e morte neonatal (9–12).

Durante a gestação, a transmissão vertical de agentes infecciosos pode levar a consequências deletérias ao desenvolvimento fetal, cujo espectro inclui malformações orgânicas diversas e óbito do concepto. Em muitos casos, tais alterações não são evidentes no nascimento, mas suas manifestações acabam sendo detectadas tardiamente ao longo do primeiro ano de vida, invariavelmente acarretando prejuízo para o indivíduo (13, 14).

Nesse contexto, a análise da placenta pode fornecer informações valiosas, considerando que vários agentes infecciosos estão associados a padrões morfológicos característicos de lesão (15–17). Todavia, são poucos os artigos que descrevem as alterações morfológicas e morfométricas de placentas de gestantes infectadas pelo SARS-CoV-2, e a associação entre o adoecimento materno e os achados placentários anormais também está sob investigação.

2 REVISÃO DA LITERATURA

2.1 SARS-CoV-2

O SARS-CoV-2 foi identificado pela primeira vez em Wuhan, China, com os primeiros casos relatados no final de dezembro de 2019. A partir daí, espalhou-se rapidamente, atingindo mais de 180 países e territórios até o final de março de 2020 (18, 19).

O vírus é transmitido primariamente por inalação e contato direto com aerossóis, gotículas de saliva e de secreção nasal de pessoas infectadas (20). Após um período de incubação de 1 a 14 dias podem ter início os sintomas da COVID-19, sendo os mais frequentes febre, tosse seca, fadiga e mialgia. Outros sintomas incluem anosmia, congestão nasal, conjuntivite, odinofagia, cefaleia, dor articular, náuseas, vômitos e diarreia. Sintomas sugestivos de gravidade incluem dispneia (presente em até 31% dos casos), dor ou sensação de peso no tórax, perda de apetite, confusão mental e temperatura corporal acima de 38°C (21). Dentre os sintomáticos, a maioria (80%) exibe quadros leves a moderados, autolimitados. Entretanto, cerca de 15% dos pacientes necessitam de internamento hospitalar com suplementação de oxigênio e ao menos 5% demandam suporte ventilatório em unidade de terapia intensiva, por vezes prolongado. Há também indivíduos que exibem sintomas persistentes mesmo após a resolução do quadro inicial (22).

Trata-se de um vírus de fita simples de ácido ribonucleico (RNA – *Ribonucleic Acid*) com múltiplas variantes reconhecidas; dessas, cinco estão associadas a aumento de transmissibilidade, aumento de virulência ou redução de efetividade dos exames diagnósticos e das vacinas disponíveis. Essas são reconhecidas como variantes de interesse (23) e estão destacadas na Tabela 1.

Tabela 1 – Variantes de SARS-CoV-2.

VARIANTE - LINHAGEM	MÊS DE IDENTIFICAÇÃO	LOCAL
Epsilon - B.1.427/B.1.429	mar/20	Estados Unidos
Zeta - P.2	abr/20	Brasil
Beta* - B.1.351	mai/20	África do Sul
Alpha* - B.1.1.7	set/20	Reino Unido
Delta* - B.1.617.2	out/20	Índia
Kappa - B.1.617.1	out/20	Índia
Gamma* - P.1	nov/20	Brasil
Iota - B.1.526	nov/20	Estados Unidos
Eta - B.1.525	dez/20	Vários
Theta - P.3	jan/21	Filipinas
Omicron* - B.1.1.529/BA.1/BA.1.1/BA.2/BA.3	nov/21	Vários

Fonte: Adaptado de *World Health Organization* (23).
* Variantes de interesse.

O SARS-CoV-2 pertence à família *Coronaviridae*, da qual fazem parte outros coronavírus causadores de resfriados (HCoV-229E, NL63, OC43 e HKU1) e de síndromes respiratórias graves como a *Severe Acute Respiratory Syndrome* – SARS (SARS-CoV) e a *Middle East Respiratory Syndrome* – MERS (MERS-CoV) (24). Ele tem mais características em comum com o SARS-CoV, que causou uma epidemia de SARS no sul da China em 2002–2003. Além de sintomas respiratórios, ambos utilizam a enzima conversora da angiotensina 2 (ACE2) como receptor celular, e sua entrada nas células dá-se através da clivagem da proteína S (*spike*) pela *transmembrane protease serine 2* (TMPRSS2) (25–27), como ilustrado na Figura 1.

A ACE2 é uma metaloprotease integrante do eixo renina-angiotensina-aldosterona, importante na manutenção da pressão arterial, balanço hídrico e de sódio. Ela está presente em vários tecidos, como nasofaringe, pulmões e intestinos (29). Ao usar a ACE2 como mecanismo de entrada, o vírus leva à desativação dessa enzima, interrompendo a sequência de reações que culminam na formação de aldosterona. Como consequência, há um aumento de seus precursores (angiotensina), resultando em vasoconstrição, ativação do complemento e trombose (30–32).

A COVID-19 está associada a uma resposta inflamatória exacerbada, geralmente proporcional à severidade da doença, conhecida como tempestade de citocinas. A magnitude dessa resposta inflamatória e sua extensão seriam responsáveis por algumas das manifestações clínicas da doença, particularmente suas complicações. Dois

Figura 1 – Representação esquemática do mecanismo de entrada do SARS-CoV-2 na célula.

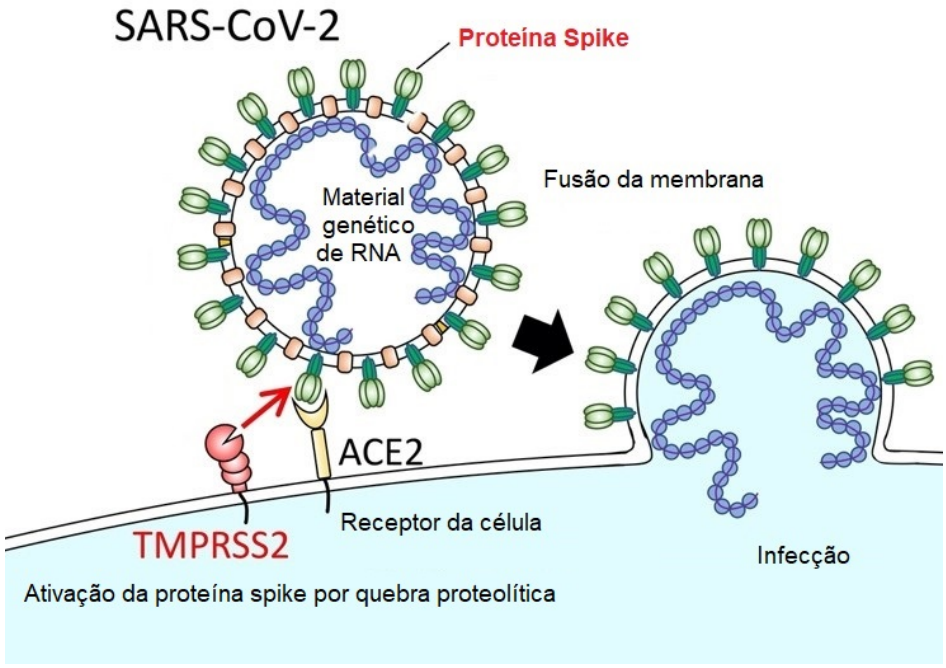

Fonte: adaptado de Jian *et al.* (28).

desdobramentos da tempestade de citocinas são a lesão endotelial e a disfunção do sistema de coagulação, que podem desempenhar um papel na fisiopatologia da doença (33).

Por fim, observou-se que o SARS-CoV-2 é endoteliotrópico; portanto, o efeito trombogênico é também potencializado pelo dano endotelial direto exercido pelo vírus (34, 35).

Os mecanismos supracitados provavelmente sobrepõem-se, e fundamentam o perfil de sintomas da COVID-19 que, além dos sintomas respiratórios, inclui relatos de pacientes com hipercoagulabilidade, gangrena de extremidades e tromboembolismo (36–38). Juntamente com a insuficiência respiratória grave, a síndrome do desconforto respiratório agudo, a sepse e a falência cardíaca, hepática e renal, os fenômenos trombóticos perfazem complicações que levam ao óbito (39–42).

2.2 SARS-CoV-2 E A GESTAÇÃO

As mudanças fisiológicas típicas da gravidez, como redução de volumes pulmonares residuais funcionais, elevação do diafragma e imunidade reduzida tornam as gestantes mais suscetíveis a infecções. Do mesmo modo, a hipercoagulabilidade característica da gravidez gera um ambiente facilitador de fenômenos trombóticos. Uma vez acometidas por doenças infecciosas, nota-se maior risco de complicações, quer sejam maternas como insuficiência respiratória, insuficiência renal e distúrbios da coagulação, quer sejam fetais como aborto espontâneo, restrição de crescimento intrauterino, parto prematuro e morte neonatal. Soma-se a isso a possibilidade de transmissão dos agentes infecciosos para o feto ou recém-nascido (43, 44).

A morbidade e mortalidade fetais não dependem necessariamente da transmissão do patógeno para o concepto, pois o estado de saúde materno por si só pode determinar o desfecho da gestação. Nas epidemias prévias de SARS e MERS, nas quais não foi documentada transmissão vertical, até 35 e 41% das grávidas, respectivamente, necessitaram de ventilação mecânica, resultando em taxas de mortalidade materna tão altas quanto 18 e 25%, respectivamente (45–47).

Consequentemente, o diagnóstico de `COVID-19` em gestantes gerou preocupação. Os dados publicados até o início deste trabalho indicavam que a gravidade da doença nesse grupo é similar a de mulheres não grávidas e adultos em geral, e parece estar relacionada à existência de comorbidades tais como hipertensão, obesidade, entre outras, de forma semelhante à população em geral (48–51).

Inicialmente, pensou-se que o `SARS-CoV-2`, a exemplo dos outros coronavírus, não pudesse ser transmitido para o concepto durante a gestação (52, 53). Entretanto, dada a identificação de ACE2 e TMPRSS2 em tecidos placentários e fetais, essa possibilidade requeria consideração (54). Com a progressão da pandemia, os relatos de infecção congênita começaram a emergir.

Infecções congênitas podem ser difíceis de caracterizar, uma vez que a detecção de patógenos geralmente requer métodos específicos (nem sempre disponíveis),

aplicados a uma miríade de amostras maternas e fetais. Como as amostras fetais são propensas a contaminação cruzada, preconiza-se metodologia rigorosa para sua coleta. Para o SARS-CoV-2, a Organização Mundial de Saúde recomenda que a detecção viral seja realizada preferencialmente em amostras estéreis, coletadas no nascimento, usando técnicas de detecção de ácido nucleico para confirmar a transmissão congênita, particularmente por via transplacentária (55).

Atualmente, a transmissão vertical anteparto ou periparto do SARS-CoV-2 está substancialmente documentada (56–61). Relatos publicados sugerem uma taxa de transmissão inferior a 2% para neonatos avaliados em até 24 horas de vida (62). Cerca de 30% dos casos ocorreram devido à transmissão transplacentária e o restante em decorrência de exposição ambiental periparto. Além disso, Raschetti *et al.* observaram que 55% de neonatos infectados desenvolveram sintomas de COVID-19 (63).

2.3 PLACENTA

A placenta é um órgão de origem fetal que constitui a interface entre os sistemas circulatórios da mãe e do concepto. Os vasos fetais, embebidos em estroma fibroconjuntivo e delimitados por trofoblasto, constituem projeções ou vilos que se ramificam por brotamento, esboçando uma arquitetura arboriforme, e estão banhados em sangue materno (Figura 2) (64, 65).

No primeiro trimestre predominam as vilosidades jovens, ou seja, vilosidades maiores, revestidas por duas camadas bem definidas de trofoblasto (cito e sinciciotrofoblasto), e dotadas de numerosos brotos sinciciais. Tais brotos consistem em massas de sinciciotrofoblasto que se projetam no espaço vilositário e representam o arcabouço a ser penetrado pelo eixo mesenquimatoso, o qual é subsequentemente vascularizado, dando origem à nova vilosidade. Ao longo da gestação, em reposta às demandas fetais, o tamanho da placenta aumenta em virtude do brotamento vilositário. São geradas vilosidades de menor tamanho, com estroma mais compacto, menor número de brotos

Figura 2 – Representação esquemática da arquitetura placentária.

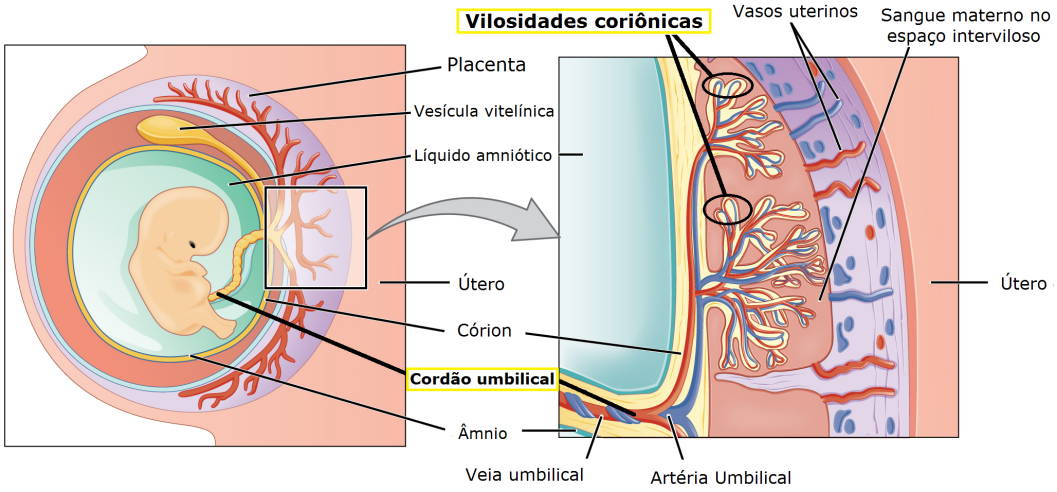

Fonte: Adaptado de Biology Forums (66).

sinciciais e significativo adelgaçamento do revestimento trofoblástico. Nas menores vilosidades observáveis, denominadas vilosidades terminais, o revestimento trofoblástico delgado, associado à distribuição periférica dos vasos fetais, leva à formação das membranas sinciciovasculares. Estas constituem a barreira placentária, região da placenta onde ocorrem as trocas materno-fetais, como ilustrado na Figura 3 (15, c. 6).

Figura 3 – Representação esquemática da arquitetura vilositária no 1º e 3º trimestres.

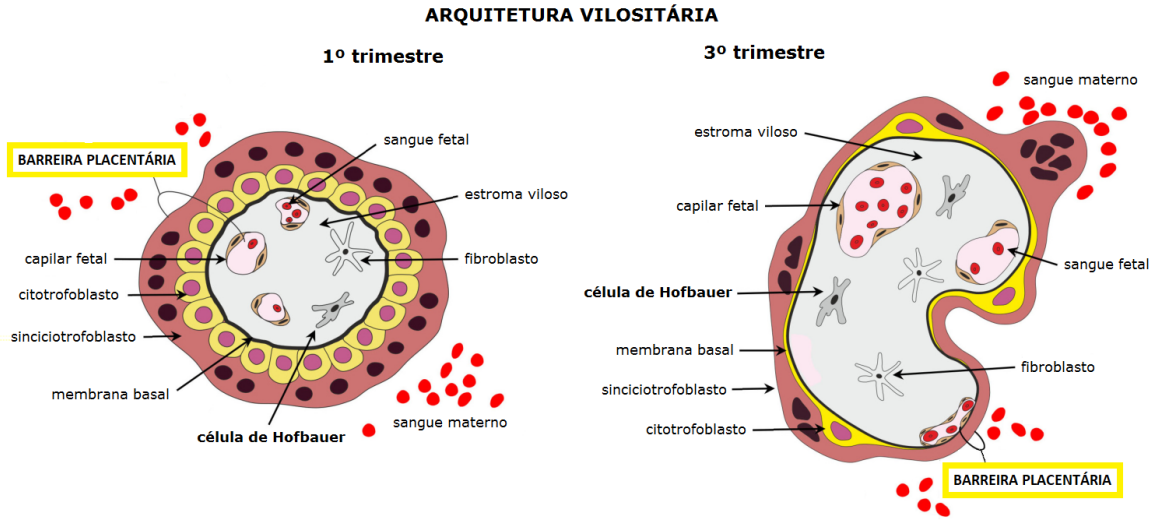

Fonte: Adaptado de Chatuphonprasert *et al.* (67).

Histologicamente, a placenta é composta por diferentes tipos celulares que desempenham funções variadas, tais como invasão endometrial, remodelamento vascular do tecido materno para ancoragem e estabelecimento da referida interface, produção

de moléculas diversas (incluindo hormônios e citocinas) e transporte de nutrientes e resíduos metabólicos (68). Sua arquitetura vilositária típica, com ramificações hierarquizadas com propriedades e tamanhos diferentes em cada trimestre gestacional, reflete seu grau de desenvolvimento e funcionalidade.

Como órgão intermediário entre a mãe e o concepto, a placenta tem um papel fundamental na inibição da transmissão de agentes infecciosos para o feto. Tal função baseia-se na separação dos suprimentos vasculares mediante a barreira placentária. Assim, a propagação por via hematogênica direta de micro-organismos é limitada por uma barreira física, embora não esteja restrita a ela. Isso porque as células do sinciciotrofoblasto, que circundam as vilosidades, são resistentes a infecções e secretam moléculas que atuam localmente na regulação gênica e imunidade adaptativa (pró-inflamatória), tais como interferon e micro-RNAs (69–72). Há macrófagos no estroma viloso, conhecidos como células de Hofbauer, que, em conjunto com o trofoblasto, integram uma barreira de natureza imunológica. Sua atuação contribui para a tolerância imunológica materna em relação ao concepto (73–75). Também secretam enzimas e citocinas que estimulam a angiogênese e o brotamento vilositário (76–78).

Entretanto, alguns micro-organismos vencem essas barreiras, seja por infecção direta e destruição do sinciotrofoblasto, por transcitose ou ainda aproveitando-se do enfraquecimento dessas barreiras em decorrência de lesão causada por outras comorbidades (79). Outro mecanismo reconhecido de transmissão transplacentária consiste na infecção das células de Hofbauer, que são suscetíveis a patógenos. Dessa interação resulta sua proliferação e ativação, por vezes com destruição de vilosidades. Parte dessas células permanecem por muitas semanas nas vilosidades coriônicas, representando um repositório de micro-organismos nas placentas de mulheres acometidas (80–83). Outra rota de contaminação proposta para o período que antecede o estabelecimento do fluxo sanguíneo placentário são a difusão de partículas virais para o embrião a partir de espermatozoides, de células imunes infectadas e de secreções de glândulas uterinas (84–86).

As alterações histopatológicas oriundas da ação de micro-organismos na pla-

centa fornecem informações relevantes. A identificação da natureza da resposta inflamatória da mãe e do feto à infecção, associada à distribuição anatômica dos efeitos na placenta, tais como influxo leucocitário e necrose, por exemplo, sugerem o mecanismo da transmissão materno-fetal (87, 88). Outro aspecto pertinente é o reconhecimento do impacto dessas alterações no desenvolvimento, maturação e suficiência placentária que, por sua vez, afetam a evolução e o desfecho da gestação (89).

Desse modo, uma etapa crítica passa a ser a definição dos padrões histológicos de lesão placentária. Em um esforço para padronizar a terminologia utilizada, delinear os critérios morfológicos mínimos para caracterização de cada lesão e sistematizar a avaliação da placenta, especialistas em patologia placentária e perinatal reuniram-se em Amsterdam em 2015. Essa iniciativa culminou no lançamento de diretrizes para a avaliação macro e microscópica da placenta, as quais são adotadas em laboratórios de anatomia patológica em todo o mundo desde seu lançamento, conhecidas como Consenso de Amsterdam (*Amsterdam Placental Workshop Group Consensus Statement*) (90).

As alterações placentárias foram agrupadas em categorias que refletissem mecanismos fisiopatológicos específicos. Assim, o reconhecimento de determinado padrão ou grupo de lesões por meio do exame morfológico permitiria inferir ou apontar quais doenças ou condições clínicas estariam vinculadas à sua presença, conforme ilustrado na Tabela 2 (91, 92).

Considerando-se as infecções transmitidas verticalmente, os achados mais comumente identificados correspondem a alterações vilositárias maturativas (ilustradas na Figura 4, p. 26) e vilosite. A vilosite, por sua vez, seria o achado mais específico, uma vez que a presença de um agente patogênico desencadeia uma reação inflamatória com recrutamento de leucócitos oriundos tanto da circulação materna quanto da circulação fetal. Eventualmente, esse processo pode levar à fibrose ou necrose das vilosidades envolvidas com subsequente deposição de fibrina e microcalcificação distrófica, ilustradas na Figura 5, p. 26 (15, c. 20) (80, 86, 93, 94).

Tabela 2 – Categorias de lesões placentárias, exemplos e sua associação com doenças maternas segundo o Consenso de Amsterdam.

CATEGORIA	ACHADOS MORFOLÓGICOS	CONDIÇÕES CLÍNICAS ASSOCIADAS
Má perfusão vascular materna (MVM)	• Infarto; • Aceleração da maturação vilosa; • Hipoplasia vilositária distal; • Vasculopatia decidual (hipertrofia mural, necrose fibrinoide vascular, ausência de remodelamento de artérias...).	Hipertensão arterial* Pré-Eclâmpsia/Eclâmpsia Obesidade Diabetes**
Má perfusão vascular fetal (MVF)	• Trombose vascular fetal; • Fibrina intramural em vasos fetais; • Vilosidades avasculares; • Obliteração vascular.	Diabetes**
Alterações maturativas	• Retardo da maturação vilosa.	Infecções (TORCHS§) Obesidade Diabetes
Alterações inflamatórias/ infecciosas	Inflamação aguda: • Subcorionite; • Intervilosite neutrofílica; • Vasculite umbilical ou coriônica; • Funisite. Inflamação crônica: • Vilosite e intervilosite (histiocitária, linfocitária, plasmocitária ou mista).	Infecção bacteriana aguda ascendente Infecções (TORCHS§) Doenças auto-imunes Idiopático
Outras	• Alterações estromais (fibrina, fibrose); • Corangiose; • Microcalcificações; • Impregnação meconial...	Várias

Fonte: adaptado de Consenso de Amsterdam (90), Matiska (91) e Redline *et al* (92).
* Hipertensão arterial sistêmica crônica ou doença hipertensiva específica da gestação (DHEG).
** Diabetes pré-gestacional e gestacional.
§ TORCHS: acrônimo para sífilis (*Treponema pallidum*), toxoplasmose, rubéola, citomegalovírus, herpes simples e que representa outros micro-organismos transmitidos verticalmente (HIV...).

2.4 SARS-CoV-2 E A PLACENTA

No contexto da infecção pelo `SARS-CoV-2`, as alterações histopatológicas descritas abrangem achados característicos de má perfusão vascular materna, incluindo vasculopatia decidual, infartos, aceleração da maturação vilosa e baixo peso placentário (95–97). Os achados do tipo má perfusão vascular materna são frequentemente

Figura 4 – Retardo maturativo placentário. Coloração: HE; magnificação: 200x. As duas figuras exemplificam placentas de termo. A figura **A** ilustra vilosidades com maturação adequada para uma placenta de 37 semanas de idade gestacional. Na figura **B**, uma placenta com a mesma idade gestacional exibe vilosidades de tamanho maior, com vasos fetais centralizados e de menor calibre, além de células do citotrofoblasto facilmente identificáveis (círculos).

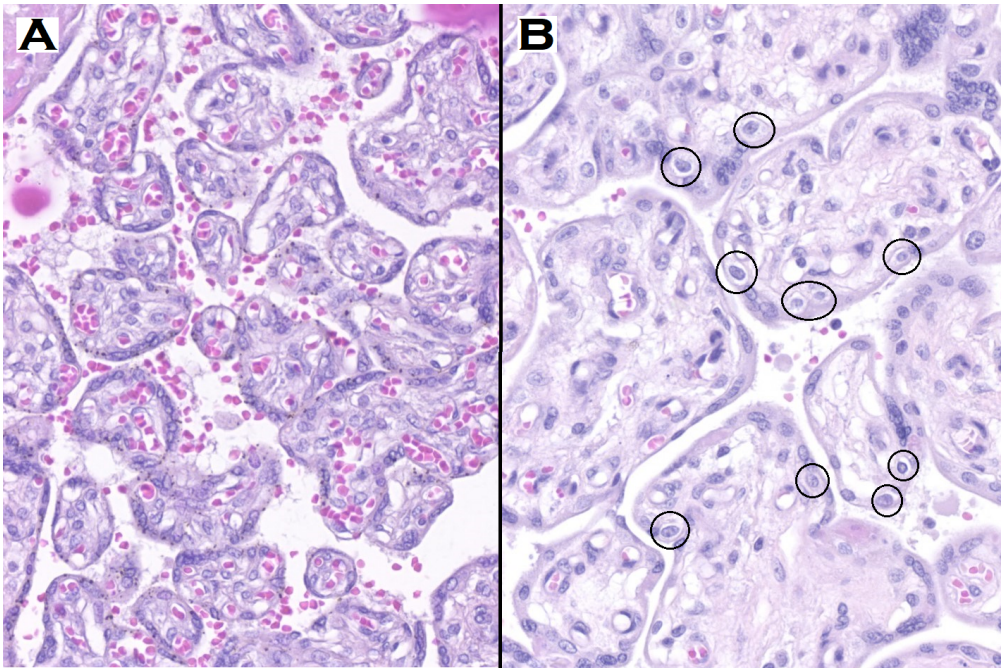

Fonte: A autora, 2021.

Figura 5 – Alterações estromais vilositárias. Coloração: HE; magnificação: 400x. Na figura **A**, há destruição vilositária devido a infiltrado linfo-histiocitário (vilosite linfo-histiocitária - estrela). A figura **B** ilustra a deposição de fibrina (seta) e fibrose (estrela); a figura **C**, foco de microcalcificação (seta).

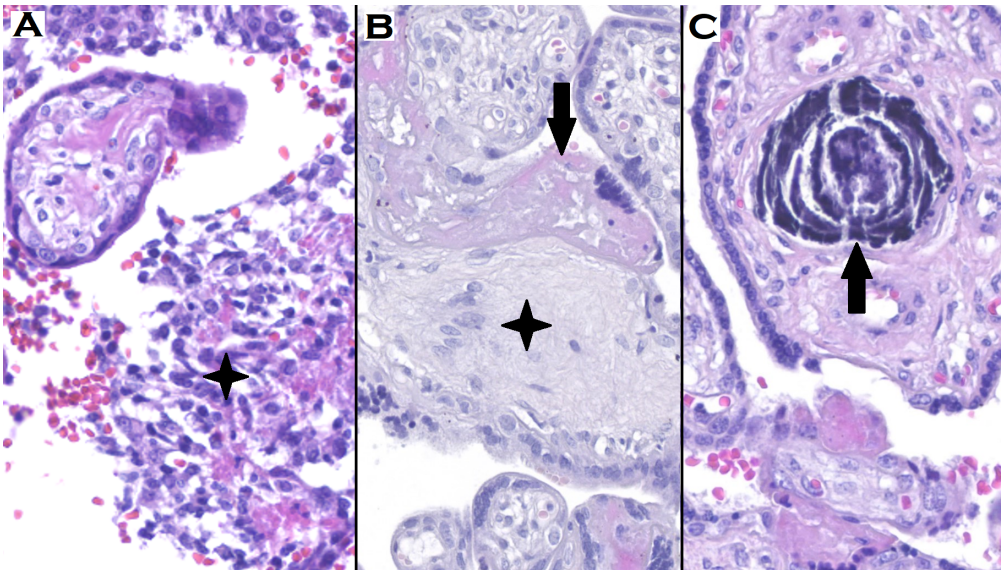

Fonte: A autora, 2021.

observados em placentas de mulheres grávidas com doenças hipertensivas, tais como hipertensão gestacional e pré-eclâmpsia, e foram associados a oligodrâmnio, nascimento prematuro e morte perinatal (90–92). Alterações sugestivas de má perfusão vascular fetal também têm sido descritas, a principal delas sendo a trombose de vasos fetais (98).

No entanto, alguns autores não identificaram uma correlação entre lesões placentárias e a infecção materna pelo SARS-CoV-2 (99), particularmente quando as amostras analisadas foram obtidas de placentas e bebês não infectados (100).

Em casos com infecção transplacentária confirmada, predominaram alterações inflamatórias. Dentre elas, a mais frequente foi intervilosite histiocitária crônica associada a necrose trofoblástica. Nestes casos, o SARS-CoV-2 foi detectado no sincitiotrofoblasto por imuno-histoquímica ou hibridização *in situ* de RNA (101, 102). Exemplos das alterações citadas estão ilustrados na Figura 6.

Ainda não está claro se a destruição do sinciciotrofoblasto é causada por um efeito viral direto ou é secundária às lesões inflamatórias ou isquêmicas às quais a placenta está sujeita. Entretanto, a despeito do mecanismo envolvido, a ruptura desta camada celular protetora da vilosidade facilita a infecção fetal (104).

Dessa forma, o reconhecimento do impacto da doença na placenta, assim como a natureza da resposta materno-fetal, podem ajudar a compreender os processos envolvidos na sua patogênese e, em última instância, fornecer uma explicação para desfechos clínicos desfavoráveis.

Figura 6 – Alterações placentárias em gestantes infectadas pelo SARS-CoV-2. **A**: Cortes seriados do disco placentário demonstram infartos recentes (delimitados em linha contínua) e hemorrágicos (linha pontilhada). Cortes histológicos corados em HE ilustram: **B** - aceleração da maturação vilosa (setas), **C** - infarto, **D** - necrose fibrinoide de vasos deciduais (*) e **E** - trombose arterial umbilical não oclusiva; **F** - Vilosite/intervilosite linfo-histiocitária caracterizada por aumento de células de Hofbauer (setas curtas), deposição de fibrina perivilositária (setas longas) e células inflamatórias no espaço interviloso (*). Ao estudo imuno-histoquímico, o marcador CD68 realça em marrom o infiltrado histiocitário que permeia as vilosidades em **G**; em **H**, identifica-se em marrom a positividade para o SARS-CoV-2 no sinciciotrofoblasto.

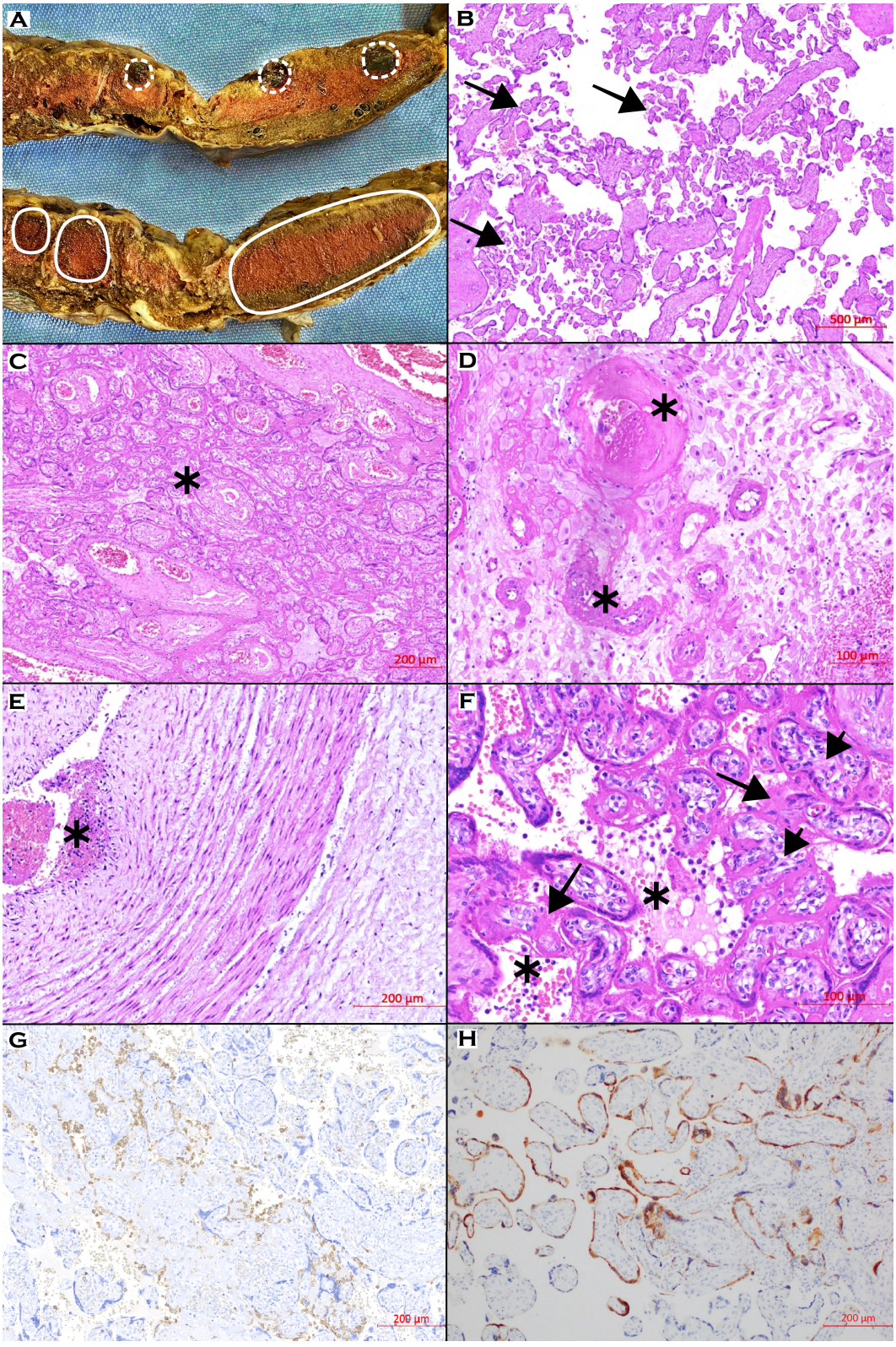

Fonte: **A** - **G**, a autora (103). **H**, adaptado de Schwartz *et al.* (101)

3 JUSTIFICATIVA

Doenças infecciosas emergentes, particularmente aquelas causadas por vírus anteriormente desconhecidos, costumam gerar ansiedade em meio à comunidade médica e científica, e também junto à população. As gestantes têm sido mais afetadas por essas doenças do que as mulheres não grávidas, com taxas mais altas de complicações e morte, tanto delas mesmas quanto de seus conceptos (105).

Considerando que os mecanismos da transmissão intrauterina, a replicação, tropismo e persistência do SARS-CoV-2 em tecidos e a gravidade dos danos para o concepto são ainda pouco entendidos, o estudo das alterações histopatológicas da placenta é essencial para a compreensão dos fenômenos relacionados à fisiopatologia da transmissão vertical, e para a identificação de alterações morfológicas que eventualmente contribuam para seu diagnóstico.

A hipótese é de que placentas de mães infectadas por SARS-CoV-2 apresentam alterações morfológicas, morfométricas e imuno-histoquímicas significativamente diferentes de placentas de mães não infectadas, e que tais achados possam estar relacionados com desfechos desfavoráveis para o concepto.

4 OBJETIVOS

4.1 OBJETIVO GERAL

Descrever e quantificar as alterações morfológicas, morfométricas e imuno-histo-químicas em placentas de gestantes com infecção documentada pelo SARS-CoV-2 (grupo estudo) em comparação com achados de placentas de gestantes não infectadas (grupo controle), pareadas por idade gestacional, idade materna e comorbidades, correlacionado com suas repercussões clínicas.

4.2 OBJETIVOS ESPECÍFICOS

a) descrever alterações morfológicas no grupo estudo em coloração de rotina (hematoxilina-eosina – HE);

b) avaliar a maturação placentária através da aferição do perímetro e do diâmetro das vilosidades e da quantificação de brotos e de nós sinciciais nos grupos estudo e controle, utilizando técnicas de morfometria em coloração de rotina (HE);

c) avaliar as alterações estromais vilositárias (fibrose e deposição de fibrina), nos grupos estudo e controle, utilizando técnicas de morfometria em colorações especiais (*sirius red* e hematoxilina fosfotúngstica, respectivamente);

d) avaliar a quantidade de células de Hofbauer por meio da identificação de células positivas para CD68 nos grupos estudo e controle utilizando técnicas de morfometria em reações imuno-histoquímicas;

e) comparar os achados dos dois grupos a fim de determinar os padrões de lesão causados pelo SARS-CoV-2 nas vilosidades placentárias;

f) estabelecer relação entre os achados morfológicos e as condições clínicas da gestante e do concepto, desde o diagnóstico até a alta hospitalar.

5 MATERIAIS E MÉTODO

5.1 APROVAÇÃO ÉTICA

O Comitê de Ética em Pesquisa em Seres Humanos do Complexo Hospital de Clínicas da Universidade Federal do Paraná aprovou o presente estudo sob o parecer número 4.183.247 (CAAE: 35129820.6.0000.0096). As gestantes foram convidadas a participar e, aquelas que aceitaram, assinaram o Termo de Consentimento Livre e Esclarecido. Os(as) pesquisadores(as) seguiram todas diretrizes, regulamentos, preceitos éticos e protocolos de segurança relevantes durante a todas as fases de execução deste estudo.

5.2 DESENHO DO ESTUDO

Trata-se de um estudo de caso-controle observacional.

5.3 SELEÇÃO DE PARTICIPANTES

Dado o momento epidemiológico no qual foi iniciada a seleção de participantes (primórdios da pandemia), havia um número limitado de casos disponíveis durante o intervalo de recrutamento. Desse modo, todas as mulheres grávidas com infecção confirmada pelo `SARS-CoV-2` durante o período perinatal atendidas no Complexo Hospital de Clínicas da Universidade Federal do Paraná (CHC-UFPR), e no Hospital Nossa

Senhora das Graças (HNSG), cujas respectivas placentas foram enviadas para exame anatomopatológico, foram consideradas elegíveis para inclusão no grupo estudo (grupo COVID-19). Foi estabelecido como único critério de exclusão o desejo da gestante de não participar da pesquisa. Inicialmente, apenas mulheres que procuraram atendimento espontaneamente no CHC-UFPR ou no HNSG, devido a sintomas de COVID-19 variando de leves a intensos durante a gestação, foram incluídas (n = 9). Após a implementação da testagem universal para infecção por SARS-CoV-2 para todas as pacientes obstétricas admitidas em ambas as instituições, foram também adicionadas as gestantes assintomáticas (n = 10). Como resultado, o grupo estudo reuniu 19 mulheres com infecção por SARS-CoV-2 confirmada no segundo (n = 3) ou no terceiro trimestre gestacional (n = 16).

Para o grupo controle, placentas de mulheres que deram à luz no CHC-UFPR em anos anteriores à epidemia foram selecionadas (de 2016 a 2018), e pareadas com os casos do grupo estudo considerando idade gestacional no parto, idade materna e comorbidades maternas (n = 19). Os controles históricos foram selecionados para garantir que mulheres com resultados falso-negativos em exames para SARS-CoV-2 não fossem incluídas. A idade gestacional no parto é uma variável universalmente usada para pareamento, uma vez que existe correlação entre o desenvolvimento da placenta e o avanço da gestação, o que poderia interferir na análise. A idade materna e comorbidades maternas foram incorporadas ao pareamento dado seu possível papel como fator de confusão ao analisar anormalidades placentárias.

5.4 INFORMAÇÕES CLÍNICAS

Os dados clínicos e laboratoriais foram obtidos de prontuários médicos nas duas instituições em que as gestantes foram atendidas; o acompanhamento da mãe e do recém-nascido deu-se até a alta hospitalar de ambos.

Informações maternas apuradas em cada prontuário médico, para ambos os

grupos, compreenderam idade materna, comorbidades, medicações em uso, paridade, idade gestacional no parto, tipo de parto, peso do concepto e pontuação do recém-nascido no escore de Apgar (106).

Todas as gestantes, nos dois grupos, submeteram-se a testes para pesquisa de infecções congênitas durante o pré-natal (toxoplasmose, sífilis, HIV e hepatite B) como parte da avaliação de rotina praticada nas duas instituições. Apenas uma delas, pertencente ao grupo estudo, teve um resultado positivo para sífilis no primeiro trimestre e recebeu o tratamento preconizado pelo Protocolo Clínico e Diretrizes Terapêuticas para prevenção da transmissão vertical de HIV, sífilis e hepatites virais do Ministério da Saúde (107).

Para o grupo estudo, também foram averiguadas a idade gestacional em que ocorreu o diagnóstico de infecção por SARS-CoV-2, o método de detecção, a presença ou ausência de sintomas tipicamente atribuídos à COVID-19 (temperatura corporal acima de 38°C, dispneia, tosse, mialgias, náuseas, vômito, diarreia, dor de cabeça, anosmia), a gravidade da doença (variando de sintomas leves à disfunção orgânica crítica), e a evolução clínica da mãe e do bebê.

5.5 AMOSTRAS PLACENTÁRIAS

Para os dois grupos, os critérios de submissão para o exame anatomopatológico das placentas incluíram anormalidades maternas e fetais diagnosticadas durante o pré-natal ou durante o parto. Portanto, comorbidades maternas, doenças relacionadas à gestação e infecção por SARS-CoV-2, por exemplo, enquadraram-se como critérios para submeter as placentas a avaliação complementar.

Todas as placentas foram examinadas de acordo com um protocolo padronizado, adaptado do Consenso de Amsterdam (90), que consistia na fixação imediata após o parto em formalina tamponada a 10% por 72 h, seguida de exame macroscópico com aferição das dimensões da placenta, do comprimento do cordão e pesagem após

secção das membranas e do cordão. Após a avaliação das faces fetal e materna, o disco placentário era cortado sequencialmente em fatias de 1,5 cm de espessura, seguido do exame da superfície de corte.

Alterações macroscópicas foram registradas e amostradas. Adicionalmente, amostras representativas do cordão umbilical (duas seções), das membranas (um rolo de membranas fetais) e da placa coriônica (ao menos duas seções de espessura total, não periféricas, incluindo faces materna e fetal) foram também escolhidas.

Todas as amostras placentárias selecionadas para estudo microscópico foram submetidas a processamento histológico de rotina, inclusão em parafina, microtomia (cortes com até 5 µm de espessura) e subsequentemente coradas em diferentes técnicas de acordo com a variável a ser analisada (Figura 7).

Figura 7 – Fluxograma com o delineamento das variáveis. Variáveis qualitativas realçadas em amarelo e laranja; varíaveis avaliadas por morfometria destacadas em azul claro.

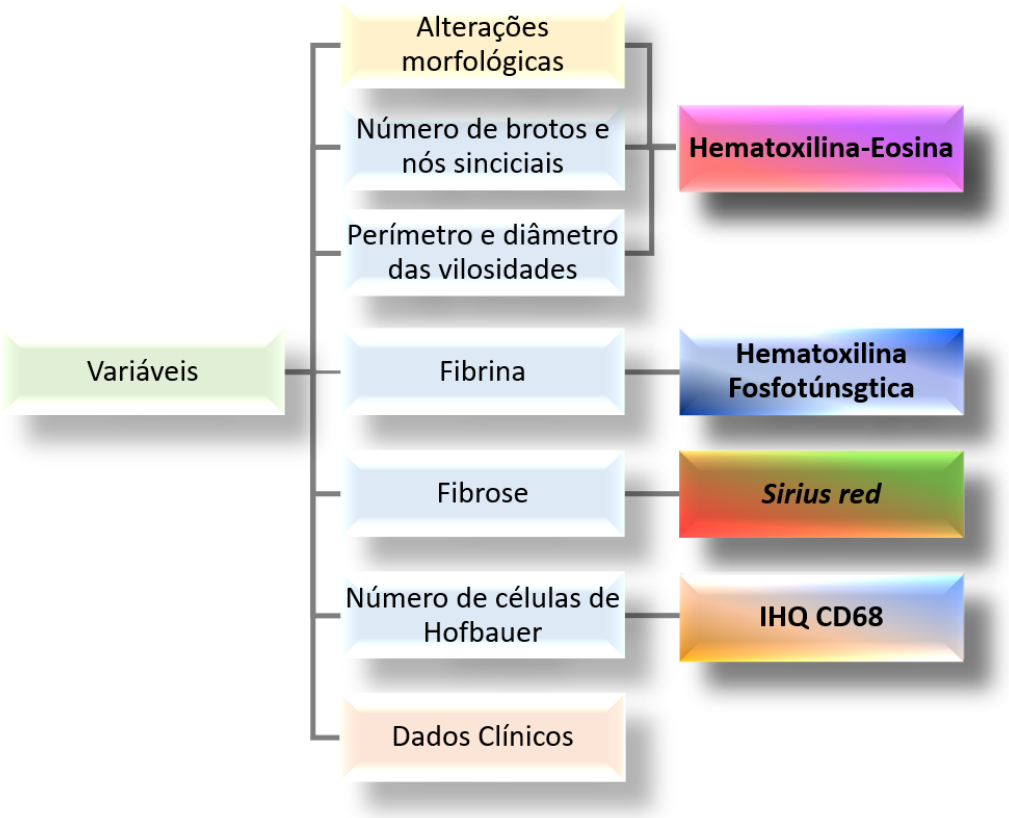

Fonte: A autora, 2021. IHQ - imuno-histoquímica.

5.6 PESQUISA DE SARS-CoV-2

A pesquisa de infecção por `SARS-CoV-2` foi realizada para todas as gestantes do grupo estudo (n = 19), assim como para maioria dos seus conceptos (n = 13), conforme disponibilidade. Para a maioria das gestantes, amostras de secreção nasofaríngea foram testadas para a identificação de RNA viral através de RT-PCR (*reverse transcription polymerase chain reaction*) (n = 17). Para as demais gestantes, o diagnóstico foi feito por teste sorológico com dosagem de IgM e IgG em amostras de sangue periférico (n = 2). A detecção do RNA viral em bebês foi executada em amostras de 13 casos, por vezes em mais de uma amostra por caso, conforme disponibilidade. Amostras testadas incluíram sangue de cordão umbilical (n = 13) e de líquido amniótico (n = 3) coletadas imediatamente após o nascimento. Também foram coletados esfregaços de secreção nasofaríngea (n = 6) em um intervalo que variou de menos de 24 h até 72 h após o parto. O leite materno também foi avaliado em três casos. Amostras teciduais fixadas em formalina e embebidas em parafina também foram examinadas para verificar a presença de RNA viral na placenta (n = 11).

Os testes de RT-PCR foram realizados tanto no CHC-UFPR quanto no HNSG, conforme procedência da gestante, usando o *kit* XGEN MASTER COVID-19 (*Mobius Life Science, Inc*, Brasil). A dosagem de IgM e IgG foi feita usando protocolos de rotina em vigência nas duas instituições. Nas amostras parafinadas, a extração do material genético viral foi efetuada com um *kit* de extração disponível comercialmente (Qiagen®), e a identificação do RNA viral usando o *kit* XGEN MASTER COVID-19 (*Mobius Life Science, Inc*, Brasil) no Instituto de Pesquisa Pelé Pequeno Príncipe.

5.7 ANÁLISE MORFOLÓGICA

Para esta análise, cortes histológicos corados em HE contendo ao menos uma amostra do cordão umbilical, do rolo de membranas e da placa coriônica de cada

caso, de ambos os grupos, foram selecionados aleatoriamente e renomeados por um membro da equipe de pesquisa não envolvido na leitura das lâminas (etapa preliminar de cegamento).

Realizou-se a avaliação morfológica através da leitura sistemática das lâminas em microscópio de luz (marca Nikkon®, modelo E200), para todas placentas dos grupos estudo e controle (n = 38), tendo por base os critérios delineados pelo Consenso de Amsterdam (90).

Os parâmetros avaliados incluíram:

a) sinais de má perfusão vascular materna: infarto viloso, maturação vilosa acelerada/aumento dos nós sinciciais, hipoplasia vilosa distal, aterose aguda decidual, necrose fibrinoide vascular decidual com ou sem células espumosas, hipertrofia mural vascular decidual, perivasculite crônica decidual, ausência de remodelamento de artéria espiralada, trombose arterial decidual e persistência de trofoblasto endovascular intramural;

b) sinais de má perfusão vascular fetal: trombose vascular fetal, deposição de fibrina intramural em vasos fetais, vilosidades avasculares, obliteração de vasos-tronco/esclerose fibromuscular, cariorrexe estromal-vascular vilosa e ectasia vascular;

c) retardo maturativo vilositário;

d) sinais de resposta inflamatória materna aguda: subcorionite, corionite, deciduíte, corioamnionite e intervilosite neutrofílicas;

e) sinais de resposta inflamatória fetal aguda: vasculite umbilical e funisite neutrofílica;

f) sinais de inflamação crônica: deciduíte crônica, vilosite e intervilosite linfo-histiocitárias;

g) outros achados: trombos intervilosos, focos de microcalcificação, corangiose, membranas com impregnação meconial ou acúmulo de hemossiderina.

Todos os parâmetros foram avaliados em todas as lâminas. Cada parâmetro foi contabilizado de modo binário, como “presente” (sim) ou “ausente” (não), e tabulado em planilha eletrônica. A intensidade e extensão dos achados foi documentada de maneira semelhante, de modo binário [“focal” (sim) ou (não); “extenso” (sim) ou (não), por exemplo], também em concordância com as definições apresentadas no Consenso de Amsterdam (90). Os demais parâmetros foram subdivididos em três categorias quantitativas: menor que 30%, de 30% à 70% e maior que 70%, de modo a registrar a extensão de todas as alterações observadas.

5.8 ANÁLISE MORFOMÉTRICA

A análise morfométrica incluiu a aferição do perímetro e diâmetro das vilosidades, contagem do número de vilosidades terciárias, brotos e nós de vilosidades terciárias, assim como quantificação de fibrina e colágeno tipo I e tipo III presentes nas vilosidades.

Esta etapa foi realizada em 11 casos do grupo estudo e 11 casos do grupo controle (n = 22), pareados pela idade gestacional, idade materna e comorbidades maternas. Antes da geração de imagens descrita a seguir, cada caso foi renomeado por um membro da equipe de pesquisa não envolvido na aquisição de dados para cegamento da análise.

5.8.1 Análise morfométrica do perímetro e diâmetro das vilosidades

Cortes histológicos de ambos os grupos (n = 22), corados em HE, foram fotografados em aumento de 200x utilizando o digitalizador *Axion Scan.Z1* (*Zeiss AG*, Oberkochen, Alemanha), resultando em cerca de 5.000 imagens de alta resolução para cada caso (*ZEN Blue Edition, Zeiss*, Alemanha). Dentre as imagens confeccionadas,

foram excluídas, além daquelas com tecido não-vilositário (membranas, cordão, decídua), as que estavam desfocadas ou com artefatos. As imagens restantes selecionadas (cerca de 1000), tinham 100% da imagem ocupada com vilosidades placentárias e foram randomizadas para a obtenção de cerca de 100 imagens para cada caso dos grupos estudo e controle.

A aferição do perímetro e do diâmetro das vilosidades foi feita com auxílio do programa *Image Pro Plus*® 4, com base em desenho feito à mão livre em 100 vilosidades em imagens consecutivas (Figura 8). Ao final do contorno de cada vilosidade, o programa fornecia dados de perímetro e diâmetros (maior e menor), entre outros, em micrômetros quadrados (μm^2). Para os cálculos estatísticos foram utilizados o menor diâmetro e o perímetro (108).

Figura 8 – Aferição do perímetro (**A**) e do diâmetro (**B**) das vilosidades no programa *Image Pro Plus*® 4.

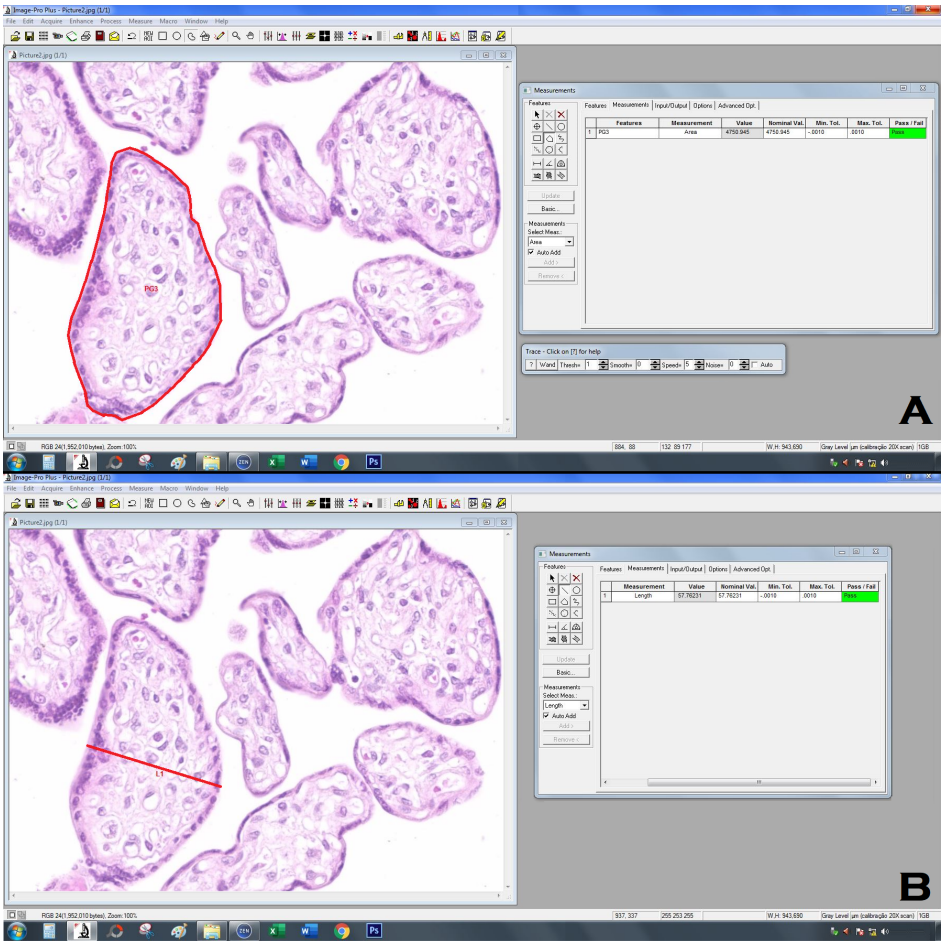

Fonte: A autora, 2021.

5.8.2 Análise morfométrica do número de nós e brotos sinciciais das vilosidades

Para avaliar os nós e brotos sinciciais, as mesmas 100 imagens em HE previamente escolhidas foram utilizadas, sendo 30 delas selecionadas de modo randomizado e submetidas a contagem simples dessas duas estruturas microscópicas, assim como do número de vilosidades. Para a contagem, foram consideradas apenas vilosidades completamente visíveis na imagem; do mesmo modo, apenas os nós sinciciais identificados nas vilosidades completamente visíveis foram contabilizados. Um nó sincicial foi definido como o agrupamento periférico ou intervilositário de quatro ou mais núcleos de sinciciotrofoblasto. Brotos sinciciais foram definidos como agrupamentos periféricos de núcleos de sinciciotrofoblasto, que se projetassem para o espaço interviloso, com ou sem estroma mesenquimal visível, porém destituídos de capilares fetais (109). Também foram contabilizados como brotos sinciciais os agrupamentos flutuantes de sinciciotrofoblasto no espaço interviloso. Essa variável foi expressa como nós ou brotos por vilosidades por campo. O método de contagem empregado foi padronizado e previamente utilizado em trabalhos já publicados (108, 110), e está ilustrado na Figura 9.

5.8.3 Análise morfométrica das alterações estromais vilositárias

Cortes histológicos de ambos os grupos (n = 22) foram corados em hematoxilina fosfotúngstica e *sirius red*, e fotografados em aumento de 200x utilizando o digitalizador *Axion Scan.Z1* (*Zeiss AG*, Oberkochen, Alemanha), resultando em cerca de 5.000 imagens de alta resolução para cada caso, para cada coloração (*ZEN Blue Edition, Zeiss*, Alemanha). O método de seleção adotado foi o mesmo descrito para o HE. As imagens resultantes foram randomizadas para a obtenção de cerca de 200 imagens para cada caso dos grupos estudo e controle, em cada coloração.

A aferição da quantidade de fibrina no estroma das vilosidades foi feita na coloração de hematoxilina fosfotúngstica, a qual cora a fibrina em roxo/azul escuro. Um controle positivo contendo níveis adequados de precipitação de pigmento foi escolhido

Figura 9 – Contagem de brotos (círculos), nós sinciciais (estrelas) conforme convencionado. Coloração: HE; magnificação 200x.

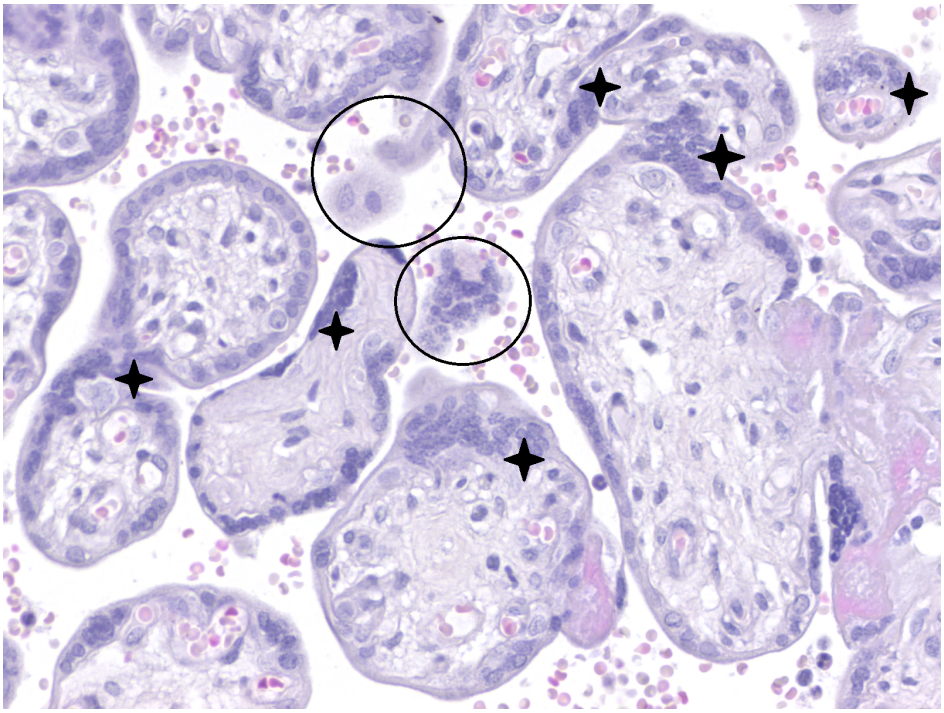

Fonte: A autora, 2021.

para a confecção de uma "máscara". Essa "máscara" foi sobreposta nas imagens e o programa *Image Pro Plus*® 4 identificou as áreas positivas, expressando os resultados como áreas de deposição de pigmento em micrômetros quadrados (μm^2).

A aferição da quantidade de fibrose no estroma das vilosidades foi feita na coloração de *sirius red*, que realça fibras colágenas tipo I e tipo III em cores diferentes quando submetida à polarização. Após a escolha da "máscara", o programa *Image Pro Plus*® 4 identificou as áreas positivas (magenta para colágeno tipo I e verde para colágeno tipo III), expressando os resultados como áreas de deposição de pigmento em micrômetros quadrados (μm^2).

Os valores obtidos da análise de deposição de fibrina e colágeno foram ainda divididos pela área total do campo observado, gerando um valor percentual para cada imagem, que foi usado para a análise estatística (111). A Figura 10 exemplifica a confecção das "máscaras" utilizadas.

Figura 10 – Composição demonstrando os processos de segmentação semiautomatizada por cores. **A**: Imagem digitalizada de uma lâmina corada com hematoxilina fosfotúngstica. **B**: A área realçada pela coloração especial (fibrina) foi delimitada artificialmente pela cor vermelho, para sua quantificação. **C**: A área total foi delimitada artificialmente pela cor verde, para sua quantificação.

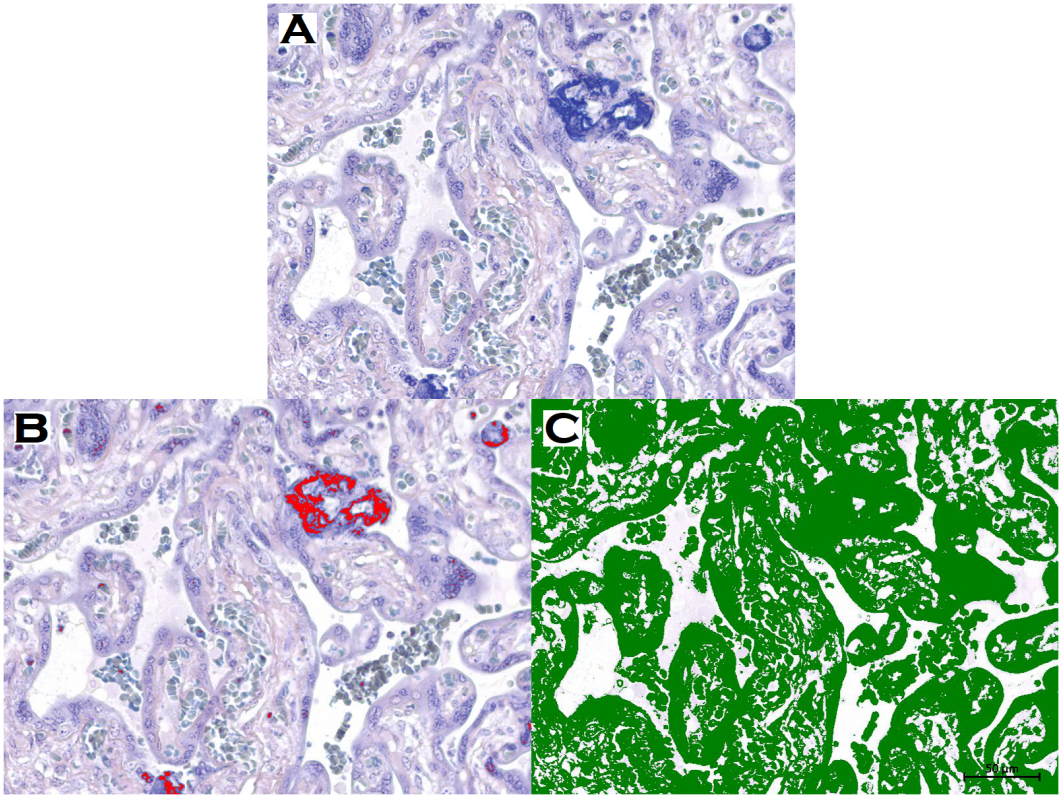

Fonte: A autora, 2021.

5.9 IMUNO-HISTOQUÍMICA

Cortes histológicos de ambos os grupos (n = 22) foram fixados em lâminas de vidro eletricamente carregadas, desparafinizados com xilol aquecido (37°C), mergulhados em banhos sucessivos de álcool etílico absoluto e re-hidratados em solução de álcool etílico com concentrações decrescentes. Foram utilizados álcool metílico e peróxido de hidrogênio para o primeiro bloqueio da peroxidase endógena e água destilada e peróxido de hidrogênio para o segundo bloqueio. Procedeu-se com a incubação com o anticorpo primário escolhido anti-CD68 (clone KP1, *mouse monoclonal, Biocare*, Califórnia, EUA) durante 1 h e com anticorpo secundário associado ao polímero de dextrana (*Spring Bioscience*, Pleasanton, EUA) durante 30 min. Para revelação foi adicionado complexo DAB/substrato (DAB, *DakoCytomation*) sobre as lâminas,

seguido de contra-coloração com hematoxilina de Mayer's, desidratação com banhos de álcool etílico em solução em concentrações crescentes, clarificação com xilol e montagem das lâminas com Bálsamo do Canadá. O protocolo desenvolvido e descrito acima já está padronizado e é usado rotineiramente no CHC-UFPR. Todos os ensaios de imuno-histoquímica incluíram um controle negativo (omissão do anticorpo primário) e controle positivo (corte histológico de linfonodo humano).

A quantificação de células de Hofbauer foi feita através da contagem do número de células positivas ao CD68 em 30 campos aleatórios de grande aumento (400x), em microscópico de luz (marca Nikkon®, modelo E200). Apenas células positivas morfologicamente compatíveis com histiócitos, com núcleos visíveis e localizadas dentro das vilosidades foram consideradas adequadas para contagem. Coloração inespecífica, positividade em quaisquer outras células e células sem núcleos visíveis foram excluídas. Foram contadas as vilosidades identificadas em cada campo, de modo a expressar o resultado desta contagem em número de células de Hofbauer por vilosidades por campo. Essa técnica de contagem foi padronizada e utilizada em trabalhos já publicados (108, 110) e está ilustrada na Figura 11.

Figura 11 – Contagem de células de Hofbauer. Imuno-histoquímica com marcador CD68; magnificação: 400x. Círculos destacam exemplos de células de Hofbauer contabilizadas. As setas apontam para áreas com deposição de pigmento desconsideradas durante a avaliação.

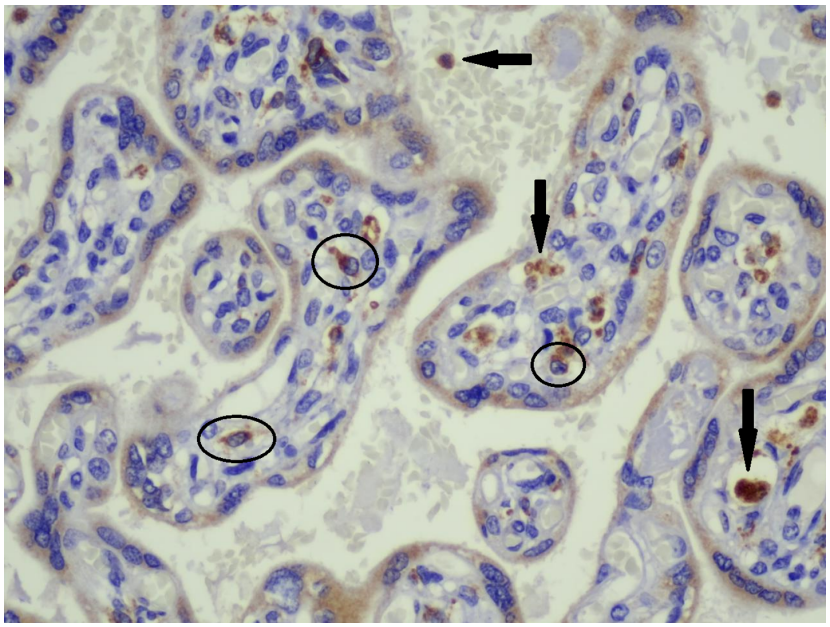

Fonte: A autora, 2021.

5.10 ANÁLISE ESTATÍSTICA

Os dados obtidos foram armazenados em planilha eletrônica e transportados para um software estatístico (*IBM SPSS Statistics software v.20.0 Armonk, NY: IBM Corp*) para execução das comparações entre os dois grupos, sob orientação de um profissional experiente. Os resultados foram expressos por médias, medianas, valores mínimos, valores máximos e desvios-padrão ou por frequências e percentuais.

As variáveis nominais foram expressas como valores reais, frequências e percentuais, e analisadas pelo teste qui-quadrado de Pearson ou pelo teste exato de Fisher. A maioria das variáveis quantitativas exibiu distribuição normal, conforme verificado pelo teste de Shapiro-Wilk, e foram comparadas com o teste T. O teste não paramétrico de Kruskal-Wallis foi utilizado para comparar os resultados da variável quantitativa restante (deposição de fibrina). Para todas as análises o nível de significância (ou probabilidade de significância) mínimo adotado foi de 5% (valor de $p<0,05$).

6 RESULTADOS E DISCUSSÃO

Os resultados obtidos neste trabalho e sua respectiva discussão constam no artigo científico a seguir, publicado no periódico *Frontiers in Immunology* em maio de 2021, cuja política de acesso aberto e direitos autorais foi incluída nos Anexos deste trabalho.

frontiers in Immunology

ORIGINAL RESEARCH
published: 26 May 2021
doi: 10.3389/fimmu.2021.685919

Association Between COVID-19 Pregnant Women Symptoms Severity and Placental Morphologic Features

Patricia Zadorosnei Rebutini[1], Aline Cristina Zanchettin[2], Emanuele Therezinha Schueda Stonoga[3], Daniele Margarita Marani Prá[1], André Luiz Parmegiani de Oliveira[1], Felipe da Silva Dezidério[1], Aline Simoneti Fonseca[2], Júlio César Honório Dagostini[3], Elisa Carolina Hlatchuk[3], Isabella Naomi Furuie[4], Jessica da Silva Longo[4], Bárbara Maria Cavalli[5], Carolina Lumi Tanaka Dino[5], Viviane Maria de Carvalho Hessel Dias[1], Ana Paula Percicote[3], Meri Bordignon Nogueira[5,6], Sonia Mara Raboni[7], Newton Sergio de Carvalho[5], Cleber Machado-Souza[2]* and Lucia de Noronha[1]*

[1] Postgraduate Program of Health Sciences, School of Medicine, Pontifícia Universidade Católica do Paraná-PUCPR, Curitiba, Brazil, [2] Postgraduate Program in Biotechnology Applied in Health of Children and Adolescent, Pelé Pequeno Príncipe, Research Institute, Faculdades Pequeno Príncipe, Curitiba, Brazil, [3] Department of Medical Pathology, Clinical Hospital, Universidade Federal do Paraná-UFPR, Curitiba, Brazil, [4] Department of Tocogynecology, Clinical Hospital, Universidade Federal do Paraná, UFPR, Curitiba, Brazil, [5] Postgraduate Program of Tocogynecology and Women's Health, Clinical Hospital, Universidade Federal do Paraná-UFPR, Curitiba, Brazil, [6] Virology Laboratory, Clinical Hospital, Universidade Federal do Paraná-UFPR, Curitiba, Brazil, [7] Department of Infectious Disease, Clinical Hospital, Universidade Federal do Paraná-UFPR, Curitiba, Brazil

OPEN ACCESS

Edited by:
Abhay P.S. Rathore, Duke University, United States

Reviewed by:
David Alan Schwartz, Augusta University, United States
Jeffery A. Goldstein, Northwestern Medicine, United States

***Correspondence:**
Cleber Machado-Souza
Cleberius@gmail.com
Patricia Zadorosnei Rebutini
rebutini@gmail.com

Specialty section:
This article was submitted to Viral Immunology, a section of the journal Frontiers in Immunology

Received: *26 March 2021*
Accepted: *05 May 2021*
Published: *26 May 2021*

Citation:
Rebutini PZ, Zanchettin AC, Stonoga ETS, Prá DMM, de Oliveira ALP, Dezidério FdS, Fonseca AS, Dagostini JCH, Hlatchuk EC, Furuie IN, Longo JdS, Cavalli BM, Dino CLT, Dias VMdCH, Percicote AP, Nogueira MB, Raboni SM, de Carvalho NS, Machado-Souza C and de Noronha L (2021) Association Between COVID-19 Pregnant Women Symptoms Severity and Placental Morphologic Features. Front. Immunol. 12:685919. doi: 10.3389/fimmu.2021.685919

Since the beginning of the pandemic, few papers describe the placenta's morphological and morphometrical features in SARS-CoV-2–positive pregnant women. Alterations, such as low placental weight, accelerated villous maturation, decidual vasculopathy, infarcts, thrombosis of fetal placental vessels, and chronic histiocytic intervillositis (CHI), have been described.

Objective: To analyze clinical data and the placental morphological and morphometric changes of pregnant women infected with SARS-CoV-2 (COVID-19 group) in comparison with the placentas of non-infected pregnant women, matched for maternal age and comorbidities, besides gestational age of delivery (Control group).

Method: The patients in the COVID-19 and the Control group were matched for maternal age, gestational age, and comorbidities. The morphological analysis of placentas was performed using Amsterdam Placental Workshop Group Consensus Statement. The quantitative morphometric evaluation included perimeter diameter and number of tertiary villi, number of sprouts and knots, evaluation of deposition of villous fibrin, and deposition of intra-villous collagen I and III by Sirius Red. Additionally, Hofbauer cells (HC) were counted within villi by immunohistochemistry with CD68 marker.

Results: Compared to controls, symptomatic women in the COVID-19 group were more likely to have at least one comorbidity, to evolve to preterm labor and infant death, and to have positive SARS-CoV-2 RNA testing in their concepts. Compared to controls, placentas in the COVID-19 group were more likely to show features of maternal and

fetal vascular malperfusion. In the COVID-19 group, placentas of symptomatic women were more likely to show CHI. No significant results were found after morphometric analysis.

Conclusion: Pregnant women with symptomatic SARS-CoV-2 infection, particularly with the severe course, are more likely to exhibit an adverse fetal outcome, with slightly more frequent histopathologic findings of maternal and fetal vascular malperfusion, and CHI. The morphometric changes found in the placentas of the COVID-19 group do not seem to be different from those observed in the Control group, as far as maternal age, gestational age, and comorbidities are paired. Only the deposition of villous fibrin could be more accentuated in the COVID-19 group (p = 0.08 borderline). The number of HC/villous evaluated with CD68 immunohistochemistry did not show a difference between both groups.

Keywords: SARS-CoV-2, COVID-19, vertical transmission, placenta, morphometric analysis, placental histopathology

INTRODUCTION

One year after the recognition of the outbreak of the severe acute respiratory distress syndrome coronavirus 2 (SARS-CoV-2), it has spread all over the world, thus developing into a global pandemic with nearly 150 million confirmed infections and more than 3.1 million deaths worldwide so far (1). Fatalities and severe courses were primarily seen in elderly patients with relevant comorbidities, but soon there were reports of younger patients showing adverse outcomes (2, 3).

No longer after its first documented appearance, SARS-CoV-2 was suspected to be perinatally transmitted (4–8). This enveloped single-stranded RNA virus infects target cells by binding to angiotensin-converting enzyme 2 (ACE2) and entry into cells after spike protein cleavage by the transmembrane serine protease 2 (TMPRSS2). Since both proteins have been detected in the placenta and fetal tissues, a possible mechanism of intrauterine transmission and neonatal infection emerged (9–14), and the coronavirus disease 2019 (COVID-19) impact on pregnant women became of particular interest.

Along with the worldwide dissemination of COVID-19, reports of adverse pregnancy outcomes have emerged in the literature, such as preeclampsia, preterm delivery, miscarriage, intrauterine fetal demise, and neonatal death (15–18). Congenital infection can be challenging to characterize since pathogen detection usually requires specific methods, not always available, applied in a myriad of maternal and fetal samples. Despite that, antepartum or peripartum vertical transmission is now substantially documented. Almost 30% of neonatal infections reported to date occurred due to transplacental transmission, and the remaining due to environmental exposure. Additionally, Raschetti et al. observed that 55% of infected neonates developed COVID-19 (19–25).

It is well recognized that analysis of the placental histopathological changes can provide valuable information, considering that a variety of pathological agents, including infectious ones, are associated with characteristic morphological findings (26–29). Regardless, few papers describe the placenta's morphological and morphometrical features in SARS-CoV-2–positive pregnant women (30–34), and the association between maternal infection and abnormal placental findings is still to be determined.

Accordingly, the purpose of this study was to analyze clinical data and the morphological and morphometric changes in placentas of pregnant women infected with SARS-CoV-2 (COVID-19 group) and to compare the placentas of non-infected pregnant women (Control group) matched in a 1:1 fashion by gestational age at delivery, maternal age, and comorbidities.

MATERIALS AND METHODS

Ethical Approvals

The Brazilian National Ethics Committee approved the presented study of Human Experimentation under the protocol number CAAE: 35129820.6.0000.0096. Families signed the informed consent forms. The authors followed all relevant guidelines, regulations, and ethics and safety protocols during this study execution at all stages. The data that support the findings of this study are available from the corresponding author.

Study Design

A prospective observational case-control study.

Study Patients and Control Group Selection

For the COVID-19 group (study group), pregnant women with laboratory-confirmed infection, whose respective placenta specimens have been sent for histologic examination, were eligible for inclusion. This group comprises 19 women who had SARS-CoV-2 infection confirmed either in the second (n = 3) or in the third gestational trimester (n = 16). Initially, we included women who spontaneously sought treatment at Complexo Hospital de Clínicas, Universidade Federal do Paraná

(CHC-UFPR) or at Hospital Nossa Senhora das Graças (HNSG), Curitiba, Brazil, for symptoms of COVID-19 varying from mild to severe (n = 9). After the implementation of universal testing for SARS-CoV-2 infection for all obstetrical patients admitted to labor and delivery in both institutions, asymptomatic pregnant women were added thereafter (n=10).

For the Control group (n = 19), placentas of pregnant women who gave birth at CHC-UFPR in years prior to the SARS-CoV-2 outbreak were selected (from 2016 to 2018) and matched in a 1:1 fashion by gestational age at delivery, maternal age, and maternal comorbidities.

Historical controls were selected to ensure that women with false-negative test results for SARS-CoV-2 infection were excluded. Gestational age at delivery is a universally used matching variable since there is a correlation between placental development and the advancing gestation, which could interfere in the analysis. Maternal age and maternal comorbidities were also incorporated as matching variables, given their possible role as confounders when analyzing placental abnormalities.

Samples

Submission criteria for placental examination included maternal or fetal conditions previously diagnosed during prenatal care or gross abnormalities noted during delivery, as routinely implemented in both institutions. Therefore, the maternal-positive SARS-CoV-2 testing result was considered an abnormal maternal condition and a placental evaluation criterion.

All placentas were examined according to a standardized protocol that consisted of immediate fixation after delivery in 10 % buffered formalin for 72 h, gross examination with measurement of placental dimensions and chord length, weight evaluation of the placental disc after trimming of the fetal membranes and umbilical cord, followed by serial sectioning through 1.5-cm interval and cut surface examination. Macroscopic alterations were recorded and sampled. Additional representative samples of the umbilical cord (two sections), the membranes (one fetal membrane roll), and the chorionic plate (at least two full-thickness, non-peripheral sections including maternal and fetal surface) were submitted to paraffin embedding.

Clinical Information

Clinical and laboratory data were obtained from medical records during hospitalization; the mother and the newborn were followed up until discharge from the hospital.

Maternal information sought from each medical record for both groups comprised maternal age and comorbidities, parity, gestational age at delivery, mode of delivery, neonatal birth weight, and APGAR score. All pregnant women in both groups were tested for congenital intrauterine infections (TORCH) during prenatal care; only one (Patient code—PC 20-3744) tested positive for syphilis in the first trimester and received the preconized treatment.

For the study group, it was also retrieved the gestational age at and method used for SARS-CoV-2 infection diagnosis, presence or absence of symptoms typically attributed to COVID-19 (body temperature over 38°C, dyspnea, cough, myalgias, nausea and vomiting, diarrhea, headache, anosmia), disease severity (ranging from mild symptoms to critical organ dysfunction), and maternal outcome.

SARS-CoV-2 Testing

Maternal nasopharyngeal swabs specimens (n = 17) were tested for SARS-CoV-2 infection by real-time reverse transcriptase-polymerase chain reaction (RT-PCR). In the remaining two cases, the diagnosis was achieved by serologic testing (n = 2).

Detection of SARS-CoV-2 RNA in infants was performed in 13 case samples (n = 13), including umbilical cord blood (n = 13), amniotic fluid (n = 3), and infants' nasopharyngeal swabs specimens (n = 6), all of them collected immediately after birth. The mothers' milk was also tested in three cases.

Samples from formalin-fixed paraffin-embedded (FFPE) tissue were also tested to verify the presence of SARS-CoV-2 RNA in the placenta (n=11). Viral RNA extraction was performed with a commercially available paraffin extraction kit (Qiagen®) in Pelé Pequeno Príncipe Research Institute.

SARS-CoV-2 RNA identification tests were performed at CHC-UFPR and HNSG using XGEN MASTER COVID-19 Kit (Mobius Life Science, Inc, Brazil). Quantitative anti-SARS-CoV-2 IgM and IgG dosage was done in peripheral blood samples in both institutions.

Morphologic Analysis

All representative placental samples taken for microscopic assessment underwent routine processing, embedding, sectioning at 5 μm, and staining with hematoxylin and eosin (H&E).

The qualitative morphological analysis was performed in all placentas from the COVID-19 and Control groups (n = 38) using the Amsterdam Placental Workshop Group Consensus Statement (35). Histological sections containing at least one sample of the umbilical cord, membrane roll, and chorionic plate of every case from both groups were randomly selected and renamed by one research team member (blinding step). Two experienced perinatal pathologists systematically evaluated the slides.

Selected parameters were computed simply as "present" (yes) or "absent" (no). The extension and intensity of specific alterations were graded following Amsterdam protocol recommendations. The remaining parameters were subdivided into three quantitative categories: <30%, 30% to 70%, and > 70%, to record both the presence and extension of most alterations.

Assessed parameters included features of maternal vascular malperfusion (villous infarction, distal villous hypoplasia, accelerated villous maturation/increase in syncytial knots, decidual acute atherosis, decidual vascular fibrinoid necrosis with or without foam cells, decidual vascular mural hypertrophy, decidual chronic perivasculitis, absence of spiral artery remodeling, decidual arterial thrombosis, persistence of intramural endovascular trophoblast), features of fetal vascular malperfusion (fetal vascular thrombosis, fetal vascular intramural fibrin deposition, avascular villi, stem vessel obliteration/fibromuscular sclerosis, villous stromal-vascular karyorrhexis, vascular ectasia), delayed villous maturation, features of maternal inflammatory response (chorionitis, chorioamnionitis), features of fetal inflammatory response (umbilical vasculitis, funisitis), features

of chronic inflammation (chronic deciduous, villitis, intervillositis), intervillous thrombi, microcalcification foci, chorangiosis, and membrane meconium and hemosiderin staining.

Morphometric Analysis

The morphometric analysis included measurement of the perimeter and diameter of the villi, counting the number of tertiary villi, sprouts and knots of tertiary villi, quantifying the villous fibrin and the intra-villous collagen I and III depositions. It was performed in 11 cases of the COVID-19 group and eleven Control group cases (n = 22), matched for gestational age, maternal age, and maternal comorbidities.

One histological section stained with H&E containing at least one sample of the chorionic plate was randomly selected from every case in both groups (n = 22). Samples of grossly identified lesions were previously excluded. Each section was subsequently photographed at a magnification of 200× (medium power field—MPF) using the Scanner Axion Scan.Z1 (Zeiss AG, Oberkochen, Germany), resulting in about 5,000 high-resolution images for each case (ZEN Blue Edition, Zeiss, Germany). Following the exclusion of unfocused images, with artifacts, with non-villous tissue, or less than 100% of the field occupied with placental villi, the remaining images were randomized to obtain about 100 images for each case of both groups. The villi's perimeter and diameter were measured using Image-Pro Plus® 4 software, based on freehand drawing on 100 villi in consecutive images. At the end of each villus' contour, the program provided perimeter and minor diameter in micrometers (μm).

The variables number of tertiary villi, number of sprouts, and knots of tertiary villi were assessed by simply counting these microscopic structures by an experienced perinatal pathologist, in 30 of those 100 images, after a new cycle of randomization.

Histological sections were also stained with phosphotungstic hematoxylin (n = 22) and Sirius Red (n = 22), aiming to evaluate villous fibrin and intra-villous collagen I and III depositions, respectively. As previously described for H&E, the slides were photographed at MPF using the Scanner Axion Scan.Z1, and the resulting images were randomized to obtain about 200 images for every case of the COVID-19 and Control group for each stain. Positive control was chosen as a "mask," which contained adequate levels of specific pigment precipitation. The mask was then superimposed on the sample images, and Image-Pro Plus 4 software identified the positive areas, expressing the results as positive pigment deposition areas per μm^2. The values obtained for the collagen analysis were further divided by the observed field's total area, generating a percentage value for each image (36).

The morphometric analysis was also blind since each case was previously renamed by one member of the research team not involved in the data acquisition, and the images were also randomly generated by the software afterward, with no investigator's interference.

Immunohistochemistry

Histological sections of the placentas from both groups (n = 22) were fixed on electrically charged glass slides and subsequently dewaxed with heated xylol (37°C), dehydrated by successive baths of absolute ethyl alcohol with decreasing solution concentrations and rehydrated with water. Methyl alcohol and hydrogen peroxide were used to block endogenous peroxidase and distilled water and hydrogen peroxide for the second block. Next, incubation with anti-CD68 primary antibody (KP1 clone, monoclonal mouse, Biocare, California, USA) for 1 h and secondary antibody associated with the dextran polymer (Spring Bioscience, Pleasanton, USA) for 30 min. For development, DAB/substrate complex (DAB, DakoCytomation) was added onto the slides, followed by counterstaining with Mayer's hematoxylin, dehydration with ethyl alcohol baths in increasing concentrations, clarification with xylol, and blending with Canada balsam. The protocol developed and described above is already standardized and routinely used in CHC-UFPR. To quantify Hofbauer cells (HC), the number of villi and CD68+ cells in those villi were counted in 30 high-power random fields (HPF= 400×). Only positive cells morphologically compatible with histocytes, with visible nuclei, and located within villi were considered suitable for counting. Unspecific staining, staining of any other cells, and cells without visible nuclei were excluded.

All immunohistochemistry assays included a negative control (missing a primary antibody) and positive control (human lymph node).

Statistical Analysis

Means, standard deviations, medians, minimum, maximum values, frequencies, or percentages were used to describe the findings. The nominal variables are expressed as actual values and frequency and analyzed by Pearson chi-square test and or by Fisher exact test. Most of the quantitative variables exhibited normal distribution, as verified by the Shapiro–Wilk test, and were compared with the t-test. The Kruskal–Wallis non-parametric test was performed to compare the remaining quantitative variable between groups (fibrin deposition). For both tests, statistical significance was defined as a p-value of <0.05. The data were analyzed using the IBM SPSS Statistics v.20.0 software. Armonk, NY: IBM Corp.

RESULTS

Relevant clinical information about each case in both groups is summarized in **Tables 1** and **2**. Comparison between groups regarding clinical data and morphologic findings are resumed in **Table 3** (n = 38). In **Table 4**, morphometric data are presented along with clinical information of the cases evaluated from both groups (n = 22). **Figure 1** exemplifies morphometric and morphological parameters evaluated.

Maternal Clinical Profile and SARS-CoV-2 Testing Results

Among the nineteen patients testing positive for SARS-CoV-2 infection, almost half (9/19, 47.4%) were symptomatic. Three had COVID-19 symptoms varying from mild (fever, cough, among others, but without dyspnea) to moderate (with dyspnea, but without the necessity of complementary life

TABLE 1 | Clinical information of the COVID-19 group.

Patient code	Maternal age (yr)	Maternal Comorbidities	COVID-19 Symptoms/ Severe Disease	SARS-CoV-2 testing			Outcome			
				RT-PCR Maternal NS swab/ Trimester	Maternal Serology	RT-PCR placenta/ RT-PCR fetal samples	Gestational age at delivery	APGAR (1 min/5 min)/ Fetal-Maternal Outcome	Fetal weight (g)	Placental weight (g)/ Macroscopic alterations
20–3594	26	Hypertensive disorder in pregnancy and hypothyroidism	+/+	+/3rd	IgM+/IgG+	–/–	33	(5/9) Preterm newborn	2450	448/Infarcts (<5%)
20–3561	38	Hypothyroidism	+/+	*/2nd	IgM+/IgG+	–/–	28+2	(na) Preterm newborn	na	245
20–3282	40	*Situs inversus totalis* with metallic stent	+/+	+/3rd	na	–/+**	33+5	(0/0) Neonatal death/ Maternal death	2300	416
20–5379	38	Gestational diabetes	+/+	+/2nd	na	–/+**	23+6	(1/5) Neonatal death/ Maternal death	610	168/Placental hypoplasia
20–3744	29	Gestational diabetes, hypothyroidism, obesity, bipolar disorder, and syphilis (treated)	+/–	+/3rd	IgM+/IgG+	–/+**	34+1	(na) Preterm newborn	na	412/Infarcts (<5%)
20–5105	29	None	–	+/3rd	na	–/na	38+6	(9/10) Term newborn	2960	462
20–3369	29	Gestational diabetes and Hyperthyroidism	+/–	+/3rd	na	–/na	37+4	(8/9) Term newborn	2600	358/Infarcts (<5%)
20–3364	42	Hypertensive disorder in pregnancy	+/+	+/2nd	IgM+/IgG+	+/+§	28+3	Intrauterine death	1020	135/Placental hypoplasia and infarcts (30–40%)
20–5776	42	None	–	+/3rd	na	–/+**	36+5	(9/10) Preterm newborn	2605	382
20–5869	27	None	+/–	+/3rd	na	–/na	37+2	(9/10) Term newborn	2345	370
20–3916	24	None	–	+/3rd	IgM+/IgG+	–/na	38+6	(9/10) Term newborn	3030	650
20–4850	25	Obesity	+/+	+/3rd	na	na/–	30+2	(na) Preterm newborn	na	410
20–5006	22	Obesity	–	+/3rd	na	na/–	41+0	(4/9) Term newborn	3110	670
20–5009	23	Hypothyroidism	–	*/3rd	IgM+/IgG+	na/–	38+4	(5/9) Term newborn	3925	775/Hydropic placenta
20–5031	35	Gestational diabetes, obesity	–	+/3rd	na	na/–	36+4	(8/9) Preterm newborn	2720	450
20–6551	32	None	–	+/3rd	na	na/na	38+5	(8/9) Term newborn	3070	448
20–6680	38	None	–	+/3rd	na	na/na	37	(9/10) Term newborn	2875	318
20–7035	34	None	–	+/3rd	na	na/–	39	(9/9) Term newborn	3115	438
20–6071	34	Hypertensive disorder in pregnancy	–	+/3rd	na	na/–	34+6	(7/8) Preterm newborn	2370	384

**rt-PCR not available—diagnostic by serology.*

*RT-PCR positive in fetal samples: **Nasofaringeal swab and §Umbilical cord blood.*

na, not available.

TABLE 2 | Clinical information of the Control group.

Patient code	Maternal age (yr)	Maternal Comorbidities	Outcome			
			Gestational age at delivery	APGAR (1 min/5 min)/ Fetal Outcome	Fetal weight (g)	Placental weight (g) Macroscopic alterations
16–7859	20	Hypothyroidism	32+3	(3/7) Preterm newborn	1180	270/Placental hypoplasia
18–13016	23	Chronic hypertension and hypothyroidism	35+2	(4/8) Preterm newborn	2223	498/none
16–8315	18	Obesity	40+4	(7/9) Term newborn	3810	514 none
18–4906	20	None	28	(7/8) Preterm newborn	1205	248/none
18–14057	42	Diabetes, chronic hypertension, bipolar disorder	33+4	(2/8) Preterm newborn	1650	243/Placental hypoplasia
16–7599	25	Gestational diabetes	39	(8/10) Term newborn	3460	480/none
16–3340	39	None	38+3	(7/9) Term newborn	3005	395/none
18–9951	24	None	37+2	(8/9) Term newborn	3690	574/none
16–6144	29	None	39	(9/10) Term newborn	3345	394/none
17–2491	35	None	32+4	(8/9) Preterm newborn	2900	416/none
16–7667	36	None	36+4	(9/9) Preterm newborn	2315	319/none
18–5040	24	None	32+4	(1/6/8) Preterm newborn	1555	297/Infarcts (5%)
16–7155	25	Obesity	40	(7/9) Term newborn	2830	375/none
16–5762	39	Hypothyroidism	39+3	(8/9) Term newborn	3490	465/Infarcts (10%)
18–11859	38	Gestational diabetes, obesity	36+1	(6/9) Preterm newborn	2925	450/none
18–5502	27	None	37+2	(7/9) Term newborn	2500	552/none
16–3787	24	None	37+4	(9/10) Term newborn	2945	461/none
18–4510	19	None	40+2	(7/8) Term newborn	1990	413/none
18–6601	16	Hypertensive disorder in pregnancy	24+5	(8/9) Preterm newborn	2235	368/none

support) (3/9, 33.3%). Six developed severe courses, requiring orotracheal intubation and hemodynamic support within less than seven days after admission (6/9, 66.6%). Two of them died due to COVID-19 associated complications (2/6, 33.3%).

Twelve patients of the COVID-19 group had at least one comorbidity (12/19, 63.2%), such as hypertension (3/19, 15.8%), diabetes (4/19, 21%), obesity (4/19, 21%), and hypothyroidism (4/19, 21%). One patient had a diagnosis of Kartagener syndrome (chronic sinusitis, bronchiectasis, and situs inversus with dextrocardia) and had a cardiac valvar replacement (metallic) for 10 years (Patient code—PC 20-3282).

Most pregnant women tested positive for SARS-CoV-2 in the third gestational trimester (16/19, 84.2%), either immediately before delivery in asymptomatic patients or within less than 15 days from delivery in symptomatic ones.

Only three patients had a positive result in the second trimester, all of them with severe COVID-19 symptoms and equally close to delivery. In this subgroup, one woman died due to COVID-19 complications along with her infant (PC 20-5379). One had an intrauterine demise (PC 20-3364) and recovered utterly afterward. The third evolved to preterm labor (PC 20-3561).

Newborns Clinical Outcome and SARS-CoV-2 Testing Results

The mode of delivery, APGAR score, placental weight, fetal weight, fetal/placental weight ratio were similar between both groups (p=NS).

Among the 19 infants in the COVID-19 group, sixteen were born alive (16/19, 84.2%). We observed three infant deaths, being one intrauterine demise and two neonatal deaths within hours of delivery (3/19, 15.8%). All infant deaths occurred in women with severe COVID-19 symptoms, including the two who died due to COVID-19 complications (PC 20-3282 and 20-5379). In the Control group, all infants were born alive.

Preterm delivery was recorded in ten cases (10/19, 52.6%), including those with infant deaths mentioned above. In the Control group, nine pregnancies ended prematurely (9/19, 47.4%), a similarity that was expected due to methodological design. However, there were no recorded infant or maternal deaths.

SARS-CoV-2 RNA was detected in samples from five infants among thirteen tested (5/13, 38.4%). It was positive in one cord blood sample (PC 20-3364) and four newborns nasopharyngeal swabs specimens (PC 20-3282, 20-5379, 20-3744, and 20-5776). All amniotic fluid and mother's milk samples tests returned negative.

From all FFPE placental tissue tested (n = 11), only one case was positive for SARS-CoV-2 RNA, being the case of intrauterine demise (PC 20-3364).

Morphologic Alterations

All parameters enumerated in *Materials and Methods* were sought systematically. Many of them were not identified in any sample. The histopathological alterations identified in both groups are listed in **Table 3** and discussed below.

Morphometric Alterations and Immunohistochemistry Evaluation

The average number of sprouts and knots (per villous) of the COVID-19 group tertiary villi was 0.19 and 0.81, respectively, compared to 0.16 and 0.81 of the Control group (p=NS). The average perimeter of the COVID-19 group tertiary villi was 271.93 μm compared to 288.42 μm in the Control group (p=0.37).

TABLE 3 | Clinical and morphological comparisons between COVID-19 group (n=19) and Control group (n=19) placentas.

		Variable	Control	COVID-19	*p*-value
Clinical data	**Maternal**	Maternal age (years)	25 (16–42)	32 (22–42)	0.21
		Gestational age (weeks)	36 (23–40)	36 (23–41)	0.97
		Comorbidities	Hypertensive disorder (3) Gestational diabetes (3) Obesity (3) Hypothyroidism (3) None (11)	Hypertensive disorder (3) Gestational diabetes (4) Obesity (4) Hypothyroidism (4) None (7)	1
	Fetal	APGAR 1 min/5 min	7 (1–9)/9 (6–10)	8(0–9)/9 (0–10)	0.41/0.33
		Fetal weight (grams)	2865 (1,180–3,810)	2663 (610–3,925)	0,94
		Placental Weight (grams)	406 (243–573)	412 (135–775)	0,79
		Placental diameter (centimeters)	17 (12–19)	16 (12–22)	0,87
		Infant death	0	3	**0.09**
		Preterm delivery	9	10	0.74
		Term delivery	10	9	0.74
Morphological variables	**MVM**	Villous infarction	5	2	0.21
		Distal villous hypoplasia	6	4	0.46
		Accelerated villous maturation/increase in syncytial knots	5	8	0.30
		Decidual vascular mural hypertrophy	5	10	**0.09**
		Absence of spiral artery remodeling	1	6	**0.03**
		Decidual vascular fibrinoid necrosis without foam cells	1	3	0.29
		Decidual vascular fibrinoid necrosis with foam cells	0	2	0.14
		Decidual arterial thrombosis	0	1	0.31
	FVM	Avascular villi small foci	1	1	1.0
		Avascular villi intermediate foci	1	0	0.31
		Fetal vascular thrombosis	1	6	**0.03**
		Fetal vascular thrombosis—umbilical cord	0	5	**0.02**
		Fetal vascular intramural fibrin deposition (non-occlusive)	0	2	0.14
		Vascular ectasia	2	1	0.54
	DVM	Delayed villous maturation (focal - <30%)	1	4	0.15
		Delayed villous maturation (extensive - >70%)	2	2	1.0
	CI	Chronic deciduitis—non-intense	17	16	0.31
		Chronic deciduitis—intense	1	0	0.29
		Villitis—low grade	1	1	1.0
		Chronic intervillositis—low grade	3	2	0.63
		Chronic intervillositis—high grade	1	2	0.54
	MIR	Subchorionitis/chorionitis	5	6	0.72
		Chorioamnionitis—non-intense	2	0	0.14
		Chorioamnionitis (necrosis)—intense	0	1	0.31
	FIR	Umbilical vasculitis	2	1	0.63
	Others	Intervillous thrombi	3	1	0.29
		Villous fibrin (focal—<30%)	15	14	0.70
		Villous fibrin (multifocal 30–70%)	3	5	0.42
		Villous fibrin (extensive—>70%)	1	0	0.31
		Villous edema	3	4	0.70
		Chorangiosis	4	3	0.42

p-value refers to the comparison between COVID-19 vs. the Control group; relevant values are highlighted (bold). p-value < 0.05. MVM, maternal vascular malperfusion; FVM, fetal vascular malperfusion; DVM, delayed vilous maturation; CI, chronic inflammation; MIR, maternal inflammatory response; FIR, fetal inflammatory response.

The mean diameter of the COVID-19 group tertiary villi was 51.78 μm than 50.52 μm in the Control group (p=0.57).

The quantitative morphometric analysis of deposition of villous fibrin revealed an average area of 686.64 μm^2 in the COVID-19 group compared to 485.36 μm^2 in the Control group (p=0.08 - borderline).

The quantitative morphometric analysis of deposition of intra-villous collagen I and III revealed that COVID-19 group average areas were 36.40% and 63.60%, respectively, compared to 41.01% and 58.99% of the Control group (p=0.45).

HC counting revealed an average number of 1,7 CD68+ cell/villous in the COVID-19 group and 1,2 CD68+ cell/villous in the Control group (p=0.12).

DISCUSSION

New insights are being acquired on SARS-CoV-2 infection pathophysiology. COVID-19 is associated with an exaggerated inflammatory response, usually proportional to the disease's

TABLE 4 | Clinical and morphometrical comparisons between COVID-19 group (n=11) and Control group (n=11) placentas.

		Variable	Control	COVID-19	*p*-value
Clinical data	**Maternal**	Maternal age (years)	28.3 (18–42)	33 (26–42)	0.41
		Gestational age (weeks)	33.9 (23–39)	33.6 (23–38)	0.78
		Comorbidities	Hypertensive disorder (2) Gestational diabetes (2) Hypothyroidism (2) None (7)	Hypertensive disorder (2) Gestational diabetes (2) Hypothyroidism (2) None (4)	1
	Fetal	APGAR 1 min/5 min	6.5 (2–9)/8.7 (7–10)	6.6(0–9)/7 (0–10)	0.59/0.48
		Fetal weight (grams)	2656 (1,180–3,810)	2213 (610–3,030)	0.94
		Placental Weight (grams)	395 (243–573)	367 (135–650)	0.87
		Fetal/Placental ratio	6.74 (4.3–8.4)	5.96(3.63–7.55)	0.61
		Placental diameter (centimeters)	16.45 (13–19)	16.2 (12–20)	0.88
		Infant death	0	3	0.11
		Preterm newborn	7	6	0.66
		Term newborn	4	4	0.66
Morphometric variables	**HE**	Villi number	9.0 (5.3–14.5)	8.3 (4.7–10.9)	0.62
		Knots/villus	0.81 (0.6–1.0)	0.81 (0.6–1.0)	0.97
		Sprouts/villus	0.16 (0.1–0.3)	0.19 (0.1–0.5)	0.92
		Villus diameter	50.52 (43.4–58.8)	51.4 (45.5–63.0)	0.57
		Villus perimeter	288.42 (202.7–368.5)	271.93(213.8–358.4)	0.37
	HPt	Fibrin area (μm^2)	485.36(61.9–1749.6)	686.64 (170.3–2053.0)	**0.08**
	SiriusRed	Collagen I percentage	41.01(10.1–66.1)	36.40(13.8–68.6)	0.45
		Collagen III percentage	58.99(33.9–89.9)	63.60 (31.4–86.2)	0.45
Immunohistochemistry		CD68+ Hofbauer cell/villous	1.2	1.7	0.12

p-value refers to the comparison between COVID-19 vs. the Control group; relevant values are highlighted (bold). p-value < 0.05. HPt, phosphotungstic hematoxylin.

severity, recognized as a cytokine storm (37). Such inflammatory alterations cause endothelial damage and disruption in the coagulation system, which may play a direct pathogenic role in the disease (38). Reports of hypercoagulability, with d-dimer elevation, development of ischemic changes as gangrene of extremities, and even disseminated intravascular coagulopathy, are not uncommon. There is emerging evidence that at least part of COVID-19 manifestations is associated with a systemic thrombotic and microvascular injury (39–45). In pregnant women, when coagulation is already altered by pregnancy itself, the impact of COVID-19 is still the object of study.

In this context, placental findings are invaluable. To date, histopathological alterations described encompass maternal vascular malperfusion (MVM) features, including low placental weight, accelerated villous maturation, decidual vasculopathy, and infarcts. The MVM findings are frequently observed in placentas from pregnant women with hypertensive disorders, such as gestational hypertension and preeclampsia, and have been associated with oligohydramnios, preterm birth, and stillbirth. Fetal vascular malperfusion (FVM) alterations have been described as well, such as focal thrombosis of fetal placental vessels (30–34, 46). However, various authors did not identify a correlation between placental lesions and maternal infection, notably when the samples analyzed were obtained from uninfected placentas and infants (47).

Interestingly, in cases with confirmed transplacental infection, inflammatory alterations were more frequently observed, particularly chronic histiocytic intervillositis with trophoblast necrosis. In these cases, SARS-CoV-2 was detected in the syncytiotrophoblast by immunohistochemistry and or RNA *in situ* hybridization (48, 49). It is not yet clear if the syncytiotrophoblast destruction is caused by a direct viral effect or is secondary to inflammatory or ischemic injury. Whichever mechanism is involved, the damage of this protective villous layer can facilitate fetal infection.

Recognition of the disease's impact on the placenta, and the maternal-fetal response's nature, may help understand the processes involved in pathogenesis, and ultimately, it may lead to an explanation for an adverse outcome.

Maternal Clinical Profile and SARS-CoV-2 Testing Results

There were no significant differences in maternal age, gestational age at delivery, and maternal comorbidities profile between groups, thus corroborating that matching variables were adequately paired (p=NS).

In our COVID-19 group, the proportion of symptomatic patients is elevated (9/19, 47.4%). Since patients' recruitment was done at the beginning of the pandemic, almost half of our cases correspond to symptomatic patients. After the universal screening was adopted, asymptomatic patients were also incorporated into the study.

In the literature, pregnant women's outcomes have not been worse when compared to non-pregnant adult individuals. The severity of the COVID-19 seems to be related to existing comorbidities, like hypertension, obesity, among others (50–53), similarly to the general population. Most symptomatic patients in our study group had at least one comorbidity (8/9, 89%), including all the severely ill ones. In comparison, less than half of asymptomatic women had one comorbidity (4/10, 40%), and only one patient without comorbidities presented with mild symptoms (1/7, 15%—PC 20-5869).

Two women died from COVID-19 complications (PC 20-3282 and PC 20-5379). Both died shortly after hospitalization (three and one days after admission, respectively).

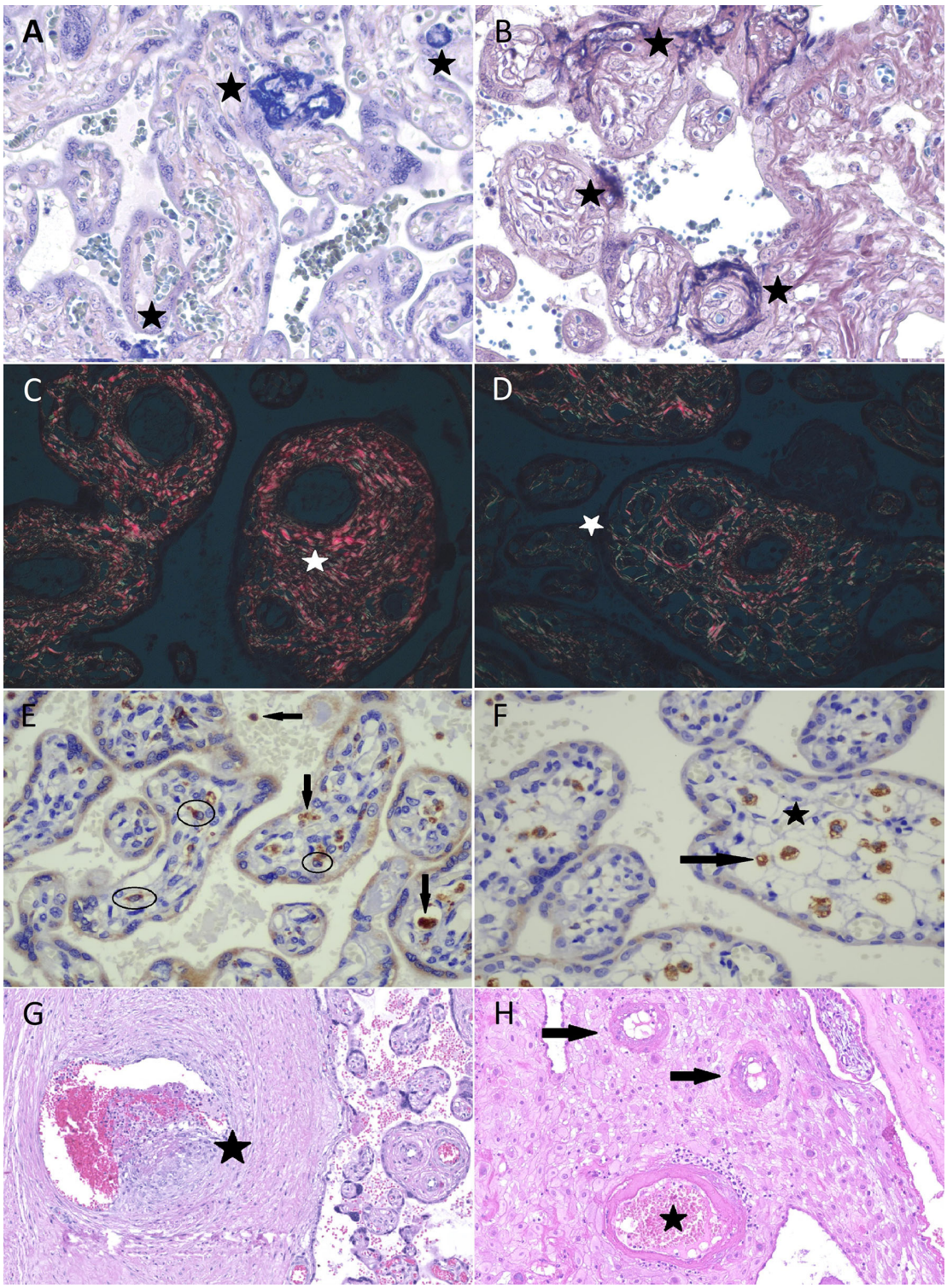

FIGURE 1 | Morphometric and morphological analysis of placental specimens from women infected with SARS-CoV-2 (COVID-19 group) and the Control Group. Fibrin deposition evaluation in COVID-19 group **(A)** and Control group **(B)** in phosphotungstic hematoxylin (star—deep blue amorphous material); both perivillous and intravillous deposition were included. Sirius Red: bright red collagen I **(C)** and green collagen III fibers **(D)** under polarized light. Photomicrography of immunostaining with CD68 (KP1 Clone, Biocare) in COVID-19 group **(E)** and in Control group **(F)**; eligible Hofbauer cells to counting (circled cells and those near the star). Macrophages outside villi and unspecific marking were excluded (arrows). Fetal vascular thrombosis **(G)** and decidual vasculopathy **(H)** in COVID-19 cases.

Newborns Clinical Outcome and SARS-CoV-2 Testing Results

The newborn outcome was directly related to the mother's health status among women with COVID-19. In patients with severe disease, the conceptus health deteriorated after Intensive Care Unit admission in all cases. Thus, not surprisingly, an adverse fetal outcome was more likely to occur in symptomatic patients (7/9, 77.7%) when compared to asymptomatic ones (3/10, 30%). Most of the asymptomatic patients had term deliveries (7/10, 70%) without recorded complications.

When considering patients with comorbidities (12/19, 63.2%), eight gestations ended prematurely (8/12, 66.6%). This proportion is slightly higher than what was observed in the Control group (5/9, 55.5%), even though clinical variables were adequately paired. Compared to the Control group, COVID-19 was also more frequently associated with maternal and infant deaths (although not statistically significant, $p = 0.09$).

Pertaining perinatal transmission of SARS-CoV-2, published reports to date suggest that it occurs, but is considered rare, with less than 2% of neonates with positive results until 24 h of life (54, 55).

Schwartz et al. proposed that positive samples for SARS-CoV-2 RNA collected within the initial 72 h of life can be considered diagnostic of early-onset COVID-19 infection. The probability that the infection resulted from the vertical transmission is even greater if the test is performed until 24 h of life (very early-onset COVID-19 infection). The authors also proposed that in cases where pregnant women and their neonates both tested positive for SARS-CoV-2, transplacental transmission could be confirmed by demonstrating the virus in fetal-derived placental tissue using immunohistochemistry to demonstrate SARS-CoV-2 antigens or RNA *in situ* hybridization to demonstrate viral nucleic acid (56). The World Health Organization recently published a manual with a definition and categorization of the timing of mother-to-child transmission of the SARS-CoV-2. Since various fetal samples are prone to cross-contamination, it preconizes rigorous methodology for sample gathering and strict criteria for establishing congenital transmission. Viral detection should be preferably performed in sterile samples, collected at birth, using nucleic acid detection techniques to confirm transplacental transmission (54).

From newborns' nasopharyngeal swabs and umbilical cord blood specimens tested, five resulted positive and were considered a possible congenital infection, or very early-onset COVID-19 infection, by the criteria above.

In two cases, the newborns were healthy until hospital discharge (PC 20-3744 and 20-5776). Two cases resulted in short-term neonatal deaths (PC 20-3282 and 20-5379); the families did not authorize postmortem evaluation in both cases. None of them exhibited symptoms attributable to SARS-CoV-2 disease.

In the fifth positive infant, a stillborn, SARS-CoV-2 RNA was detected in the umbilical cord blood sample collected immediately after delivery and in the placental FFPE tissue (PC 20-3364). An autopsy was performed, and evaluation of fetal tissues showed mild microglial hyperplasia, mild lymphocytic infiltrate, and edema in skeletal muscle. Other findings were unspecific and probably caused by intrauterine asphyxia. All fetal tissue samples tested negative for viral RNA. The authors (57) previously reported those results.

Morphologic Alterations

Our samples exhibited alterations spanning all major Amsterdam Placental Workshop Group Consensus Statement categories (MVM, FVM, delayed villous maturation, and inflammatory features). Most of them exhibited similar distribution between the two groups, which was expected due to the matching process. However, some results were unexpected.

Although maternal age and comorbidities were adequately matched, COVID-19 group placentas were more likely to show some MVM features when compared to controls, particularly signs of decidual vasculopathy. Decidual vascular mural hypertrophy was more frequently observed in the COVID-19 group (but did not reach statistical significance, $p = 0.09$). Ten patients exhibited this alteration (10/19, 56.6%), the majority without a recorded hypertensive disorder (7/10, 70%). In contrast, three of the five women with decidual vascular mural hypertrophy in the Control group had a hypertensive disorder.

The absence of spiral artery remodeling was significantly more frequent in the COVID-19 group ($p=0,03$). Six patients (6/19, 31.6%) exhibited this alteration combined with decidual vascular fibrinoid necrosis, mainly in women without the hypertensive disorder (5/6, 83.3%). In the Control group, those findings were noticed in only two cases, both in women with hypertension. Decidual arterial thrombosis was observed in only one case that ended with maternal and fetal death (PC 20-5379).

Accelerated villous maturation or increase in syncytial knots was similar in both groups, and those findings are supported by the morphometric analysis results discussed below. On the other hand, villous infarction and distal villous hypoplasia were less frequent in the study group.

Those findings are in consonance with previous reports describing higher decidual arteriopathy rates as a maternal vascular malperfusion feature in SARS-CoV-2 infected women. According to Shanes et al., though at least some of those alterations are thought to be chronic, its precise time of development is not precisely known, and as decidual arteriopathy appears to be more strongly related to COVID-19, it may be originating from a different mechanism (30).

Fetal vascular thrombosis was the FVM feature more frequently observed in our COVID-19 group. It was present in six cases (6/19, 31,5%), a significantly higher rate than in the Control group ($p = 0.03$). Of note, one case corresponded to the mother with Kartagener syndrome that evolved to maternal and neonatal death (PC 20-3282). In the Control group, this finding was detected only in one case, the mother showing no comorbidity (PC 20-5502). The distal lesions in villi indicative of fetal malperfusion were similar between both groups.

The frequency of inflammatory changes was similar between groups. Chronic histiocytic intervillositis, characterized by the accumulation of histocytes in the intervillous space, belongs to this category. In the context of COVID-19, such alteration is not frequently reported, and when present, was associated with

adverse fetal outcomes and or with documented newborn infection by SARS-CoV-2 (30–33, 48, 49).

We identified chronic histiocytic intervillositis in four of our cases (PC 20-3282, PC 20-5379, PC 20-3364, and PC 20-4850). All four mothers with placentas having this finding had a severe COVID-19 course; two of them died. Their infants were prematurely born; three of them were positive for SARS-CoV-2 RNA in nasopharyngeal swab or umbilical cord blood samples. Those three died as well.

In the three cases that resulted in maternal and or infant death (PC 20-3282, PC 20-5379, PC 20-3364), features of MVM, FVM, and inflammatory changes were identified in various combinations. However, only in one case (PC 20-3364), MVM and FVM features were more intense and exhibited a broader distribution throughout the placenta than other specimens from both groups. This patient had a hypertensive disorder as well; because of that, those alterations cannot be attributed entirely to viral injury, even though COVID-19 may have a contributory role in the pathophysiology. Of note, chronic histiocytic intervillositis was observed in all three, two of them categorized as high grade (PC 20-5379, PC 20-3364).

Considering only the two cases that resulted in maternal deaths, placental findings were similar to those observed in the COVID-19 group, except for the presence of chronic histiocytic intervillositis.

Although the frequency of chronic histiocytic intervillositis was similar in COVID-19 and Control groups, this finding was not associated with adverse outcomes in the Control group. Interestingly, in the COVID-19 group, this finding was more frequently observed in placentas of severely ill patients, including those that died from COVID-19 complications, those associated with infant deaths, and with a positive SARS-CoV-2 RNA test in fetal tissues.

Morphometric Alterations and Immunohistochemistry Evaluation

Measurements of villi, such as diameter and perimeter, and counting of sprouts and knots in tertiary villi, aimed to evaluate villi maturity objectively (58, 59). Changes found in the placentas of the COVID-19 group do not seem to be different from those observed in the Control group, as far as maternal age, gestational age, and comorbidities are paired. Those data corroborate the morphological impression that villous maturity retardation or acceleration was not different between our COVID-19 and Control groups.

Fibrosis can be the final event after villi damage, following inflammatory, infectious, or vascular insults, such as described in FVM physiopathology (60). The relative amount of villous fibrosis estimated by evaluation of collagen I and III depositions with Sirius Red histochemical stain showed no difference between groups. There was no difference between groups for global collagen deposition analysis as well, meaning that there was no relative increase in the amount of villous fibrosis in the COVID-19 group.

The amount of fibrin deposited in the villi evaluated by the phosphotungstic hematoxylin histochemical stain could be more accentuated in the COVID-19 group since the difference between groups was borderline. However, such borderline difference between COVID-19 and Control groups was not perceived at the morphological analysis. In the qualitative evaluation, fibrin deposition seemed to be similarly increased in both groups, both in perivillous and intravillous topography.

The number of HC per tertiary villi was also similar between groups. This finding suggests that, at least in perinatally infected women, villous histocytes did not proliferate, and HC hyperplasia may not be as involved in the physiopathology of COVID-19 in the placenta as described for other viruses like Zika virus or HIV (28, 61–63).

In conclusion, pregnant women with symptomatic SARS-CoV-2 infection, particularly with the severe course, are more likely to exhibit an adverse fetal outcome, with slightly more frequent histopathologic findings of maternal and fetal vascular malperfusion, and chronic histiocytic intervillositis. The morphometric changes found in the placentas of the COVID-19 group do not seem to be different from those observed in the Control group, as far as maternal age, gestational age, and comorbidities are paired. Only the deposition of villous fibrin could be more accentuated in the COVID-19 group ($p = 0.08$ borderline). The number of HC/villous evaluated with CD68 immunohistochemistry did not show a difference between both groups.

DATA AVAILABILITY STATEMENT

The original contributions presented in the study are included in the article/supplementary material. Further inquiries can be directed to the corresponding authors.

ETHICS STATEMENT

The studies involving human participants were reviewed and approved by Comitê de Ética em Pesquisa em Seres Humanos do Hospital de Clínicas da Universidade Federal do Paraná. The patients/participants provided their written informed consent to participate in this study.

AUTHOR CONTRIBUTIONS

DP, AO, and VD contributed to collecting SARS-CoV-2 patients' samples and medical records in HNSG. IF and JL contributed to the collection of SARS-CoV-2 patients' samples and medical records in CHC-UFPR. AZ and AF contributed to the RNA extraction and RT-PCR reactions in HNSG. MN, BC, and CD were responsible for the RT-PCR reactions in CHC-UFPR. ES was responsible for selecting the controls and contributed to the immunohistochemistry analysis. PR was responsible for morphological and morphometrical analysis, interpretation of data, and drafted the manuscript. JD and EH contributed to the literature review and morphometrical analysis (Phosphotungstic hematoxylin). FD contributed with morphometrical analysis (Sirius

Red). AP contributed with morphological analysis. SR supported the experiments and contributed to the RT-PCR reactions in CHC-UFPR. CM-S supported the experiments and was responsible for the statistical analysis. NC contributed to the manuscript revision. LN supported the experiments, supervised the project, and was a significant contributor to the manuscript review. All authors contributed to the article and approved the submitted version.

FUNDING

This research was funded by productivity research level 2 of the National Council for Scientific and Technological Development (CNPq) and by Pontificia Universidade Católica do Paraná with resources from BRDE, Banco Regional de Desenvolvimento do Extremo Sul.

ACKNOWLEDGMENTS

The authors express their gratitude to Seigo Nakashima for performing the image acquisition from slides and support with software usage (ZEN Blue Edition and Image-Pro Plus 4) and Maurício de Oliveira and Katiucia Thiara Fantinel Picolli for histochemical and immunohistochemical techniques. Also, to CAPES, CNPq, and BRDE/PUC-PR for financial support.

REFERENCES

1. World Health Organization. *Coronavirus (COVID-19) Dashboard* (2021). Available at: https://covid19.who.int/ (Accessed April 26, 2021).
2. Petrilli CM, Jones SA, Yang J, Rajagopalan H, O'Donnell L, Chernyak Y, et al. Factors Associated With Hospital Admission and Critical Illness Among 5279 People With Coronavirus Disease 2019 in New York City: Prospective Cohort Study. *BMJ* (2020) 369:m1966. doi: 10.1136/bmj.m1966
3. Docherty AB, Harrison EM, Green CA, Hardwick HE, Pius R, Norman L, et al. ISARIC4C Investigators. Features of 20 133 UK Patients in Hospital With covid-19 Using the ISARIC Who Clinical Characterization Protocol: Prospective Observational Cohort Study. *BMJ* (2020) 369:m1985. doi: 10.1136/bmj.m1985
4. Zhu H, Wang L, Fang C, Peng S, Zhang L, Chang G, et al. Clinical Analysis of 10 Neonates Born to Mothers With 2019-nCoV Pneumonia. *Transl Pediatr* (2020) 9(1):51–60. doi: 10.21037/tp.2020.02.06
5. Zeng H, Xu C, Fan J, Tang Y, Deng Q, Zhang W, et al. Antibodies in Infants Born to Mothers With COVID-19 Pneumonia. *JAMA* (2020) 323(18):1848–9. doi: 10.1001/jama.2020.4861
6. Dong L, Tian J, He S, Zhu C, Wang J, Liu C, et al. Possible Vertical Transmission of SARS-CoV-2 From an Infected Mother to Her Newborn. *JAMA* (2020) 323(18):1846–8. doi: 10.1001/jama.2020.4621
7. Alzamora MC, Paredes T, Caceres D, Webb CM, Valdez LM, La Rosa M. Severe COVID-19 During Pregnancy and Possible Vertical Transmission. *Am J Perinatol* (2020) 37(8):861–5. doi: 10.1055/s-0040-1710050
8. Zeng L, Xia S, Yuan W, Yan K, Xiao F, Shao J, et al. Neonatal Early-Onset Infection With SARS-CoV-2 in 33 Neonates Born to Mothers With COVID-19 in Wuhan, China. *JAMA Pediatr* (2020) 174(7):722–5. doi: 10.1001/jamapediatrics.2020.0878
9. Hecht JL, Quade B, Deshpande V, Mino-Kenudson M, Ting DT, Desai N, et al. SARS-CoV-2 can Infect the Placenta and is Not Associated With Specific Placental Histopathology: A Series of 19 Placentas From COVID-19-positive Mothers. *Mod Pathol* (2020) 33(11):2092–103. doi: 10.1038/s41379-020-0639-4
10. Mulvey JJ, Magro CM, Ma LX, Nuovo GJ, Baergen RN. Analysis of Complement Deposition and Viral RNA in Placentas of COVID-19 Patients. *Ann Diagn Pathol* (2020) 46:151530. doi: 10.1016/j.anndiagpath.2020.151530
11. Smithgall MC, Liu-Jarin X, Hamele-Bena D, Cimic A, Mourad M, Debelenko L, et al. Third-Trimester Placentas of Severe Acute Respiratory Syndrome Coronavirus 2 (SARS-CoV-2)-positive Women: Histomorphology, Including Viral Immunohistochemistry and in-Situ Hybridization. *Histopathology* (2020) 77(6):994–9. doi: 10.1111/his.14215
12. Penfield CA, Brubaker SG, Limaye MA, Lighter J, Ratner AJ, Thomas KM, et al. Detection of Severe Acute Respiratory Syndrome Coronavirus 2 in Placental and Fetal Membrane Samples. *Am J Obstet Gynecol MFM* (2020) 2(3):100133. doi: 10.1016/j.ajogmf.2020.100133
13. Patanè L, Morotti D, Giunta MR, Sigismondi C, Piccoli MG, Frigerio L, et al. Vertical Transmission of Coronavirus Disease 2019: Severe Acute Respiratory Syndrome Coronavirus 2 RNA on the Fetal Side of the Placenta in Pregnancies With Coronavirus Disease 2019-Positive Mothers and Neonates at Birth. *Am J Obstet Gynecol MFM* (2020) 2(3):100145. doi: 10.1016/j.ajogmf.2020.100145
14. Lamouroux A, Attie-Bitach T, Martinovic J, Leruez-Ville M, Ville Y. Evidence for and Against Vertical Transmission for Severe Acute Respiratory Syndrome Coronavirus 2. *Am J Obstet Gynecol* (2020) 223(1):91.e1–4. doi: 10.1016/j.ajog.2020.04.039
15. Joudi N, Henkel A, Lock WS, Lyell D. Preeclampsia Treatment in Severe Acute Respiratory Syndrome Coronavirus 2. *Am J Obstet Gynecol MFM* (2020) 2(3):100146. doi: 10.1016/j.ajogmf.2020.100146
16. Gidlöf S, Savchenko J, Brune T, Josefsson H. COVID-19 in Pregnancy With Comorbidities: More Liberal Testing Strategy is Needed. *Acta Obstet Gynecol Scand* (2020) 99(7):948–9. doi: 10.1111/aogs
17. Lokken EM, Walker CL, Delaney S, Kachikis A, Kretzer NM, Erickson A, et al. Clinical Characteristics of 46 Pregnant Women With a Severe Acute Respiratory Syndrome Coronavirus 2 Infection in Washington State. *Am J Obstet Gynecol* (2020) 223(6):911.e1–911.e14. doi: 10.1016/j.ajog.2020.05.031
18. Pierce-Williams RAM, Burd J, Felder L, Khoury R, Bernstein PS, Avila K, et al. Clinical Course of Severe and Critical Coronavirus Disease 2019 in Hospitalized Pregnancies: A United States Cohort Study. *Am J Obstet Gynecol MFM* (2020) 2(3):100134. doi: 10.1016/j.ajogmf.2020.100134
19. Kirtsman M, Diambomba Y, Poutanen SM, Malinowski A, Vlachodimitropoulou E, Parks W, et al. Probable Congenital SARS-CoV-2 Infection in a Neonate Born to a Woman With Active SARS-CoV-2 Infection. *CMAJ* (2020) 192(24):E647–50. doi: 10.1503/cmaj.200821
20. Vivanti AJ, Vauloup-Fellous C, Prevot S, Zupan V, Suffee C, Do Cao J, et al. Transplacental Transmission of SARS-CoV-2 Infection. *Nat Commun* (2020) 11(1):3572. doi: 10.1038/s41467-020-17436-6
21. Sisman J, Jaleel MA, Moreno W, Rajaram V, Collins RRJ, Savani RC, et al. Intrauterine Transmission of SARS-COV-2 Infection in a Preterm Infant. *Pediatr Infect Dis J* (2020) 39(9):e265–7. doi: 10.1097/INF.0000000000002815
22. Baud D, Greub G, Favre G, Gengler C, Jaton K, Dubruc E, et al. Second-Trimester Miscarriage in a Pregnant Woman With SARS-CoV-2 Infection. *JAMA* (2020) 323(21):2198–200. doi: 10.1001/jama.2020.7233
23. Walker KF, O'Donoghue K, Grace N, Dorling J, Comeau JL, Li W, et al. Maternal Transmission of SARS-COV-2 to the Neonate, and Possible Routes for Such Transmission: A Systematic Review and Critical Analysis. *BJOG* (2020) 127(11):1324–36. doi: 10.1111/1471-0528.16362
24. Schwartz DA, Thomas KM. Characterizing COVID-19 Maternal-Fetal Transmission and Placental Infection Using Comprehensive Molecular Pathology. *EBioMedicine* (2020) 60:102983. doi: 10.1016/j.ebiom.2020.102983
25. Raschetti R, Vivanti AJ, Vauloup-Fellous C, Loi B, Benachi A, De Luca D. Synthesis and Systematic Review of Reported Neonatal SARS-CoV-2 Infections. *Nat Commun* (2020) 11(1):5164. doi: 10.1038/s41467-020-18982-9
26. Benirschke B, Burton GJ, Baergen RN. *Pathology of the Human Placenta. 6th ed.* Berlin, Heidelberg: Springer (2012). doi: 10.1007/978-3-642-23941-0
27. Garcia AG, Fonseca EF, Marques RL, Lobato YY. Placental Morphology in Cytomegalovirus Infection. *Placenta* (1989) 10(1):1–18. doi: 10.1016/0143-4004(89)90002-7

28. de Noronha L, Zanluca C, Burger M, Suzukawa AA, Azevedo M, Rebutini PZ, et al. Zika Virus Infection at Different Pregnancy Stages: Anatomopathological Findings, Target Cells and Viral Persistence in Placental Tissues. *Front Microbiol* (2018) 9:2266. doi: 10.3389/fmicb.2018.02266
29. Ribeiro CF, Silami VG, Brasil P, Nogueira RM. Sickle-Cell Erythrocytes in the Placentas of Dengue-Infected Women. *Int J Infect Dis* (2012) 16(1):e72. doi: 10.1016/j.ijid.2011.09.005
30. Shanes ED, Mithal LB, Otero S, Azad HA, Miller ES, Goldstein JA. Placental Pathology in COVID-19. *Am J Clin Pathol* (2020) 154(1):23–32. doi: 10.1093/ajcp/aqaa089
31. Baergen RN, Heller DS. Placental Pathology in Covid-19 Positive Mothers: Preliminary Findings. *Pediatr Dev Pathol* (2020) 23(3):177–80. doi: 10.1177/1093526620925569
32. Hosier H, Farhadian SF, Morotti RA, Deshmukh U, Lu-Culligan A, Campbell KH, et al. SARS-CoV-2 Infection of the Placenta. *J Clin Invest* (2020) 130 (9):4947–53. doi: 10.1172/JCI139569
33. Gulersen M, Prasannan L, Tam Tam H, Metz CN, Rochelson B, Meirowitz N, et al. Histopathologic Evaluation of Placentas After Diagnosis of Maternal Severe Acute Respiratory Syndrome Coronavirus 2 Infection. *Am J Obstet Gynecol MFM* (2020) 2(4):100211. doi: 10.1016/j.ajogmf.2020.100211
34. Smithgall MC, Liu-Jarin X, Hamele-Bena D, Cimic A, Mourad M, Debelenko L, et al. Third-Trimester Placentas of Severe Acute Respiratory Syndrome Coronavirus 2 (SARS-CoV-2)-positive Women: Histomorphology, Including Viral Immunohistochemistry and in-Situ Hybridization. *Histopathology* (2020) 77(6):994–9. doi: 10.1111/his.14215
35. Khong TY, Mooney EE, Ariel I, Balmus NC, Boyd TK, Brundler MA, et al. Sampling and Definitions of Placental Lesions: Amsterdam Placental Workshop Group Consensus Statement. *Arch Pathol Lab Med* (2016) 140 (7):698–713. doi: 10.5858/arpa.2015-0225-CC
36. Malaquias MAS, Oyama LA, Jericó PC, Costa I, Padilha G, Nagashima S, et al. Effects of Mesenchymal Stromal Cells Play a Role the Oxidant/Antioxidant Balance in a Murine Model of Asthma. *Allergol Immunopathol* (2018) 46 (2):136–43. doi: 10.1016/j.aller.2017.06.003
37. Fajgenbaum DC, June CH. Cytokine Storm. *N Engl J Med* (2020) 383 (23):2255–73. doi: 10.1056/NEJMra2026131
38. Nagashima S, Mendes MC, Martins APC, Borges NH, Godoy TM, Miggiolaro AFRS, et al. Endothelial Dysfunction and Thrombosis in Patients With COVID-19—Brief Report. *Arterioscler Thromb Vasc Biol* (2020) 40:2404–7. doi: 10.1161/atvbaha.120.314860
39. Lippi G, Plebani M. Laboratory Abnormalities in Patients With COVID-2019 Infection. *Clin Chem Lab Med* (2020) 58(7):1131–4. doi: 10.1515/cclm-2020-0198
40. Lippi G, Plebani M, Henry BM. Thrombocytopenia is Associated With Severe Coronavirus Disease 2019 (COVID-19) Infections: A Meta-Analysis. *Clin Chim Acta* (2020) 506:145–8. doi: 10.1016/j.cca.2020.03.022
41. Tang N, Li D, Wang X, Sun Z. Abnormal Coagulation Parameters are Associated With Poor Prognosis in Patients With Novel Coronavirus Pneumonia. *J Thromb Haemost* (2020) 18(4):844–7. doi: 10.1111/jth.14768
42. Benhamou D, Keita H, Ducloy-Bouthors ASCARO Working Group. Coagulation Changes and Thromboembolic Risk in COVID-19 Obstetric Patients. *Anaesth Crit Care Pain Med* (2020) 39(3):351–3. doi: 10.1016/j.accpm.2020.05.003
43. Ribes A, Vardon-Bounes F, Mémier V, Poette M, Au-Duong J, Garcia C, et al. Thromboembolic Events and Covid-19. *Adv Biol Regul* (2020) 77:100735. doi: 10.1016/j.jbior.2020.100735
44. Klok FA, Kruip MJHA, van der Meer NJM, Arbous MS, Gommers D, Kant KM, et al. Confirmation of the High Cumulative Incidence of Thrombotic Complications in Critically Ill ICU Patients With COVID-19. *Thromb Res* (2020) 191:148–50. doi: 10.1016/j.thromres.2020.04.041
45. Zhang Y, Cao W, Xiao M, Li YJ, Yang Y, Zhao J, et al. [Clinical and Coagulation Characteristics of 7 Patients With Critical COVID-2019 Pneumonia and Acro-Ischemia]. *Zhonghua Xue Ye Xue Za Zhi* (2020) 41 (0):E006. doi: 10.3760/cma.j.issn.0253-2727.2020.0006
46. Menter T, Mertz KD, Jiang S, Chen H, Monod C, Tzankov A, et al. Placental Pathology Findings During and After SARS-CoV-2 Infection: Features of Villitis and Malperfusion. *Pathobiology* (2021) 88(1):69–77. doi: 10.1159/000511324
47. Levitan D, London V, McLaren RA, Mann JD, Cheng K, Silver M. Histologic and Immunohistochemical Evaluation of 65 Placentas From Women With Polymerase Chain Reaction-Proven Severe Acute Respiratory Syndrome Coronavirus 2 (SARS-CoV-2) Infection. *Arch Pathol Lab Med* (2021). doi: 10.5858/arpa.2020-0793-SA
48. Schwartz DA, Morotti D. Placental Pathology of COVID-19 With and Without Fetal and Neonatal Infection: Trophoblast Necrosis and Chronic Histiocytic Intervillositis as Risk Factors for Transplacental Transmission of SARS-CoV-2. *Viruses* (2020) 12(11):1308. doi: 10.3390/v12111308
49. Schwartz DA, Baldewijns M, Benachi A, Bugatti M, Collins RRJ, De Luca D, et al. Chronic Histiocytic Intervillositis With Trophoblast Necrosis are Risk Factors Associated With Placental Infection From Coronavirus Disease 2019 (COVID-19) and Intrauterine Maternal-Fetal Severe Acute Respiratory Syndrome Coronavirus 2 (SARS-CoV-2) Transmission in Liveborn and Stillborn Infants. *Arch Pathol Lab Med* (2020) 145(5):517–28. doi: 10.5858/arpa.2020-0771-SA
50. Knight M, Bunch K, Vousden N, Morris E, Simpson N, Gale C, et al. UK Obstetric Surveillance System SARS-CoV-2 Infection in Pregnancy Collaborative Group. Characteristics and Outcomes of Pregnant Women Admitted to Hospital With Confirmed SARS-CoV-2 Infection in UK: National Population-Based Cohort Study. *BMJ* (2020) 369:m2107. doi: 10.1136/bmj.m2107
51. Breslin N, Baptiste C, Gyamfi-Bannerman C, Miller R, Martinez R, Bernstein K, et al. Coronavirus Disease 2019 Infection Among Asymptomatic and Symptomatic Pregnant Women: Two Weeks of Confirmed Presentations to an Affiliated Pair of New York City Hospitals. *Am J Obstet Gynecol MFM* (2020) 2(2):100118. doi: 10.1016/j.ajogmf.2020.100118
52. Blitz MJ, Grünebaum A, Tekbali A, Bornstein E, Rochelson B, Nimaroff M, et al. Intensive Care Unit Admissions for Pregnant and Non-Pregnant Women With Coronavirus Disease 2019. *Am J Obstet Gynecol* (2020) 223 (2):290–1. doi: 10.1016/j.ajog.2020.05.004
53. Kayem G, Lecarpentier E, Deruelle P, Bretelle F, Azria E, Blanc J, et al. A Snapshot of the Covid-19 Pandemic Among Pregnant Women in France. *J Gynecol Obstet Hum Reprod* (2020) 49(7):101826. doi: 10.1016/j.jogoh.2020.101826
54. World Health Organization. *Definition and Categorization of the Timing of Mother-to-Child Transmission of SARS-CoV-2* (2021). Available at: https://www.who.int/publications/i/item/WHO-2019-nCoV-mother-to-child-transmission-2021 (Accessed April 26, 2021).
55. Egloff C, Vauloup-Fellous C, Picone O, Mandelbrot L, Roques P. Evidence and Possible Mechanisms of Rare Maternal-Fetal Transmission of SARS-CoV-2. *J Clin Virol* (2020) 128:104447. doi: 10.1016/j.jcv.2020.104447
56. Schwartz DA, Morotti D, Beigi B, Moshfegh F, Zafaranloo N, Patanè L. Confirming Vertical Fetal Infection With Coronavirus Disease 2019: Neonatal and Pathology Criteria for Early Onset and Transplacental Transmission of Severe Acute Respiratory Syndrome Coronavirus 2 From Infected Pregnant Mothers. *Arch Pathol Lab Med* (2020) 144(12):1451–6. doi: 10.5858/arpa.2020-0442-SA
57. Stonoga ES, de Almeida Lanzoni L, Rebutini P, Permegiani de Oliveira A, Chiste J, Fugaça C, et al. Intrauterine Transmission of SARS-CoV-2. *Emerg Infect Dis* (2021) 27(2):638–41. doi: 10.3201/eid2702.203824
58. Jackson MR, Mayhew TM, Boyd PA. Quantitative Description of the Elaboration and Maturation of Villi From 10 Weeks of Gestation to Term. *Placenta* (1992) 13(4):357–70. doi: 10.1016/0143-4004(92)90060-7
59. Vangrieken P, Vanterpool SF, van Schooten FJ, Al-Nasiry S, Andriessen P, Degreef E, et al. Histological Villous Maturation in Placentas of Complicated Pregnancies. *Histol Histopathol* (2020) 35(8):849–62. doi: 10.14670/HH-18-205
60. Redline RW, Ravishankar S. Fetal Vascular Malperfusion, An Update. *APMIS* (2018) 126(7):561–9. doi: 10.1111/apm.12849
61. Schwartz DA. Viral Infection, Proliferation, and Hyperplasia of Hofbauer Cells and Absence of Inflammation Characterize the Placental Pathology of Fetuses With Congenital Zika Virus Infection. *Arch Gynecol Obstet* (2017) 295 (6):1361–8. doi: 10.1007/s00404-017-4361-5
62. Simoni MK, Jurado KA, Abrahams VM, Fikrig E, Guller S. Zika Virus Infection of Hofbauer Cells. *Am J Reprod Immunol* (2017) 77(2):10.1111/aji.12613. doi: 10.1111/aji.12613

63. Rosenberg AZ, Yu W, Hill DA, Reyes CA, Schwartz DA. Placental Pathology of Zika Virus: Viral Infection of the Placenta Induces Villous Stromal Macrophage (Hofbauer Cell) Proliferation and Hyperplasia. *Arch Pathol Lab Med* (2017) 141(1):43–8. doi: 10.5858/arpa.2016-0401-OA

Conflict of Interest: The authors declare that the research was conducted in the absence of any commercial or financial relationships that could be construed as a potential conflict of interest.

7 CONCLUSÃO

Considerando os objetivos propostos para o desenvolvimento deste trabalho, verificou-se que placentas de mulheres infectadas pelo SARS-CoV-2 exibiram alterações histológicas ao exame anatomopatológico realizado em coloração de rotina (HE). Tais alterações incluíam todo o espectro de lesões definidas no Consenso de Amsterdam (90), destacando-se os achados de má perfusão vascular materna, má perfusão vascular fetal e alterações inflamatórias. Todavia, apenas os parâmetros de ausência de remodelamento de artérias espiraladas e trombose de vasos fetais foram significativamente mais frequentes quando as placentas do grupo estudo foram comparadas àquelas do grupo controle.

A infecção pelo SARS-CoV-2 não esteve associada com alterações placentárias maturativas em comparação ao grupo controle, avaliadas por meio da aferição do perímetro e diâmetros das vilosidades e da contagem de brotos e nós sinciciais, utilizando técnicas de morfometria em coloração de rotina (HE).

A infecção pelo SARS-CoV-2 também não esteve associada com a presença de marcadores de dano vilositário, cuja expressão morfológica é a fibrose estromal e a deposição de fibrina, em comparação com o grupo controle, na avaliação morfométrica em colorações especiais (*sirius red* e hematoxilina fosfotúngstica, respectivamente).

Tendo em vista a correlação entre os achados morfológicos com o quadro clínico das gestantes infectadas pelo SARS-CoV-2, observou-se que:

a) gestantes com COVID-19 moderada a grave exibiram mais frequentemente alterações histológicas placentárias quando comparadas às gestantes infectas pelo SARS-CoV-2, porém assintomáticas, incluindo achados de má perfusão vascular materna, má perfusão vascular fetal e alterações inflamatórias, conforme definições constantes no Consenso de Amsterdam (90);

b) gestantes com COVID-19 moderada a grave exibiram mais frequentemente um desfecho fetal adverso, tal como parto prematuro e óbito perinatal, quando comparadas às gestantes infectas pelo SARS-CoV-2, porém assintomáticas;

c) conceptos de gestantes com COVID-19 moderada a grave exibiram mais frequentemente teste positivo para SARS-CoV-2 no período perinatal quando comparados a conceptos de gestantes infectas pelo SARS-CoV-2, porém assintomáticas;

d) gestantes com COVID-19 moderada a grave exibiram mais frequentemente uma ou mais comorbidades, tais como hipertensão arterial, diabetes e obesidade, quando comparadas às gestantes infectas pelo SARS-CoV-2, porém assintomáticas.

8 CONSIDERAÇÕES FINAIS

O presente trabalho foi executado no início da pandemia de COVID-19, em um momento em que os mecanismos de transmissão do SARS-CoV-2, sua virulência, período de incubação e perfil de sintomas, por exemplo, não estavam bem definidos. Somando-se a isso as altas taxas de mortalidade inicialmente documentadas (112), não é surpresa que a epidemia tenha gerado tamanha inquietação.

Uma das muitas preocupações naquele momento era como a infecção afetaria as gestantes e seus conceptos. Há poucos anos, testemunhou-se os efeitos da infecção pelo vírus ZIKA nessa população. Há poucas décadas, observou-se os efeitos de doenças respiratórias graves por outros coronavírus, que resultaram em elevada mortalidade materna.

Ao selecionar as participantes do grupo estudo no início da pandemia, obteve-se uma proporção de indivíduos sintomáticos maior do que na população geral; cerca de metade das gestantes infectadas pelo SARS-CoV-2 exibiam sintomas. Nesse subgrupo, particularmente naquelas com COVID-19 moderada a grave, foram frequentes as alterações histopatológicas na placenta. Todavia, nesse subgrupo também estavam concentradas as mulheres com comorbidades. Na comparação com o grupo controle, que contemplava mulheres com as mesmas comorbidades, apenas dois parâmetros morfológicos diferiram significativamente. Isso aponta para o fato de que as comorbidades exibidas pelas gestantes tiveram, provavelmente, mais impacto sobre as alterações placentárias do que a própria infecção viral. Ressalta-se que os casos analisados consistiam em mulheres que foram infectadas em até 15 dias antes do parto. Desse modo, possíveis efeitos crônicos associados à infecção viral não seriam reconhecidos no presente estudo.

Embora não tenha atingido significância estatística na comparação entre grupos, uma alteração exibiu distribuição peculiar no grupo estudo e merece destaque. Trata-se da vilosite/intervilosite histiocitária, observada mais frequentemente em ges-

tantes com COVID-19 moderada a grave, e cuja presença esteve associada a testes positivos para SARS-CoV-2 em bebês. Esse achado tem sido apontado como relevante (101, 102) uma vez que sugere um possível mecanismo de transmissão transplacentária. A infecção e destruição do revestimento sinciotrofoblástico permitiria ao vírus atingir a circulação fetal, sendo a intervilosite a expressão morfológica dessa alteração.

Ainda, analisando-se sob outra perspectiva, a presença de comorbidades esteve associada a uma maior suscetibilidade para desenvolver sintomas moderados a graves de COVID-19. Nessas mulheres, os desfechos fetais adversos foram também mais frequentes. É cabível, nesse contexto, considerar a necessidade de um acompanhamento obstétrico mais estrito, seja pela orientação quanto às medidas de prevenção, seja pela avaliação periódica em intervalos menores, ou pela possibilidade de intervenção precoce em casos de extrema gravidade.

Por fim, a infecção tardia pelo SARS-CoV-2, no terceiro trimestre, não parece interferir na evolução da gestação em mulheres que não tenham comorbidades, sejam assintomáticas ou exibam apenas sintomas leves de COVID-19 (Figura 12).

Figura 12 – Súmula gráfica da metodologia e dos principais resultados.

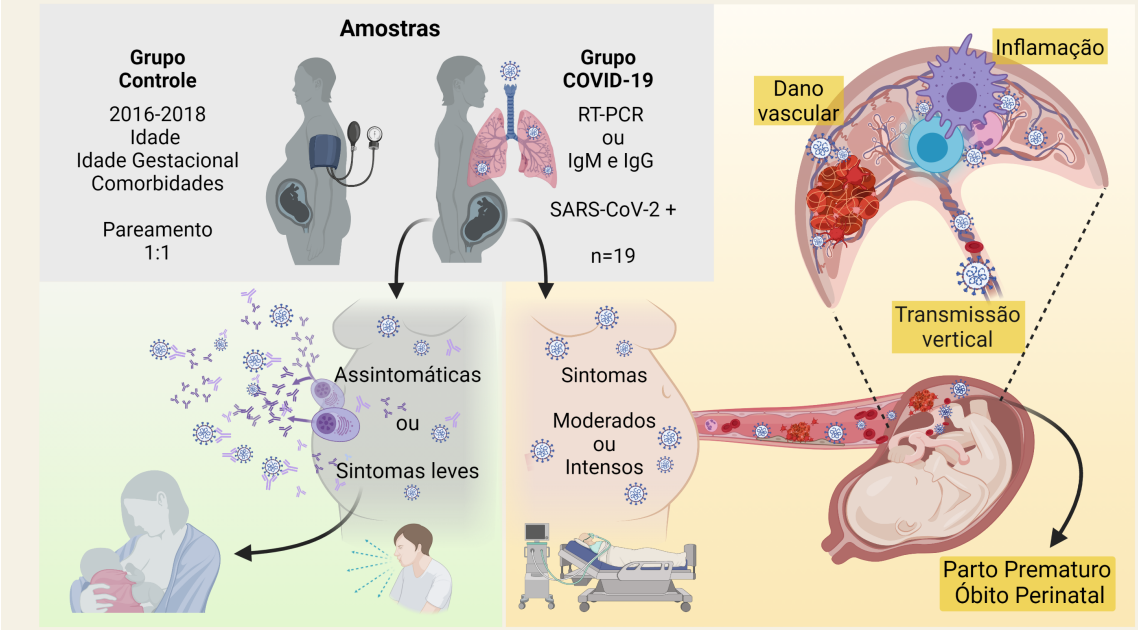

Fonte: A autora, 2021. Confeccionado com BioRender.com

8.1 SUGESTÕES PARA TRABALHOS FUTUROS

Embora os resultados publicados e discutidos previamente sejam relevantes, faz-se necessário continuar a estudar os efeitos da infecção pelo SARS-CoV-2 na placenta e, portanto, seu impacto para a gestação.

É pertinente ampliar a população de estudo para incorporar gestantes infectadas durante as fases iniciais da gestação, de modo a avaliar o impacto imediato da infecção viral nesse contexto, assim como a possibilidade de persistência do vírus na placenta e seus efeitos no longo prazo.

Tendo-se em vista a descrição de transmissão transplacentária do SARS-CoV-2, sugere-se documentar a presença e localização de antígenos virais em tecido placentário, de modo a contribuir para o entendimento dos possíveis mecanismos de transmissão do vírus, o que pode ser realizado por técnica de imuno-histoquímica, por exemplo.

Por fim, considerando os mecanismos propostos na literatura para explicar a fisiopatologia da COVID-19, que incluem dano endotelial, assim como os achados histológicos placentários relatados neste trabalho, que englobam lesões de natureza vascular, sugere-se avaliar marcadores de dano endotelial na placenta.

REFERÊNCIAS

1 WORLD HEALTH ORGANIZATION. **Coronavirus (COVID-19) Dashboard**. 2022. Disponível em: <https://covid19.who.int/>. Acesso em: fevereiro de 2022.

2 WORLD HEALTH ORGANIZATION. **Coronavirus (COVID-19) Dashboard**. 2022. Disponível em: <https://covid19.who.int/region/amro/country/br>. Acesso em: fevereiro de 2022.

3 PETRILLI, C. M.; JONES, S. A.; YANG, J.; RAJAGOPALAN, H.; O'DONNELL, L.; CHERNYAK, Y.; et al. Factors associated with hospital admission and critical illness among 5279 people with coronavirus disease 2019 in New York City: Prospective cohort study. **British Medical Journal**, v. 369, 2020.

4 DOCHERTY, A. B.; HARRISON, E. M.; GREEN, C. A.; HARDWICK, H. E.; PIUS, R.; NORMAN, L.; et al. Features of 20133 UK patients in hospital with COVID-19 using the ISARIC WHO Clinical Characterisation Protocol: prospective observational cohort study. **British Medical Journal**, v. 369, 2020.

5 ZHU, H.; WANG, L.; FANG, C.; PENG, S.; ZHANG, L.; CHANG, G.; et al. Clinical analysis of 10 neonates born to mothers with 2019-nCoV pneumonia. **Translational Pediatrics**, v. 9, n. 1, p. 51–60, 2020.

6 ZENG, H.; XU, C.; FAN, J.; TANG, Y.; DENG, Q.; ZHANG, W.; LONG, X. Antibodies in infants born to mothers with COVID-19 pneumonia. **JAMA**, v. 323, n. 18, p. 1848–1849, 2020.

7 DONG, L.; TIAN, J.; HE, S.; ZHU, C.; WANG, J.; LIU, C.; YANG, J. Possible vertical transmission of SARS-CoV-2 from an infected mother to her newborn. **JAMA**, v. 323, n. 18, p. 1846–1848, 05 2020.

8 ZENG, L.; XIA, S.; YUAN, W.; YAN, K.; XIAO, F.; SHAO, J.; ZHOU, W. Neonatal early-onset infection with SARS-CoV-2 in 33 neonates born to mothers with COVID-19 in Wuhan, China. **JAMA Pediatrics**, v. 174, n. 7, p. 722–725, 2020.

9 JOUDI, N.; HENKEL, A.; LOCK, W. S.; LYELL, D. Preeclampsia treatment in severe acute respiratory syndrome coronavirus 2. **American Journal of Obstetrics and Gynecology MFM**, v. 2, n. 3, p. 100146, 2020.

10 GIDLÖF, S.; SAVCHENKO, J.; BRUNE, T.; JOSEFSSON, H. COVID-19 in pregnancy with comorbidities: More liberal testing strategy is needed. **Acta Obstetricia et Gynecologica Scandinavica**, v. 99, n. 7, p. 948–949, 2020.

11 PIERCE-WILLIAMS, R. A. M.; BURD, J.; FELDER, L.; KHALIFEH, A.; ANDERSON, K.; BERGHELLA, V.; et al. Clinical course of severe and critical coronavirus disease 2019 in hospitalized pregnancies: a United States cohort

study. **American Journal of Obstetrics and Gynecology MFM**, v. 2, n. 2, p. 100134, 2020.

12 LOKKEN, E. M.; WALKER, C. L.; DELANEY, S.; LACOURSE, S. M.; DEUTSCH, G.; WALDORF, K. M. A.; et al. Disease severity, pregnancy outcomes, and maternal deaths among pregnant patients with severe acute respiratory syndrome coronavirus 2 infection in Washington State. **American Journal of Obstetrics and Gynecology**, v. 223, n. 6, 2020.

13 HONEIN, M. A.; DAWSON, A. L.; PETERSEN, E. E.; JONES, A. M.; LEE, E. H.; YAZDY, M. M.; AHMAD, N.; MACDONALD, J.; EVERT, N.; BINGHAM, A.; ELLINGTON, S. R.; SHAPIRO-MENDOZA, C. K.; ODUYEBO, T.; FINE, A. D.; BROWN, C. M.; SOMMER, J. N.; GUPTA, J.; CAVICCHIA, P.; SLAVINSKI, S.; WHITE, J. L.; OWEN, S. M.; PETERSEN, L. R.; BOYLE, C.; MEANEY-DELMAN, D.; JAMIESON, D. J. Birth defects among fetuses and infants of us women with evidence of possible Zika virus infection during pregnancy. **JAMA**, v. 317, n. 1, p. 59–68, 2017.

14 ARAGAO, M. F. V. V.; HOLANDA, A. C.; BRAINER-LIMA, A. M.; PETRIBU, N. C. L.; CASTILLO, M.; LINDEN, V. van der; SERPA, S. C.; TENÓRIO, A. G.; TRAVASSOS, P. T. C.; CORDEIRO, M. T.; SARTESCHI, C.; VALENCA, M. M.; COSTELLO, A. Nonmicrocephalic infants with congenital Zika syndrome suspected only after neuroimaging evaluation compared with those with microcephaly at birth and postnatally: How large is the Zika virus "iceberg"? **American Journal of Neuroradiology**, v. 38, n. 7, p. 1427–1434, 2017.

15 BENIRSCHKE, K.; BURTON, G. J.; BAERGEN, R. N. **Pathology of the Human Placenta**. 6. ed. Heidelberg: Springer, 2012.

16 GARCIA, A. G. P.; MARQUES, R. L. S.; LOBATO, Y. Y.; FONSECA, M. E. F.; WIGG, M. dutra. Placental pathology in congenital rubella. **Placenta**, v. 6, n. 4, p. 281–295, 1985.

17 RIBEIRO, C. F.; SILAMI, V. G.; BRASIL, P.; NOGUEIRA, R. M. Sickle-cell erythrocytes in the placentas of dengue-infected women. **International Journal of Infectious Disease**, v. 16, n. 1, 2012.

18 WORLD HEALTH ORGANIZATION. **Coronavirus (COVID-19) Question and answers – What it is?** 2021. Disponível em: <https://www.who.int/emergencies/diseases/novel-coronavirus-2019/question-and-answers-hub/q-a-detail/coronavirus-disease-covid-19>. Acesso em: junho de 2021.

19 WORLD HEALTH ORGANIZATION. **Coronavirus disease 2019 (COVID-19) Situation Report – 71 (March-2020)**. 2020. Disponível em: <https://www.who.int/docs/default-source/coronaviruse/situation-reports/20200331-sitrep-71-covid-19.pdf?sfvrsn=4360e92b_8>. Acesso em: junho de 2021.

20 WORLD HEALTH ORGANIZATION. **Coronavirus (COVID-19) Question and answers – How is it transmitted?** 2021. Disponível em: <https://www.who.int/emergencies/diseases/novel-coronavirus-2019/question-and-

answers-hub/q-a-detail/coronavirus-disease-covid-19-how-is-it>. Acesso em: junho de 2021.

21 WORLD HEALTH ORGANIZATION. **Coronavirus (COVID-19) Question and answers – Symptoms**. 2021. Disponível em: <https://www.who.int/emergencies/diseases/novel-coronavirus-2019/question-and-answers-hub/q-a-detail/coronavirus-disease-covid-19>. Acesso em: junho de 2021.

22 JOHNS HOPKINS ABX GUIDE. **Coronavirus COVID-19 (SARS-CoV-2)**. 2021. Disponível em: <https://www.hopkinsguides.com/hopkins/view/Johns_Hopkins_ABX_Guide/540747/all/Coronavirus_COVID_19__SARS_CoV_2_>. Acesso em: junho de 2021.

23 WORLD HEALTH ORGANIZATION. **Coronavirus (COVID-19) Question and answers – Variants**. 2022. Disponível em: <https://www.who.int/en/activities/tracking-SARS-CoV-2-variants/>. Acesso em: fevereiro 2022.

24 GATTA, A. N. D.; RIZZO, R.; PILU, G.; SIMONAZZI, G. Coronavirus disease 2019 during pregnancy: a systematic review of reported cases. **American Journal of Obstetrics & Gynecology**, v. 223, n. 1, p. 36–41, 2020.

25 GUAN, W.; NI, Z.; HU, Y.; LIANG, W.; OU, C.; HE, J.; et al. Clinical characteristics of coronavirus disease 2019 in China. **New England Journal of Medicine**, v. 382, n. 18, p. 1708–1720, 2020.

26 PAN, L.; MU, M.; YANG, P.; SUN, Y.; WANG, R.; YAN, J.; et al. Clinical characteristics of COVID-19 patients with digestive symptoms in Hubei, China: A descriptive, cross-sectional, multicenter study. **American Journal of Gastroenterology**, v. 115, n. 5, p. 766–773, 2020.

27 MATSUYAMA, S.; NAGATA, N.; SHIRATO, K.; KAWASE, M.; TAKEDA, M.; TAGUCHI, F. Efficient activation of the severe acute respiratory syndrome coronavirus spike protein by the transmembrane protease TMPRSS2. **Journal of Virology**, v. 84, n. 24, p. 12658–12664, 2010.

28 JIAN, L.; YI, W.; ZHANG, N.; WEN, W.; KRYSKO, O.; SONG, W. J.; BACHERT, C. Perspective: COVID-19, implications of nasal diseases and consequences for their management. **The Journal of Allergy and Clinical Immunology**, v. 146, n. 1, p. 67–69, 2020.

29 GUPTA, A.; MADHAVAN, M. V.; SEHGAL, K.; NAIR, N.; MAHAJAN, S.; SEHRAWAT, T. S.; et al. Extrapulmonary manifestations of COVID-19. **Nature Medicine**, v. 26, p. 1017–1032, 2020.

30 VADUGANATHAN, M.; VARDENY, O.; MICHEL, T.; MCMURRAY, J. J.; PFEFFER, M. A.; SOLOMON, S. D. Renin–angiotensin–aldosterone system inhibitors in patients with COVID-19. **New England Journal of Medicine**, v. 382, n. 17, p. 1653–1659, 2020.

31 MURUGAN, D.; LAU, Y. S.; LAU, W. C.; MUSTAFA, M. R.; HUANG, Y. Angiotensin 1-7 protects against angiotensin II-induced endoplasmic reticulum stress and endothelial dysfunction via mas receptor. **PLOS One**, v. 11, n. 1, p. e0147892, 2015.

32 MULVEY, J. J.; MAGRO, C. M.; MA, L. X.; NUOVO, G. J.; BAERGEN, R. N. Analysis of complement deposition and viral rna in placentas of COVID-19 patients. **Annals of Diagnostic Pathology**, v. 46, p. 151530, 2020.

33 FAJGENBAUM, D. C.; JUNE, C. H. Cytokine storm. **New England Journal of Medicine**, v. 383, n. 23, p. 2255–2273, 2020.

34 MAGRO, C.; MULVEY, J. J.; BERLIN, D.; NUOVO, G.; SALVATORE, S.; HARP, J.; et al. Complement associated microvascular injury and thrombosis in the pathogenesis of severe COVID-19 infection: A report of five cases. **Translational Research**, v. 220, p. 1–13, 2020.

35 NAGASHIMA, S.; MENDES, M. C.; MARTINS, A. P. C.; BORGES, N. H.; GODOY, T. M.; MIGGIOLARO, A. F. R. S.; et al. Endothelial dysfunction and thrombosis in patients with COVID-19—brief report. **Arteriosclerosis, Thrombosis, and Vascular Biology**, v. 40, p. 2404—-2407, 2020.

36 LIPPI, G.; PLEBANI, M. Laboratory abnormalities in patients with COVID-19 infection. **Clinical Chemistry and Laboratory Medicine**, v. 58, n. 7, p. 1131–1134, 2020.

37 LIPPI, G.; PLEBANI, M.; HENRY, B. M. Thrombocytopenia is associated with severe coronavirus disease 2019 (COVID-19) infections: A meta-analysis. **Clinica Chimica Acta**, v. 506, p. 145–148, 2020.

38 TANG, N.; LI, D.; WANG, X.; SUN, Z. Abnormal coagulation parameters are associated with poor prognosis in patients with novel coronavirus pneumonia. **Journal of Thrombosis and Haemostasis**, v. 18, n. 4, p. 844–847, 2020.

39 BENHAMOU, D.; KEITA, H.; DUCLOY-BOUTHORS, A. S.; CARO working group. Coagulation changes and thromboembolic risk in COVID-19 obstetric patients. **Anaesthesia Critical Care & Pain Medicine**, v. 39, n. 3, p. 351–353, 2020.

40 RIBES, A.; VARDON-BOUNES, F.; MÉMIER, V.; POETTE, M.; AU-DUONG, J.; GARCIA, C.; et al. Thromboembolic events and COVID-19. **Advances in Biological Regulatio**, v. 77, p. 100735, 2020.

41 KLOK, F. A.; KRUIP, M. J. H. A.; VAN DER MEER, N. J. M.; ARBOUS, M. S.; GOMMERS, D.; KANT, K. M.; et al. Confirmation of the high cumulative incidence of thrombotic complications in critically ill icu patients with COVID-19: An updated analysis. **Thrombosis Research**, v. 191, p. 148–150, 2020.

42 TOMBOLINI, A.; SCENDONI, R. SARS-CoV-2-related deaths in routine forensic autopsy practice: histopathological patterns. **International Journal of Legal Medicine**, v. 134, p. 2205–2208, 2020.

43 QIAO, J. What are the risks of COVID-19 infection in pregnant women? **The Lancet Journal**, v. 395, p. 760–762, 2020.

44 LOPES DE SOUSA, A. F.; CARVALHO, H. E. F.; OLIVEIRA, L. B.; SCHNEIDER, G.; CAMARGO, E. L. S.; WATANABE, E.; et al. Effects of

COVID-19 infection during pregnancy and neonatal prognosis: What is the evidence? **International Journal of Environmental Research and Public Health**, v. 17, n. 11, 2020.

45 ALZAMORA, M. C.; PAREDES, T.; CACERES, D.; WEBB, C. M.; VALDEZ, L. M.; ROSA, M. L. Severe COVID-19 during pregnancy and possible vertical transmission. **American journal of perinatology**, v. 37, n. 8, p. 861–865, 2020.

46 SCHWARTZ, D. A.; GRAHAM, A. L. Potential maternal and infant outcomes from (Wuhan) coronavirus 2019-nCoV infecting pregnant women: Lessons from SARS, MERS, and other human coronavirus infections. **Viruses**, v. 12, n. 2, p. 194, 2020.

47 RASMUSSEN, S. A.; SMULIAN, J. C.; LEDNICKY, J. A.; WEN, T. S.; JAMIESON, D. J. Coronavirus disease 2019 (COVID-19) and pregnancy: what obstetricians need to know. **American Journal of Obstetrics & Gynecology**, v. 222, n. 5, p. 415–426, 2020.

48 KNIGHT, M.; BUNCH, K.; VOUSDEN, N.; MORRIS, E.; SIMPSON, N.; GALE, C.; O'BRIEN, P.; QUIGLEY, M.; BROCKLEHURST, P.; KURINCZUK, J. J. Characteristics and outcomes of pregnant women admitted to hospital with confirmed SARS-CoV-2 infection in UK: national population based cohort study. **BMJ**, v. 369, 2020.

49 BRESLIN, N.; BAPTISTE, C.; GYAMFI-BANNERMAN, C.; SIMPSON, L. L.; D'ALTON, M. E.; GOFFMAN, D. Coronavirus disease 2019 infection among asymptomatic and symptomatic pregnant women: two weeks of confirmed presentations to an affiliated pair of New York city hospitals. **American Journal of Obstetrics & Gynecology MFM**, v. 2, n. 2, p. 100118, 2020.

50 BLITZ, M. J.; GRüNEBAUM, A.; TEKBALI, A.; BORNSTEIN, E.; ROCHELSON, B.; NIMAROFF, M.; CHERVENAK, F. A. Intensive care unit admissions for pregnant and nonpregnant women with coronavirus disease 2019. **American Journal of Obstetrics & Gynecology**, v. 223, n. 2, p. 290–291, 2020.

51 KAYEM, G.; LECARPENTIER, E.; DERUELLE, P.; BRETELLE, F.; AZRIA, E.; BLANC, J. A snapshot of the COVID-19 pandemic among pregnant women in france. **Journal of Gynecology Obstetrics and Human Reproduction**, v. 49, n. 7, p. 101826, 2020.

52 LAMOUROUX, A.; ATTIE-BITACH, T.; MARTINOVIC, J.; LERUEZ-VILLE, M.; VILLE, Y. Evidence for and against vertical transmission for severe acute respiratory syndrome coronavirus 2. **American Journal of Obstetrics & Gynecology**, v. 223, n. 1, p. 91.E1–91.E4, 2020.

53 CELIK, O.; SAGLAM, A.; BAYSAL, B.; DERWIG, I. E.; CELIK, N.; AK, M.; et al. Factors preventing materno-fetal transmission of SARS-CoV-2. **Placenta**, v. 97, p. 1–5, 2020.

54 SMITHGALL, M. C.; LIU-JARIN, X.; HAMELE-BENA, D.; CIMIC, A.; MOURAD, M.; DEBELENKO, L.; CHEN, X. Third-trimester placentas of severe acute respiratory syndrome coronavirus 2 (SARS-CoV-2)-positive women: histomorphology, including viral immunohistochemistry and in-situ hybridization. **Histopathology**, v. 77, n. 6, p. 994–999, 2020.

55 WORLD HEALTH ORGANIZATION. **Definition and categorization of the timing of mother-to-child transmission of SARS-CoV-2**. 2021. Disponível em: <https://www.who.int/publications/i/item/WHO-2019-nCoV-mother-to-child-transmission-2021>. Acesso em: junho de 2021.

56 KIRTSMAN, M.; DIAMBOMBA, Y.; POUTANEN, S. M.; MALINOWSKI, A. K.; VLACHODIMITROPOULOU, E.; PARKS, W. T.; ERDMAN, L.; MORRIS, S. K.; SHAH, P. S. Probable congenital SARS-CoV-2 infection in a neonate born to a woman with active SARS-CoV-2 infection. **CMAJ**, v. 192, n. 24, p. E647–E650, 2020.

57 VIVANTI, A. J.; VAULOUP-FELLOUS, C.; PREVOT, S.; ZUPAN, V.; SUFFEE, C.; CAO, J. D. Transplacental transmission of SARS-CoV-2 infection. **Nature Communications**, n. 3572, 2020.

58 SISMAN, J.; JALEEL, M. A.; MORENO, W.; RAJARAM, V.; COLLINS, R. R. J.; SAVANI, R. Intrauterine transmission of SARS-CoV-2 infection in a preterm infant. **The Pediatric Infectious Disease Journal**, v. 39, n. 9, p. e265–e267, 2020.

59 BAUD, D.; GREUB, G.; FAVRE, G.; GENGLER, C.; JATON, K.; DUBRUC, E.; POMAR, L. Second-Trimester Miscarriage in a Pregnant Woman With SARS-CoV-2 Infection. **JAMA**, v. 323, n. 21, p. 2198–2200, 2020.

60 WALKER, K. F.; O'DONOGHUE, K.; GRACE, N.; DORLING, J.; COMEAU, J. L.; LI, W.; THORNTON, J. G. Maternal transmission of SARS-CoV-2 to the neonate, and possible routes for such transmission: a systematic review and critical analysis. **BJOG: An International Journal of Obstetrics & Gynaecology**, v. 127, n. 11, p. 1324–1336, 2020.

61 SCHWARTZ, D. A.; THOMAS, K. M. Characterizing COVID-19 maternal-fetal transmission and placental infection using comprehensive molecular pathology. **EBioMedicine - The Lancet**, v. 60, n. 102983, 2020.

62 SCHWARTZ, D. A.; MOROTTI, D.; BEIGI, B.; MOSHFEGH, F.; ZAFARANLOO, N.; PATANè, L. Confirming vertical fetal infection with coronavirus disease 2019: Neonatal and pathology criteria for early onset and transplacental transmission of severe acute respiratory syndrome coronavirus 2 from infected pregnant mothers. **Archives of Pathology & Laboratory Medicine**, v. 144, n. 12, p. 1451–1456, 2020.

63 RASCHETTI, R.; VIVANTI, A. J.; VAULOUP-FELLOUS, C.; LOI, B.; BENACHI, A.; LUCA, D. D. Synthesis and systematic review of reported neonatal SARS-CoV-2 infections. **Nature Communications**, n. 5164, 2020.

64 MOORE, K. L.; PERSAUD, T. V. N.; TORCHIA, M. G. **The Developing Human: Clinically Oriented Embryology**. 10. ed. Philadelphia: Elsevier, 2012.

65 GARCIA, A.; AZOUBEL, R. **A Placenta Humana: Morfologia e Patologia Fetal e Perinatal**. 1. ed. Rio de Janeiro: Atheneu, 1986.

66 BIOLOGY FORUMS. **Placenta**. 2020. Disponível em: <https://biology-forums.com/index.php?action=gallery;sa=view;id=1263\#images>. Acesso em: junho de 2021.

67 CHATUPHONPRASERT, W.; JARUKAMJORN, K.; ELLINGER, I. Physiology and pathophysiology of steroid biosynthesis, transport and metabolism in the human placenta. **Frontiers in Pharmacology**, v. 9, n. 1027, p. 1–29, 2018.

68 MALTEPE, E.; FISHER, S. J. Placenta: the forgotten organ. **Annual Review of Cell and Developmental Biology**, v. 31, n. 1, p. 523–552, 2015.

69 ZELDOVICH, V. B.; CLAUSEN, C. H.; BRADFORD, E.; FLETCHER, D. A.; MALTEPE, E.; ROBBINS, J. R.; BAKARDJIEV, A. I. Placental syncytium forms a biophysical barrier against pathogen invasion. **PLoS Pathogens**, v. 9, n. 12, p. e1003821, 2013.

70 CORRY, J.; ARORA, N.; GOOD, C. A.; SADOVSKY, Y.; COYNE, C. B. Organotypic models of type III interferon-mediated protection from Zika virus infections at the maternal–fetal interface. **Proceedings of the National Academy of Sciences**, v. 114, n. 35, p. 9433–9438, 2017.

71 BAYER, A.; LENNEMANN, N. J.; OUYANG, Y.; BRAMLEY, J. C.; MOROSKY, S.; MARQUES JR., E. T. de A.; CHERRY, S.; SADOVSKY, Y.; COYNE, C. B. Type III interferons produced by human placental trophoblasts confer protection against Zika virus infection. **Cell Host Microbe**, v. 19, n. 5, p. 705–712, 2016.

72 CAO, B.; DIAMOND, M. S.; MYSOREKAR, I. U. Maternal-fetal transmission of Zika virus: routes and signals for infection. **Journal of Interferon and Cytokine Research**, v. 37, n. 7, p. 287–294, 2017.

73 SCHLIEFSTEINER, C.; PEINHAUPT, M.; KOPP, S.; LÖGL, J.; LANG-OLIP, I.; HIDEN, U.; HEINEMANN, A.; DESOYE, G.; WADSACK, C. Human placental Hofbauer cells maintain an anti-inflammatory M2 phenotype despite the presence of gestational diabetes mellitus. **Frontiers in Immunology**, v. 8, p. 888, 2017.

74 BROWN, M. B.; VON CHAMIER, M.; ALLAM, A. A.; REYES, L. M1/M2 macrophage polarity in normal and complicated pregnancy. **Frontiers in Immunology**, v. 5, p. e606, 2014.

75 JOERINK, M.; RINDSJÖ, E.; VAN RIEL, B.; ALM, J.; PAPADOGIANNAKIS, N. Placental macrophage (Hofbauer cell) polarization is independent of maternal allergen-sensitization and presence of chorioamnionitis. **Placenta**, v. 32, n. 5, p. 380–385, 2011.

76 DELORME-AXFORD, E.; DONKER, R. B.; MOUILLET, J.-F.; CHU, T.; BAYER, A.; OUYANG, Y.; WANG, T.; STOLZ, D. B.; SARKAR, S. N.; MORELLI, A. E.; SADOVSKY, Y.; COYNE, C. B. Human placental trophoblasts confer viral resistance to recipient cells. **Proceedings of the National Academy of Sciences of the United States of America**, v. 110, n. 29, p. 12048—-12053, 2013.

77 REYES, L.; GOLOS, T. G. Hofbauer cells: Their role in healthy and complicated pregnancy. **Frontiers in Immunology**, v. 9, 2018.

78 GRIGORIADIS, C.; TYMPA, A.; CREATSA, M.; BAKAS, P.; LIAPIS, A.; KONDI-PAFITI, A.; CREATSAS, G. Hofbauer cells morphology and density in placentas from normal and pathological gestations. **Revista Brasileira de Ginecologia e Obstetrícia**, v. 35, p. 407–412, 2013.

79 EGLOFF, C.; VAULOUP-FELLOUS, C.; PICONE, O.; MANDELBROT, L.; ROQUES, P. Evidence and possible mechanisms of rare maternal-fetal transmission of SARS-CoV-2. **Journal of Clinical Virology**, v. 128, p. 104447, 2020.

80 ROSENBERG, A. Z.; YU, W.; HILL, A. D.; REYES, C. A.; SCHWARTZ, D. A. Placental pathology of Zika virus: viral infection of the placenta induces villous stromal macrophage (Hofbauer cell) proliferation and hyperplasia. **Archives of Pathology and Laboratory Medicine**, v. 141, n. 1, p. 43–48, 2016.

81 ANTEBY, E. Y.; NATANSON-YARON, S.; GREENFIELD, C.; GOLDMAN-WOHL, D.; HAIMOV-KOCHMAN, R.; HOLZER, H.; YAGEL, S. Human placental Hofbauer cells express sprouty proteins: a possible modulating mechanism of villous branchin? **Placenta**, v. 26, n. 6, p. 476–483, 2005.

82 SIMONI, M. K.; JURADO, K. A.; ABRAHAMS, V. M.; FIKRIG, E.; GULLER, S. Zika virus infection of Hofbauer cells. **American Journal of Reproductive Immunology**, v. 77, n. 2, p. e12613, 2017.

83 ZANLUCA, C.; DE NORONHA, L.; DOS SANTOS, C. N. D. Maternal-fetal transmission of the Zika virus: an intriguing interplay. **Tissue Barriers**, v. 3, n. 19, p. e1402143, 2018.

84 COYNE, C. B.; LAZEAR, H. M. Zika virus – reigniting the TORCH. **Nature Reviews Microbiology**, v. 14, p. 707–715, 2016.

85 ADIBI, J. J.; MARQUES JR., E. T. A.; CARTUS, A.; BEIGI, R. H. Teratogenic effects of the Zika virus and the role of the placenta. **The Lancet**, v. 387, n. 10027, p. 1587–1590, 2016.

86 LUO, H.; WINKELMANN, E. R.; FERNANDEZ-SALAS, I.; LI, L.; MAYER, S. V.; DANIZ-LOZANO, R.; SANCHEZ-CASAS, R. M.; VASILAKIS, N.; TESH, R.; BARRETT, A. D.; WEAVER, S. C.; WANG, T. Zika, dengue and yellow fever viruses induce differential anti-viral immune responses in human monocytic and first trimester trophoblast cells. **Antiviral Research**, v. 151, p. 55–62, 2018.

87 REDLINE, R. W. Placental pathology: a systematic approach with clinical correlations. **Placenta**, v. 29, p. S86—-91, 2008.

88 REDLINE, R. W. Classification of placental lesions. **American Journal of Obstetrics and Gynecology**, v. 213, p. S21—-28, 2015.

89 GOLDSTEIN, J. A.; GALLAGHER, K.; BECK, C.; KUMAR, R.; GERNAND, A. D. Maternal-fetal inflammation in the placenta and the developmental origins of health and disease. **Frontiers in Immunology**, v. 11, 2020.

90 KHONG, T. Y.; MOONEY, E. E.; ARIEL, I.; BALMUS, N. C. M.; BOYD, T. K.; BRUNDLER, M. A.; et al. Sampling and definitions of placental lesions - Amsterdam Placental Workshop Group Consensus Statement. **Archives of Pathology & Laboratory Medicine**, v. 140, n. 7, p. 698–713, 2016.

91 MATSIKA, A. Clinical correlates of histopathological entities of the placenta. **Australian Journal of General Practice**, v. 50, p. 62—-69, 2021.

92 REDLINE, R. W.; RAVISHANKAR, S.; BAGBY, C. M.; SAAB, S. T.; ZAREI, S. Four major patterns of placental injury: a stepwise guide for understanding and implementing the 2016 amsterdam consensus. **Modern Pathology**, v. 34, p. 1074—-1092, 2021.

93 D. A. SCHWARTZ. Viral infection, proliferation, and hyperplasia of Hofbauer cells and absence of inflammation characterize the placental pathology of fetuses with congenital Zika virus infection. **Archives of Gynecology and Obstetrics**, v. 295, n. 6, p. 1361–1368, 2017.

94 DE NORONHA, L.; ZANLUCA, C.; AZEVEDO, M. L. V.; LUZ, K. G.; DOS SANTOS, C. N. D. Zika virus damages the human placental barrier and presents marked fetal neurotropism. **Memórias do Instituto Oswaldo Cruz**, v. 111, n. 5, p. 287–293, 2016.

95 SHANES, E. D.; MITHAL, L. B.; OTERO, S.; AZAD, H. A.; MILLER, E. S.; GOLDSTEIN, J. A. Placental pathology in COVID-19. **American Journal of Clinical Pathology**, v. 154, n. 1, p. 23–32, 2020.

96 MENTER, T.; MERTZ, K. D.; JIANG, S.; CHEN, H.; MONOD, C.; TZANKOV, A. Placental pathology findings during and after SARS-CoV-2 infection: Features of villitis and malperfusion. **Pathobiology: Journal of Immunopathology, Molecular and Cellular Biology**, v. 88, n. 1, p. 69–77, 2020.

97 HOSIER, H.; FARHADIAN, S. F.; MOROTTI, R. A.; DESHMUKH, U.; LU-CULLIGAN, A.; CAMPBELL, K. H.; et al. SARS-CoV-2 infection of the placenta. **The Journal of Clinical Investigation**, v. 130, n. 9, p. 4947—4953, 2020.

98 BAERGEN, R.; HELLER, D. Placental pathology in COVID-19 positive mothers: Preliminary findings. **Pediatric and Developmental Pathology**, v. 23, n. 3, p. 177–180, 2020.

99 GULERSEN, M.; PRASANNAN, L.; TAM, H. T.; METZ, C. N.; ROCHELSON, B.; MEIROWITZ, N. Histopathologic evaluation of placentas after diagnosis of maternal severe acute respiratory syndrome coronavirus 2 infection. **American Journal of Obstetrics and Gynecology MFM**, v. 2, n. 4, 2020.

100 SCHWARTZ, D. A.; MOROTTI, D. Placental pathology of COVID-19 with and without fetal and neonatal infection: Trophoblast necrosis and chronic histiocytic intervillositis as risk factors for transplacental transmission of SARS-CoV-2. **Viruses**, v. 12, n. 11, 2020.

101 SCHWARTZ, D. A.; BALDEWIJNS, M.; BENACHI, A.; BUGATTI, M.; COLLINS, R. R. J.; LUCA, D. Chronic histiocytic intervillositis with trophoblast necrosis is a risk factor associated with placental infection from coronavirus disease 2019 (COVID-19) and intrauterine maternal-fetal severe acute respiratory syndrome coronavirus 2 (SARS-CoV-2) transmission in live-born and stillborn infants. **Archives of Pathology and Laboratory Medicine**, v. 145, n. 5, 2021.

102 LEVITAN, D.; LONDON, V.; MCLAREN, R. A.; MANN, J. D.; CHENG, K.; SILVER, M.; BALHOTRA, K. S.; MCCALLA, S.; LOUKERIS, K. Histologic and immunohistochemical evaluation of 65 placentas from women with polymerase chain reaction-proven severe acute respiratory syndrome coronavirus 2 (SARS-CoV-2) infection. **Archives of Pathology and Laboratory Medicine**, v. 145, n. 6, p. 648–656, 2021.

103 STONOGA, E. T. S.; LANZONI, L. A.; REBUTINI, P. Z.; OLIVEIRA, A. L. P.; CHISTE, J. A.; FUGAçA, C. A.; PRá, D. M. M.; PERCICOTE, A. P.; ROSSONI, A.; NOGUEIRA, M. B.; NORONHA, L.; RABONI, S. M. Intrauterine transmission of SARS-CoV-2. **Emerging Infectious Diseases**, v. 27, n. 21, p. 638–641, 2021.

104 PATANE, L.; MOROTTI, D.; GIUNTA, M. R.; SIGISMONDI, C.; PICCOLI, M. G.; FRIGERIO, L.; et al. Vertical transmission of coronavirus disease 2019: severe acute respiratory syndrome coronavirus 2 RNA on the fetal side of the placenta in pregnancies with coronavirus disease 2019–positive mothers and neonates at birth. **American Journal of Obstetrics and Gynecology MFM**, v. 2, n. 3, p. 100145, 2020.

105 SCHWARTZ, D. A.; LEVITAN, D. Severe acute respiratory syndrome coronavirus 2 (SARS-CoV-2) infecting pregnant women and the fetus, intrauterine transmission and placental pathology during the coronavirus disease 2019 (COVID-19) pandemic: It's complicated. **Archives of Pathology and Laboratory Medicine**, 2021.

106 WATTERBERG, K. L.; AUCOTT, S.; BENITZ, W. E.; CUMMINGS, J. J.; EICHENWALD, E. C.; GOLDSMITH, J.; et al. The Apgar Score. **American Academy of Pediatrics**, v. 136, n. 4, p. 819–822, 2015.

107 MINISTÉRIO DA SAÚDE. Secretaria de Vigilância em Saúde. Departamento de Doenças de Condições Crônicas e Infecções Sexualmente Transmissíveis. **Protocolo Clínico e Diretrizes Terapêuticas para prevenção da transmissão vertical de HIV, sífilis e hepatites virais**. Brasília, DF, 2019.

Disponível em: <http://www.aids.gov.br/pt-br/pub/2015/protocolo-clinico-e-diretrizes-terapeuticas-para-prevencao-da-transmissao-vertical-de-hiv>. Acesso em: junho de 2021.

108 BAURAKIADES, E.; MARTINS, A. P. C.; MORESCHI, N. V.; SOUZA, C. D. A.; ABUJAMRA, K.; SAITO, A. O.; MECATTI, M. C.; SANTOS, M. G.; PIMENTEL, C. R.; SILVA, L. L. G.; CRUZ, C. R.; DE NORONHA, L. Histomorphometric and immunohistochemical analysis of infectious agents, T-cell subpopulations and inflammatory adhesion molecules in placentas from HIV-seropositive pregnant women. **Diagnostic Pathology**, v. 6, n. 1, p. e101, 2011.

109 LOUKERIS, K.; SELA, R.; BAERGEN, R. N. Syncytial knots as a reflection of placental maturity: reference values for 20 to 40 weeks' gestational age. **Pediatric and Developmental Pathology**, v. 13, n. 4, p. 305–309, 2010.

110 DE NORONHA, L.; ZANLUCA, C.; BURGER, M.; SUZUKAWA, A.; AZEVEDO, M.; REBUTINI, P.; NOVADZKI, I.; TANABE, L.; PRESIBELLA, M.; SANTOS, C. Zika virus infection at different pregnancy stages: Anatomopathological findings, target cells and viral persistence in placental tissues. **Frontiers in Microbiology**, v. 9, 2018.

111 MALAQUIAS, M.; OYAMA, L. A.; JERICO, P. C.; COSTA, I.; PADILHA, G.; NAGASHIMA, S.; et al. Effects of mesenchymal stromal cells play a role the oxidant/antioxidant balance in a murine model of asthma. **Allergologia et Immunopathologia**, v. 46, n. 2, p. 136–143, 2018.

112 OUR WORLD IN DATA. UNIVERSITY OF OXFORD. **Mortality Risk of COVID-19**. 2022. Disponível em: <https://ourworldindata.org/mortality-risk-covid>. Acesso em: março de 2022.

ANEXOS

ANEXO 1 – Política de direitos autorais do periódico *Frontiers in Immunology* referente ao artigo *Association Between COVID-19 Pregnant Women Symptoms Severity and Placental Morphologic Features* incluído no Capítulo Resultados desta tese.

1. Frontiers Policies

1.1. Open Access and Copyright

All Frontiers articles from July 2012 onwards are published with open access under the CC-BY Creative Commons attribution license (the current version is CC-BY, version 4.0). This means that the author(s) retains copyright, but the content is free to download, distribute, and adapt for commercial or non-commercial purposes, given appropriate attribution to the original article.

Upon submission, the author(s) grants Frontiers a license to publish, including to display, store, copy, and reuse the content. The CC-BY Creative Commons attribution license enables anyone to use the publication freely, given appropriate attribution to the author(s) and citing Frontiers as the original publisher. The CC-BY Creative Commons attribution license does not apply to third-party materials that display a copyright notice to prohibit copying. Unless the third-party content is also subject to a CC-BY Creative Commons attribution license, or an equally permissive license, the author(s) must comply with any third-party copyright notices.

This page is available in the following languages:

Creative Commons License Deed

Attribution 4.0 International (CC BY 4.0)

This is a human-readable summary of (and not a substitute for) the license.

You are free to:

Share — copy and redistribute the material in any medium or format

Adapt — remix, transform, and build upon the material

for any purpose, even commercially.

The licensor cannot revoke these freedoms as long as you follow the license terms.

Under the following terms:

Attribution — You must give appropriate credit, provide a link to the license, and indicate if changes were made. You may do so in any reasonable manner, but not in any way that suggests the licensor endorses you or your use.

No additional restrictions — You may not apply legal terms or technological measures that legally restrict others from doing anything the license permits.

Notices:

You do not have to comply with the license for elements of the material in the public domain or where your use is permitted by an applicable exception or limitation.

No warranties are given. The license may not give you all of the permissions necessary for your intended use. For example, other rights such as publicity, privacy, or moral rights may limit how you use the material.

ANEXO 2 – Produção adicional: artigo intitulado *Intrauterine Transmission of SARS-CoV-2* publicado no periódico *Emerging Infectious Diseases* em fevereiro de 2021 e política de direitos autorais do periódico/editora.

Centers for Disease Control and Prevention

ISSN: 1080-6059

Volume 27, Number 2—February 2021

Research Letter

Intrauterine Transmission of SARS-CoV-2

Emanuele T. S. Stonoga[1], Laura de Almeida Lanzoni[1], Patricia Zadorosnei Rebutini[1]✉, André Luiz Permegiani de Oliveira, Jullie Anne Chiste, Cyllian Arias Fugaça, Daniele M. M. Prá, Ana Paula Percicote, Andrea Rossoni, Meri Bordignon Nogueira, Lucia de Noronha, and Sonia Mara Raboni

Author affiliations: Hospital de Clínicas da Universidade Federal do Paraná, Parana, Brazil (E.T.S. Stonoga, L.A. Lanzoni, J.A. Chiste, C.A. Fugaça, M.B. Nogueira); Pontifícia Universidade Católica do Paraná, Parana (P.Z. Rebutini, A.L.P. Oliveira, D.M. Marani Prá, L. de Noronha); Universidade Federal do Paraná, Parana (A.P. Percicote, A. Rossoni, S.M. Raboni)

Cite This Article

Abstract

We documented fetal death associated with intrauterine transmission of severe acute respiratory syndrome coronavirus 2. We found chronic histiocytic intervillositis, maternal and fetal vascular malperfusion, microglial hyperplasia, and lymphocytic infiltrate in muscle in the placenta and fetal tissue. Placenta and umbilical cord blood tested positive for the virus by PCR, confirming transplacental transmission.

A woman 42 years of age at 27 weeks' gestation sought treatment at Hospital de Clínicas da Universidade Federal do Paraná, Parana, Brazil, for symptoms of coronavirus disease (COVID-19). Dyspnea, dry cough, high temperature (38.5°C), anosmia, nausea, vomiting, and diarrhea had developed 2 days before hospitalization. At admission, we collected a nasopharyngeal swab sample and tested it for severe acute respiratory syndrome coronavirus 2 (SARS-CoV-2) and rhinovirus by reverse transcription PCR (RT-PCR) (XGEN MASTER COVID-19 Kit; Mobius Life Science, Inc, https://mobiuslife.com.br) (Appendix). The sample tested positive for both viruses. We prescribed azithromycin, oseltamivir, prophylactic enoxaparin, and corticosteroids for fetal lung maturation. A chest computed tomography scan revealed bilateral ground glass opacities and interlobular septal thickening. After 4 days, the patient needed ventilatory and hemodynamic support.

The patient's prenatal care had been uneventful. She had undergone routine tests and ultrasound scans; the most recent had been at 25 weeks' gestation. Her medical history included a previous pregnancy complicated by hypertension that resolved with delivery. The current pregnancy was her seventh; she previously had delivered 3 children and had 2 abortions and 1 ectopic pregnancy.

Six days after admission, obstetric ultrasound demonstrated a single intrauterine pregnancy. The fetus was in a transverse position with shoulder presentation; the ultrasound showed reduced amniotic fluid volume and absence of fetal movements and heart rate. Because misoprostol failed to induce labor, we conducted a cesarean delivery. The fetus was stillborn. Immediately after delivery, we used an aseptic technique to collect samples of amniotic fluid (before amniotic membranes ruptured), umbilical cord blood, placental membranes, and cotyledon fragments (Table).

We obtained informed written consent for fetal autopsy, placental grossing, and histologic examination. External examination showed a female concept with skin discoloration and moderate peeling; the fetus had gestational age of »28 weeks and weighed 1,020 g (50th percentile). Internal examination revealed red serous effusions in the chest and abdomen and petechial hemorrhage in the heart and lungs. We conducted evisceration using the Letulle method and separated the organs into functional groups. We noted hepatic discoloration and friability and lung and kidney hypoplasia (both <5th percentile). We did not identify other macroscopic abnormalities.

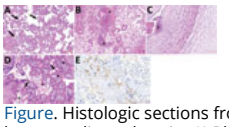

Figure. Histologic sections from the placenta of stillborn fetus of a woman with severe acute respiratory syndrome coronavirus 2 infection, Brazil, 2020. Tissue stained with hematoxylin and eosin. A) Placenta shows...

The placental disc was round and had tan and glistening membranes peripherally attached. The umbilical cord had 3 vessels; it was 28 cm long, inserted eccentrically, and under coiled. The fetal surface was gray with normal chorionic plate vessels. The trimmed placental disc weighed 135 g and measured 12 × 12 cm (<3rd percentile) (Appendix). We collected additional samples of fetal liver, spleen, lung, central nervous system tissue, ovary, and muscle for RT-PCR (Table). Tissue samples were fixed in 10% buffered formalin, routinely processed, stained in hematoxylin and eosin, and underwent immunohistochemical staining using CD68 antibodies (Figure; Appendix).

Few reports have described the effects of SARS-CoV-2 infection in utero; because pathogen detection requires multiple samples, it has been difficult to characterize congenital infection (*1*,*2*). According to Shah et al. (*3*), congenital SARS-CoV-2 infection can be confirmed by PCR of placental tissue. We detected SARS-CoV-2 RNA in cotyledon samples, membranes, and umbilical cord blood aspirate, suggesting a breakdown of the placental barrier and fetal intrauterine viremia. We used immunohistochemical staining with CD68 antibodies to identify multifocal chronic histiocytic intervillositis in the placenta (Figure, panels D, E). This condition was also described in other pregnant women with COVID-19 (*4*,*5*). We also noted microglial hyperplasia, mild lymphocytic infiltrate, and edema in skeletal muscle (Appendix). These findings might suggest infection. However, all fetal tissue samples tested negative for SARS-CoV-2 RNA (Table). Other findings might have been caused by intrauterine asphyxia (Appendix).

COVID-19 is associated with cytokine storm, an exaggerated inflammatory response that is usually indicative of disease severity (*6*). Excessive inflammation could cause endothelial damage and disrupt the coagulation system; some evidence suggests that thrombotic and microvascular injury might affect manifestations of COVID-19 (*7*,*8*). We noted severe maternal vascular malperfusion injuries in the placenta, including substantial recent infarcts, decidual vasculopathy, accelerated villous maturation, and low placental weight. Similar findings are often observed in placentas from women with hypertensive disorders and have been associated with oligohydramnios, preterm birth, and stillbirth. Although the patient's blood pressure was within reference limits, her age and history of gestational hypertension are risk factors for such alterations and the probable cause of placental insufficiency and fetal demise (*9*,*10*). We also observed multifocal small intervillous thrombi and focal thrombosis of fetal placental vessels. Therefore, the extent and apparently rapid development of these findings suggests that infection contributed to vascular damage.

The effects of congenital transmission of SARS-CoV-2 remain largely unknown. This study highlights the need for placental and fetal gross and microscopic evaluation, which can help elucidate the pathophysiology of COVID-19.

Dr. Stonoga is a first-year pathology resident at Hospital de Clínicas da Universidade Federal do Paraná, Parana. Her research interests include perinatal pathology and infectious disease research.

Top

References

1. Alzamora MC, Paredes T, Caceres D, Webb CM, Valdez LM, La Rosa M. Severe COVID-19 during pregnancy and possible vertical transmission. Am J Perinatol. 2020;37:861–5. DOI PubMed Google Scholar
2. Kirtsman M, Diambomba Y, Poutanen SM, Malinowski AK, Vlachodimitropoulou E, Parks WT, et al. Probable congenital SARS-CoV-2 infection in a neonate born to a woman with active SARS-CoV-2 infection. CMAJ. 2020;192:E647–50. DOI PubMed Google Scholar
3. Shah PS, Diambomba Y, Acharya G, Morris SK, Bitnun A. Classification system and case definition for SARS-CoV-2 infection in pregnant women, fetuses, and neonates. Acta Obstet Gynecol Scand. 2020;99:565–8. DOI PubMed Google Scholar
4. Sisman J, Jaleel MA, Moreno W, Rajaram V, Collins RRJ, Savani RC, et al. Intrauterine transmission of SARS-COV-2 infection in a preterm infant. Pediatr Infect Dis J. 2020;39:e265–7.
5. Vivanti AJ, Vauloup-Fellous C, Prevot S, Zupan V, Suffee C, Do Cao J, et al. Transplacental transmission of SARS-CoV-2 infection. Nat Commun. 2020;11:3572. DOI PubMed Google Scholar
6. Huang C, Wang Y, Li X, Ren L, Zhao J, Hu Y, et al. Clinical features of patients infected with 2019 novel coronavirus in Wuhan, China. [Erratum in: Lancet. 2020;395:496]. Lancet. 2020;395:497–506. DOI PubMed Google Scholar
7. Nagashima S, Mendes MC, Camargo Martins AP, Borges NH, Godoy TM, Miggiolaro AFRDS, et al. Endothelial dysfunction and thrombosis in patients with COVID-19—brief report. Arterioscler Thromb Vasc Biol. 2020;40:2404–7. DOI PubMed Google Scholar
8. Benhamou D, Keita H, Ducloy-Bouthors AS, Benhamou D, Bonnet MP, Bonnin M, et al.; Obstetric Anaesthesia and Critical Care Club Working Group. Coagulation changes and thromboembolic risk in COVID-19 obstetric patients. Anaesth Crit Care Pain Med. 2020;39:351–3. DOI PubMed Google Scholar
9. Shanes ED, Mithal LB, Otero S, Azad HA, Miller ES, Goldstein JA. Placental Pathology in COVID-19. Am J Clin Pathol. 2020;154:23–32. DOI PubMed Google Scholar
10. Baergen RN, Heller DS. Placental pathology in Covid-19 positive mothers: preliminary findings. Pediatr Dev Pathol. 2020;23:177–80. DOI PubMed Google Scholar

Top

Figure

Figure. Histologic sections from the placenta of stillborn fetus of a woman with severe acute respiratory syndrome coronavirus 2 infection, Brazil, 2020. Tissue stained with hematoxylin and eosin. A) Placenta...

Table

Table. Results of PCR for severe acute respiratory syndrome coronavirus 2 in a pregnant woman and fetus, Brazil, 2020

Top

Cite This Article
DOI: 10.3201/eid2702.203824

[1]These first authors contributed equally to this article.

Table of Contents – Volume 27, Number 2—February 2021

EID Search Options

Advanced Article Search – Search articles by author and/or keyword.

Articles by Country Search – Search articles by the topic country.

Article Type Search – Search articles by article type and issue.

Top

Comments

Please use the form below to submit correspondence to the authors or contact them at the following address:

Patricia Zadorosnei Rebutini, Postgraduate Program of Health Sciences, Pontifícia Universidade Católica do Paraná, Rua Imaculada Conceição, 1155, Prado Velho, Curitiba, Parana, Brazil

Return Address

Send To

Authors Editors

Comments

10000 character(s) remaining.

Send

Top

Page created: November 09, 2020
Page updated: January 24, 2021
Page reviewed: January 24, 2021

Centers for Disease Control and Prevention

ISSN: 1080-6059

Copyright

Emerging Infectious Diseases is published by the Centers for Disease Control and Prevention, a U.S. Government agency. Therefore, materials published in *Emerging Infectious Diseases*, including text, figures, tables, and photographs are in the public domain and can be reprinted or used without permission with proper citation.

Open Access and Usage

Emerging Infectious Diseases is an open access journal in the public domain. All content is freely available without charge to users or their institutions. In accordance with the Budapest Open Access Initiative definition of Open Access, users are allowed to read, download, copy, distribute, print, search, or link to the full texts of the articles, or use them for any other lawful purpose, without asking prior permission from the publisher or the author. Because the journal is in the public domain, its usage policy also conforms to conditions set for by Creative Commons.

Emerging Infectious Diseases requests a proper citation be included for its content and that any user indicate clearly if changes have been made. Each article includes citation information.

Emerging Infectious Diseases grants authors permission to self-archive their articles without fees or permission and grants institutions permission to preserve a second copy of articles published by their researchers in the institutional repository.

Disclaimer

The conclusions, findings, and opinions expressed by authors contributing to this journal do not necessarily reflect the official position of the U.S. Department of Health and Human Services, the Public Health Service, the Centers for Disease Control and Prevention, or the authors' affiliated institutions.

Use of trade names is for identification only and does not imply endorsement by the Public Health Service or by the U.S. Department of Health and Human Services.

Registration

EMERGING INFECTIOUS DISEASES® is a registered service mark of the U.S. Department of Health and Human Services. Its Registration Number 4,972,553 is issued by the United States Patent & Trademark Office (USPTO).

Page created: February 04, 2010
Page updated: April 22, 2021
Page reviewed: April 22, 2021

The conclusions, findings, and opinions expressed by authors contributing to this journal do not necessarily reflect the official position of the U.S. Department of Health and Human Services, the Public Health Service, the Centers for Disease Control and Prevention, or the authors' affiliated institutions. Use of trade names is for identification only and does not imply endorsement by any of the groups named above.

ANEXO 3 – Produção adicional: artigo intitulado *Placental Morphologic Similarities Between ZIKV-Positive and HIV-Positive Pregnant Women* no periódico *Frontiers in Immunology* em junho de 2021 e política de direitos autorais do periódico/editora.

frontiers in Immunology

PERSPECTIVE
published: 09 June 2021
doi: 10.3389/fimmu.2021.684194

Placental Morphologic Similarities Between ZIKV-Positive and HIV-Positive Pregnant Women

Daiane Cristine Martins Ronchi[1], *Mineia Alessandra Scaranello Malaquias*[1], *Patrícia Zadorosnei Rebutini*[1], *Letícia Arianne Panini do Carmo*[1], *Plínio Cézar Neto*[1], *Emily Scaranello Marini*[1], *Amanda Prokopenko*[1], *Seigo Nagashima*[1], *Camila Zanluca*[2], *Claudia Nunes Duarte dos Santos*[2] *and Lúcia de Noronha*[1]*

[1] Laboratory of Experimental Pathology, Postgraduate Program of Health Sciences, School of Medicine, Pontifícia Universidade Católica do Paraná, Curitiba, Brazil, [2] Molecular Virology Laboratory, Instituto Carlos Chagas, Fundação Oswaldo Cruz, Curitiba, Brazil

OPEN ACCESS

Edited by:
Ashley L. St John,
Duke-NUS Medical School,
Singapore

Reviewed by:
Elizabeth Ann Lieser Enninga,
Mayo Clinic, United States
Nicholas Lennemann,
University of Alabama at Birmingham,
United States

***Correspondence:**
Lúcia de Noronha
lnno.noronha@gmail.com

Specialty section:
This article was submitted to Viral Immunology, a section of the journal Frontiers in Immunology

Received: 22 March 2021
Accepted: 19 May 2021
Published: 09 June 2021

Citation:
Martins Ronchi DC, Scaranello Malaquias MA, Rebutini PZ, Panini do Carmo LA, Neto PC, Marini ES, Prokopenko A, Nagashima S, Zanluca C, Duarte dos Santos CN and de Noronha L (2021) Placental Morphologic Similarities Between ZIKV-Positive and HIV-Positive Pregnant Women. Front. Immunol. 12:684194. doi: 10.3389/fimmu.2021.684194

Zika virus (ZIKV) caused global concern due to Brazil's unexpected epidemic, and it was associated with congenital microcephaly and other gestational intercurrences. The study aimed to analyze the placenta morphometric changes of ZIKV-infected pregnant women (ZIKV group; n = 23) compared to placentas of HIV-infected (HIV group; n = 24) and healthy pregnant women (N-control group; n = 22). It also analyzed the relationship between the morphometric results and pathological alterations on conventional microscopy, gestational trimester of infection, and presence of the congenital Zika syndrome (CZS). There was a significant increase in area ($p = 0.0172$), as well as a higher number of knots ($p = 0.0027$), sprouts ($p < 0.0001$), and CD163 +Hofbauer cells (HCs) ($p < 0.0001$) in the ZIKV group compared to the N-control group, suggesting that villous dysmaturity and HCs hyperplasia could be associated with ZIKV infections. The HIV group had a higher area ($p < 0.0001$), perimeter ($p = 0.0001$), sprouts ($p < 0.0001$), and CD163 + HCs ($p < 0.0001$) compared to the N-control group, demonstrating that the morphometric abnormalities found in the ZIKV and HIV group are probably similar. However, when ZIKV and HIV groups are compared, it was observed a higher number of sprouts ($p = 0.0066$) and CD163+ HCs ($p < 0.0001$) in the first one, suggesting that placental ZIKV congenital changes could be more pronounced.

Keywords: Zika virus, HIV, vertical transmission, placenta, morphometric analysis

INTRODUCTION

During pregnancy, Zika virus (ZIKV) infection has been associated with fetal malformations, such as microcephaly, lissencephaly, cerebellar hypoplasia, hydrocephalus, polymicrogyria, abnormal development of the corpus callosum, and changes in neuronal migration and subcortical calcifications that configure the Congenital Zika Syndrome (1–9).

Recently, ZIKV caused global concern due to the unexpected epidemic of infection in Brazil, associated with congenital microcephaly and abortions, both of which have been more common

when ZIKV infection occurred during the first trimester of gestation. Besides, severe cerebral malformations have not been described when the infection occurred in the third trimester, suggesting that the brain's abnormal development associated with ZIKV could become the organogenesis period (10, 11).

CZS has been associated with placental alterations like an increase in the number of syncytial knots and sprouts, stromal disorders, villous immaturity, Hofbauer cells (HCs) hyperplasia, and vascular abnormalities (12, 13). The direct infection and replication of ZIKV in placenta tissues can be triggered by the infection of HCs (placental macrophage) in the chorionic villi (10). HCs appear to be the most frequently observed ZIKV-positive cells in the naturally infected human placentas and also may remain persistently infected until delivery. Even in the placenta samples with a short interval between the acute phase of infection and delivery time, ZIKV appears to be detected exclusively in HCs. Furthermore, villous immaturity may be related to congenital disorders caused by ZIKV infection, and it is also associated with an increase in HCs. The persistence of ZIKV-positive HCs in full-term placentas may indicate that these cells could provide a viral source for continued fetal infection and may be responsible for the transplacental transmission mediated by its migratory ability to reach the fetal vessels (12).

Human immunodeficiency virus (HIV) has also been associated with abortion, stillborn, preterm delivery, and other gestational intercurrences, but not with the congenital syndrome. However, the effects of HIV on the placentas remain poorly understood. The main target of HIV is CD4 T lymphocytes, but other cells expressing CD4 are also infected, like monocytes, macrophages, and dendritic cells, where HCs are included. Some of the alterations described include chorioamnionitis and deciduitis, and villitis, an increase in the number of syncytial knots and sprouts, stromal disorders like fibrin deposition and fibrosis, abnormalities of the villous maturation and infarction. Other authors have described placentas of HIV-infected pregnant with no pathological alterations on the conventional microscopy. On the other hand, morphometric techniques have usually shown alterations in villus diameter and perimeter, suggesting changes in villous maturation (14–18).

Given that, despite having different vertical transmission routes and outcomes, both HIV and ZIKV may produce similar morphological changes in placental tissues, such as villous immaturity and hyperplasia of HCs. Severe villitis, for example, does not appear to be a common form of placental injury in both cases. In addition, these two viruses can break through the placental barrier causing only subtle morphological alterations, resulting in placentas of the usual histological aspect under conventional microscopy (14–18).

Because of this, the present study aimed to analyze the placental morphometric changes in ZIKV-infected pregnant women and compare these changes with that found in HIV-infected pregnant women, considering gestational trimester of infection, presence of CZS, and pathological alterations on conventional microscopy as variables. In addition, this study also compares both groups (ZIKV and HIV) to the placentas of healthy (non-infected) pregnant women.

MATERIALS AND METHODS

Ethical Approvals

The Brazilian National Ethics Committee approved the presented study under the number CAAE: 42481115.7.0000.5248. The authors confirm that all methods were carried out following relevant guidelines and regulations. Furthermore, the sample collection followed all relevant ethics and safety protocols. The data that support the findings of this study are available from the corresponding author upon reasonable request.

Samples

The ZIKV-infected placenta group (ZIKV group) comprises 23 placentas that were formalin-fixed paraffin-embedded (FFPE) (12). The 23 patients gave birth to 15 term healthy and eight malformed babies, between 34 and 40 gestational weeks (average = 38; median = 38; SD = 2.17). All the 15 term healthy babies (37–40 gestational weeks) are alive. Of the eight malformed babies, five were preterm (34–36 gestational weeks). Still, regarding this group of malformed babies, four of them are alive, two had perinatal death and two were stillborn. The 23 mothers have at least two positive tests for ZIKV infection: anti-ZIKV IgM positive in the maternal blood and/or colostrum, positive RT-PCR in the maternal blood and/or urine, positive RT-PCR in the frozen placenta samples, positive RT-PCR and/or immunohistochemical test in the FFPE placenta samples. The newborn/stillborn additional samples were also positive: brain tissue RT-PCR and anti-ZIKV IgM in the blood (12).

The HIV-infected placenta group (HIV group) consisted of 24 FFPE placenta samples of HIV-positive pregnant women with no comorbidities. Pregnant women gave birth to healthy newborns between 33 and 40 weeks (average = 38.08; median = 38; SD = 1.99) of gestation in 2004 to 2005, when ZIKV was not circulating in Brazil. The placentas showed no pathological changes on the conventional microscopy. We did not observe villous maturation changes, and weights of the newborns were normal for gestational age (average = 2789.29 g; median = 2730 g; SD = 497.19 g; min-max = 1780–3890 g). Maternal age of this group ranged from 17 to 42 years (average = 26; median = 26; SD = 6.53). The placentas were from pregnant women who had been diagnosed with HIV before or during their pregnancy. The newborns were followed up until their HIV infection condition was defined as negative. All the babies are alive e HIV-seronegative. The viral loads and CD4/CD8 ratio were measured three to six times for most patients. The viral loads ranged from 13047.5 to 5760 (copies), and the CD4/CD8 ratio ranged from 0.65 to 0.35 during the 9 months of pregnancy. Antiretroviral therapy was administered at least 1 month before the birth in all patients (16).

The non-infected placenta group (N-control group) comprises 22 pregnant women that had prenatal without comorbidities. They gave birth to healthy newborns, between 34 and 40 gestational weeks (average = 38.19; median = 38; SD = 1.65), from 2004 to 2005, when ZIKV was not circulating in Brazil. The placentas did not present anatomopathological alterations. We did not observe villous maturation changes,

and weights of the newborns were normal for gestational age (average = 2957.27 g; median = 2887.5 g; SD = 762.63 g; min–max = 1770–4410 g). Maternal age of this group ranged from 15 to 40 years (average = 26.06; median = 24; SD = 7.14). The pregnant woman and the newborn were followed up until discharge from the hospital (16).

The samples of three groups were matched by gestational age, which varied from 33 to 38 weeks. All the pregnant women were submitted to laboratory tests for congenital intrauterine infections (*TORCH = toxoplasmosis, rubella, cytomegalovirus, syphilis, and herpes*) with negative results. Analysis of gestational age showed no significant differences between the groups.

Morphometric Analysis

Histological sections of all placentas were stained with hematoxylin & eosin (H&E) to evaluate the perimeter, diameter, and area of villi, the number of sprouts, syncytial knots, and villi numbers per medium power field (MPF). H&E sections were photographed at a magnification of 200× (MPF) using the Scanner Axion Scan.Z1, generating an average of 5,000 images. Unfocused, with artifacts, non-villous tissue representative (membranes, cord, decidua) images were excluded. The remaining images selected (about 1,000) had 100% of the field occupied with placental villi and were randomized to obtain about 100 images for each case of the three groups.

For all placentas, the perimeter, diameter, area of the villi, and basal membrane thickness were measured using Image-Pro Plus® 4 software, based on freehand drawing on 100 consecutive villi. After freehand villus' contour, the program provided perimeter, diameters (major), area, and basal membrane thickness in micrometers or square micrometers ($\mu m/\mu m^2$) (16).

To evaluate the syncytial knots and sprouts per villi, the same 100 MPF/H&E images were used and submitted to simple counting of these microscopic structures (12).

Immunohistochemical Analysis

Histological sections of the placentas were fixed on electrically charged glass slides and subsequently dewaxed with heated xylol (37°C), dehydrated with successive baths of absolute ethyl alcohol, and rehydrated with water. Methyl alcohol and hydrogen peroxide were used to block endogenous peroxidase and distilled water and hydrogen peroxide for the second block. They were incubated with anti-CD163 primary antibody (type: polyclonal/rabbit; clone/code: 14215; dilution: 1:1000; source: Thermo Fisher) for 1 h and with secondary antibody associated with the dextran polymer (Spring Bioscience, Pleasanton, USA) for 30 min. DAB/substrate complex (DAB, DakoCytomation) was added onto the slides, followed by counterstaining with Mayer's hematoxylin, dehydration with ethyl alcohol baths, clarification with xylol, and blending with Canada balsam (12).

The 30 HPF (high power field = 400×) were analyzed by counting the number of villi and CD163+ HCs per villi in all three study groups.

The images were obtained from random sample regions without the interference of an observer. The morphometric measurements and the score of CD163 positive cells were performed blindly.

Statistical Analyses

The results were described by means, standard deviations, medians, minimum, and maximum values. The comparison of the groups concerning quantitative variables was performed using the non-parametric Kruskal-Wallis test or t-test. The Shapiro-Wilk test evaluated the normality condition. Values of $p < 0.05$ indicated statistical significance. The data were analyzed using the IBM SPSS Statistics v.20.0 software. Armonk, NY, USA: IBM Corp.

RESULTS

Morphometric Alterations of the HIV and ZIKV Groups

The analysis of the area ($p = 0.0172$) and the number of knots ($p = 0.0027$), sprouts ($p < 0.0001$), and CD163+ HCs ($p < 0.0001$) in the ZIKV group demonstrated larger immature chorionic villi with a higher number of knots and sprouts and HCs hyperplasia when compared with the N-control group (**Figure 1** and **Supplementary Figure 1**).

HIV group placentas with no pathological alterations on conventional microscopy also showed changes in villous maturation and HC hyperplasia by morphometry analysis compared to the N-control group. The area ($p < 0.0001$), perimeter (p = 0.0001), number sprouts ($p < 0.0001$), and CD163+ HCs ($p < 0.0001$) of HIV group were higher than the N-control group (**Figure 1** and **Supplementary Figure 1**).

The ZIKV group placentas showed higher values of the number of sprouts ($p < 0.0066$) and CD163+ HCs ($p < 0.0001$) compared to the HIV group (**Figure 1** and **Supplementary Figure 1**).

Trimester of ZIKV Infection

Morphometric analyses were performed in placental samples from mothers who were infected with ZIKV during the first (n = 4), second (n = 8), and third trimesters of pregnancy (n = 6). In five placenta samples, the trimester of infection was unknown. The perimeter ($p = 0.0292$), number of knots ($p = 0.0062$), sprouts ($p < 0.0001$), and CD163+ HCs ($p < 0.0001$) showed significant differences by the trimester of infection. The most relevant differences were observed between the second trimester and third trimester of infection versus the N-control group, revealing second-/third-trimester ZIKV placentas with villous dysmaturity and HCs hyperplasia compared to the control placentas (**Table 1**).

Pathological Alterations

ZIKV group placentas with and without pathological alterations by conventional microscopy were compared. It was observed that placentas with pathological changes presented higher diameter ($p = 0.0226$), perimeter ($p = 0.0212$), number of knots ($p = 0.0101$), number of sprouts ($p < 0.0001$), and CD163+ HCs ($p < 0.0001$) compared to placentas without pathological alterations (**Table 1**). However, placentas considered within normal standards also presented morphometric changes characterized by higher area, perimeter, number of knots, sprouts, and CD163+ HCs compared to the N-control group ($p < 0.05$).

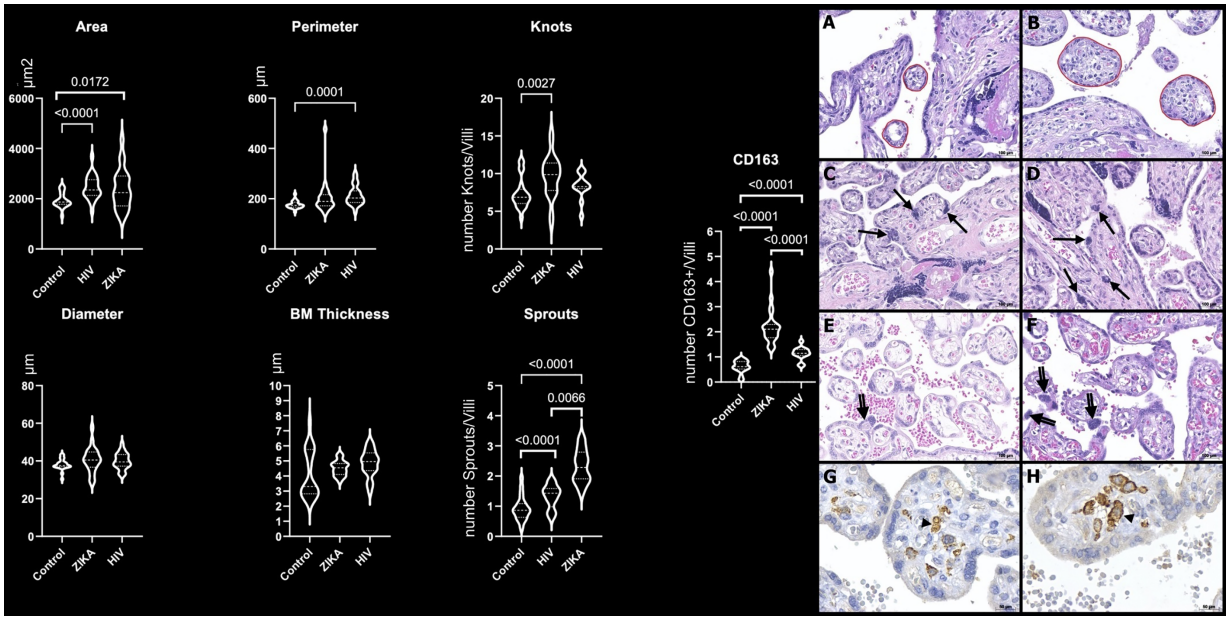

FIGURE 1 | Morphometric analysis of placental specimens from women infected with ZIKV during the pregnancy compared to the HIV and N-control groups. Perimeter, diameter, and basal membrane (BM) thickness in μm; area in μm^2; number of knots, sprouts, and CD163+ HCs per villi (CD163/villi). Photomicrography of a placental sample stained with H&E showing the perimeter of villi (red freehand drawing) in N-control group **(A)** and ZIKV group **(B)**; the number of syncytial knots/villi (arrows) in N-control group **(C)** and ZIKV-group **(D)**; the number of sprouts/villi (double arrows) in N-control group **(E)** and ZIKV group **(F)**. Original magnification: 200×. Scale bars: 100 μm. Photomicrography of immunostaining with CD163 highlighting Hofbauer cell (arrowhead) in the N-control group **(G)** and ZIKV group **(H)**. Original magnification: 400×. Scale bars: 50 μm.

Congenital Zika Syndrome

The status of the newborns (with or without CZS) was also analyzed. The diameter ($p = 0.0109$), area ($p = 0.0102$), perimeter ($p = 0.0035$), number of knot ($p = 0.0054$), number of sprouts ($p < 0.0001$), and CD163+ HCs ($p < 0.0001$) were higher in placentas of newborns with CZS compared with placentas of newborns without this condition (**Table 1**).

DISCUSSION

Morphometric Alterations of HIV and ZIKV Groups

The findings showed significant enlargement of the area of the ZIKV group when compared with the N-control group. A higher number of knots, sprouts, and CD163+ HCs were also noticed.

Syncytial knots are syncytiotrophoblasts' specializations, and their severe increase in late gestation indicates early maturation (12). Syncytial sprouts are markers of trophoblast proliferation; they are seen frequently during early pregnancy and are increased in the villous dysmaturity (19, 20).

HCs, the most frequently ZIKV-positive cells, are placental villous macrophages of fetal origin, and alterations in their numbers (hyperplasia) and biological features are associated with complications in pregnancy. HCs play a role in diverse functions, such as placental vasculogenesis, immune regulation, and the secretion of enzymes and cytokines across the maternal-fetal barrier. In addition, there is some evidence suggesting the involvement of HCs in the development of placental villi (12).

This study's findings corroborate with studies that showed a delay in villous maturation and signs of the HCs hyperplasia in ZIKV-infected placentas. These alterations could damage the chorionic villi, such as calcification, necrosis, Wharton jelly sclerosis, fibrin deposition, and a significant villi size increase (11, 21–23). We could conclude that all of the anatomopathological parameters could be confirmed by the morphometric data and may be used to describe ZIKV-infected placentas.

Other findings showed that the HIV group had a larger area, perimeter, number of sprouts, and CD163+ HCs compared to the N-control group. Studies also revealed that placentas exposed to HIV infection exhibited the following microscopic features: edema, villous immaturity, focal necrosis of trophoblasts, numerous HCs, intervillous fibrin deposition, and chorangiosis (17, 18, 24). However, when those patterns are subtle or minimal, pathologists cannot make the diagnosis. Given that, morphometric techniques may be helpful to identify subtle abnormalities.

Rabelo et al. (22) showed ZIKV NS1 protein in the decidual and endothelial cells of the maternal decidua and CTB, STB, and HCs in the third trimester placental tissues associated with an HIV-exposed, but uninfected, infant with severe congenital Zika syndrome. Nonetheless, the maternal HIV infection could have contributed to the permissiveness of other placental cell types to ZIKV infection.

Finally, when both groups (ZIKV and HIV) were compared, no statistically significant results were found, except for the number of

TABLE 1 | Median (max-min) and *p*-value of morphometric data in the gestational trimester of infection, presence of placenta pathological alterations, and CZS.

Variables	N-CONTROL	Gestational Trimester of Infection†			Pathological Alterations of Placenta on Conventional Microscopy§		Congenital Zika Syndrome*	
		First (n = 4)	Second (n = 8)	Third (n = 6)	No (n = 15)	Yes (n = 8)	No (n = 15)	Yes (n = 8)
Diameter (μm)	37.6 (43.4–30.4)	38.3 (46.3–29.1)	40.2 (45.3–32.1)	39.8 (44.6–29.1)	40.1 (50.6–29.1)	44.9 (57.7–36.6)	40.0 (45.3–29.1)	45.5 (57.7–36.6)
			NS		**0.0226**		**0.0109**	
Area (μm^2)	1867 (2496–1314)	1812.9 (3536.9–1228.8)	2119.4 (2927.2–1377.9)	2241.8 (2917.7–1527.3)	2165.1 (3671.2–1228.8)	2907.4 (4354.4–1673.3)	2119.4 (2927.2–1228.8)	2897.1 (4354.4–1673.3)
			NS		NS		**0.0102**	
Perimeter (μm)	174 (219–148)	174.2 (237.2–142.2)	182.1 (477.7–163.2)	186.2 (203.8–154.3)	181.2 (477.7–142.2)	208.9 (257.6–163.2)	180.3 (477.7–142.2)	214.0 (257.6–176.9)
			0.0292[a]		**0.0212**		**0.0035**	
Number of knots/villi	6.9 (11.7–4.2)	9.9 (11.6–7.9)	11.1 (14.3–9.3)	8.6 (15.5–4.7)	9.8 (15.5–4.7)	10.2 (11.6–3.5)	10.1 (15.5–4.7)	9.8 (11.6–3.5)
			0.0062[a]		**0.0101**		**0.0054**	
Number of sprouts/villi	0.9 (1.9–0.3)	1.9 (3.2–1.6)	2.4 (3.1–1.4)	2.1 (2.6–1.8)	2.4 (3.2–1.6)	2.0 (3.3–1.4)	2.2 (3.2–1.4)	2.8 (3.3–1.7)
			<0.0001[b]		**<0.0001**		**<0.0001**	
Number of cells CD163+/villi	0.6 (1.0–0.1)	2.7 (3.3–2.0)	2.2 (2.3–1.7)	1.9 (2.3–1.7)	2.0 (2.4–1.3)	2.5 (4.4–1.7)	2.0 (2.4–1.3)	2.8 (4.4–1.4)
			<0.0001[c]		**<0.0001**		**<0.0001**	

Analysis only for the ZIKV group.

†Five cases of unknown gestational trimester.

§Main pathological findings: umbilical artery agenesis (1), mild acute funisitis (1), and villous immaturity (6).

**Major central nervous malformations: microcephaly (3), spina bifida (1), hydrocephalus (2), and encephalocele (1).*

[a]p value refers to the second trimester vs. N-control.

[b]p-value refers to the e third trimester vs. N-control and first vs. the third trimester.

[c]p-value refers to the third trimester vs. N-control; first vs. the second and third trimester. Kruskal-Wallis test and t-test; values of $p < 0.05$ indicated statistical significance.

NS, not significant p-value.

Bold values = Statistically significant values.

sprouts and CD163+ HCs higher in the ZIKV group. Thus, it seems that HCs hyperplasia and sprouting/dysmaturity villi may be more pronounced and characteristic in the ZIKV-infected placentas (12, 17). Even though placental changes, such as dysmaturity and hyperplasia of HCs, can be seen in other maternal-fetal diseases, such as congenital infections (TORCH) and diabetes, in the absence of these comorbidities, this aspect may help the pediatric pathologists to suspect the diagnosis of ZIKV vertical transmission. This study also demonstrates that the morphometrical abnormalities finding in ZIKV and HIV groups are very similar, despite having different vertical transmission routes and outcomes since ZIKV is a teratogenic virus and HIV is not. In addition, vertical HIV transmission is much rarer than that of ZIKV, but it can increase perinatal and intrauterine deaths (**Supplementary Figure 1**) (14, 17, 18).

Trimester of ZIKV Infection

When the gestational trimester of infection was analyzed, it was observed that most of the differences between the ZIKV and N-control groups appear to be when infection occurred in the second or third trimester. Since all newborns of this study were in the third trimester (term or preterm), the shorter time that elapsed between the moment of ZIKV infection and the birth may be an explanation for more pronounced changes in these placentas.

The number of HCs also showed differences between groups, suggesting that these cells may have early hyperplasia, and this hyperplasia seems to be maintained throughout the gestational period, although it decreases in intensity over the months. This fact appears to agree with the hypothesis that these cells can work as a reservoir of ZIKV (12, 25).

Regardless of the trimester in which the infection occurred, as ZIKV is detected in placental cells until the end of pregnancy, it is plausible to speculate that the infection of the fetus could happen as a secondary event. In some cases, those abnormalities are only detected months after the delivery (20, 26–29).

Pathological Alterations

Fifteen of 23 ZIKV group placentas were diagnosed without pathological alterations for the pediatric pathologist. However, eight of them had pathological alterations on conventional microscopy, mainly villous immaturity. When placentas with and without pathological alterations were compared, placentas diagnosed with villous immaturity had a higher diameter, perimeter, number of knots, and CD163+ cells. This means that pathologists probably identified those alterations on conventional microscopy and, altogether, termed villous immaturity, so they did not need morphometry techniques to make these diagnoses.

On the other hand, ZIKV-group placentas with no pathological alterations also showed higher diameter, perimeter, and number of knots, sprouts, and CD163+ cells to the N-control group. Therefore, conventional microscopy cannot identify subtle alterations that morphometry could find.

Congenital Zika Syndrome

This study showed significant enlargement of the villi's diameter, area, and perimeter and the number of sprouts and CD163+ HCs in the group that had CZS. In addition, eight infants had fetal malformations related to ZIKV infection during pregnancy. However, 15 women had the onset of ZIKV symptoms during pregnancy and gave birth to infants without CZS.

This study observed that ZIKV causes essential alterations in the placenta's villous, leading to congenital disorders, stillborn, and neonatal death. We could also conclude that morphometric parameters may be biomarkers for CZS since they are more pronounced in malformed newborns. These data could help in the clinical follow-up of newborns with subclinical congenital disorders or even unapparent at birth.

In conclusion, there are placental dysmaturity alterations after ZIKV infection during pregnancy. Very similar placental alterations could be demonstrated on the HIV-infected pregnant women, but sprouting and HCs hyperplasia may be less pronounced in this group. Also, the morphometric analysis revealed villous dysmaturity even in placentas diagnosed within the usual standards by the routine exams. The second and third gestational trimester infections generated more villous dysmaturity and HCs hyperplasia than those pregnant women who became infected in the first trimester. In addition, placentas whose babies had CZS showed more pronounced changes than those without CZS. These alterations may help understand the aspect of ZIKV infection related to placental damage and congenital disabilities and possible deficiencies that might appear after birth.

DATA AVAILABILITY STATEMENT

The raw data supporting the conclusions of this article will be made available by the authors, without undue reservation.

ETHICS STATEMENT

The studies involving human participants were reviewed and approved by the ethics committee of the Oswaldo Cruz Foundation (Fiocruz) Brazilian National Ethics Committee of Human Experimentation. The patients/participants provided their written informed consent to participate in this study.

AUTHOR CONTRIBUTIONS

LN, CZ, and CNDS contributed to the study design. CZ performed the experiments. SN prepared the materials for analyses. DCMR, PZR, LAPC, PCN, and AP performed the morphometric analyses. PZR participated in the patient follow-up. MASM and ESM participated in sample identification/distribution. DCMR, MASM, PZR, and LN analyzed the results and wrote the manuscript. All authors contributed to the article and approved the submitted version.

FUNDING

This research was funded by Fiocruz, CNPq (439968/2016-0), CAPES Zika Fast Track 481-2016 (88887.116626/2016-01), and

Fundação Araucária (CP04/2016). CNDS and LN have a CNPq fellowship.

SUPPLEMENTARY MATERIAL

The Supplementary Material for this article can be found online at: https://www.frontiersin.org/articles/10.3389/fimmu.2021.684194/full#supplementary-material

Supplementary Figure 1 | Illustrative figure shows the morphometric differences between N-control and ZIKV group and between N-control and HIV group, respectively. However, it also represents similar morphometrics results when the ZIKV group was compared with the HIV group. The N-control group's syncytial membranes are more efficient in exchanges because the vessels are closer to the cytotrophoblast. In ZIKV- and HIV-infected placentas, villus increases in size, moving the vessel away from the trophoblast layer, distancing the syncytiotrophoblast membranes cause intrauterine death, premature, low birth weight babies, and/or other malformations. Created with www.biorender.com.

REFERENCES

1. Neu N, Duchon J, Zachariah P. TORCH Infections. *Clin Perinatol* (2015) 42 (1):77–103(viii). doi: 10.1016/j.clp.2014.11.001
2. Noronha Ld, Zanluca C, Azevedo ML, Luz KG, Santos CN. Zika Virus Damages the Human Placental Barrier and Presents Marked Fetal Neurotropism. *Mem Inst Oswaldo Cruz* (2016) 111(5):287–93. doi: 10.1590/0074-02760160085
3. Ayres CFJ. Identification of Zika Virus Vectors and Implications for Control. *Lancet Infect Dis* (2016) 16(3):278–9. doi: 10.1016/S1473-3099
4. Solomon IH, Milner DA, Folkerth RD. Neuropathology of Zika Virus Infection. *J Neuroinfect Dis* (2016) 7(2):220. doi: 10.4172/2314-7326.1000220
5. Hughes BW, Addanki KC, Sriskanda AN, McLean E, Bagasra O. Infectivity of Immature Neurons to Zika Vírus: A Link to Congenital Zika Syndrome. *EBioMedicine* (2016) 10):65–70. doi: 10.1016/j.ebiom.2016.06.026
6. Oehler E, Watrin L, Larre P, Leparc-Goffart I, Lastère S, Valour F, et al. ZIKV Infection Complicated by Guillain-Barré Syndrome: Case Report, French Polinesia, December 2013. *Euro Surveill* (2014) 19(9):1–3. doi: 10.2807/1560-7917.es2014.19.9.20720
7. Brasil P, Pereira JP, Moreira ME, Nogueira RMR, Damasceno L, Wakimoto M, et al. Zika Virus Infection in Pregnant Women in Rio De Janeiro. *N Engl J Med* (2016) 375:2321–34. doi: 10.1056/NEJMoa1602412
8. Melo AS, Aguiar RS, Amorim MMR, Arruda MB, Melo FO, Ribeiro STC, et al. Congenital Zika Virus Infection: Beyond Neonatal Microcephaly. *JAMA Neurol* (2016) 73:1407–16. doi: 10.1001/jamaneurol.2016.3720
9. Schuler-Faccini L, Ribeiro EM, Feitosa IM, Horovitz DDG, Cavalcanti DP, Pessoa A, et al. Brazilian Medical Genetics Society–Zika Embryopathy Task Forceet. Possible Association Between Zika Virus Infection and Microcephaly–Brazil, 2015. Morb. *Mortal Wkly Rep* (2016) 65:59–62. doi: 10.15585/mmwr.mm6503e2
10. Petersen LR, Jamieson DJ, Powers AM, Honein MA. Zika Virus. Baden LR, Editor. *N Engl J Med* (2016) 374(16):1552–63. doi: 10.1056/NEJMra1602113
11. Bhatnagar J, Rabeneck DB, Martines RB, Reagan-Steiner S, Ermias Y, Estetter LBC, et al. Zika Vírus RNA Replication and Persistence in Brain and Placental Tissue. *Emerging Infect Dis* (2017) 23(3):405–14. doi: 10.3201/eid2303.161499
12. Noronha L, Zanluca C, Burger M, Suzukawa AA, Azevedo M, Rebutini PZ, et al. Zika Virus Infection At Different Pregnancy Stages: Anatomopathological Findings, Target Cells and Viral Persistence in Placental Tissues. *Front Microbiol* (2018) 9:2266. doi: 10.3389/fmicb.2018.02266
13. Souza AS, Dias CM, Braga FDCB, Terzian ACB, Estofolete CF, Oliani AH, et al. Fetal Infection by Zika Virus in the Third Trimester: Report of 2 Cases. *Clin Infect Dis* (2016) 63:1622–5. doi: 10.1093/cid/ciw613
14. Maartens G, Celum C, Lewin SR. HIV Infection: Epidemiology, Pathogenesis, Treatment, and Prevention. *Lancet* (2014) 384(9939):258–71. doi: 10.1016/S0140-6736(14)60164-1
15. Yang SW, Cho EH, Choi SY, Lee YK, Park JH, Kim MK, et al. Dc-SIGN Expression in Hofbauer Cells may Play an Important Role in Immune Tolerance in Fetal Chorionic Villi During the Development of Preeclampsia. *J Reprod Immunol* (2017) 124:30–7. doi: 10.1016/j.jri.2017.09.012
16. Baurakiades E, Martins APC, Moreschi V, Souza CDA, Abujamra K, Saito AO, et al. Histomorphometric and Immunohistochemical Analysis of Infectious Agents, T-cell Subpopulations and Inflammatory Adhesion Molecules in Placentas From HIV-seropositive Pregnant Women. *Diagn Pathol* (2011) 6:101. doi: 10.1186/1746-1596-6-101
17. López CL, Pires ARC, Fonseca EC, Rodrigues FR, Braga Neto AR, Herdy GVH, et al. Anatomopathological Characterization of Placentas From HIV+ Patients Associated With p24 Expression. *J Bras Patol Med Lab* (2013) 49 (6):437–45. doi: 10.1590/S1676-24442013000600010
18. Obimbo MM, Zhou Y, McMaster MT, Cohen CR, Qureshi Z, Ong'ech J, et al. Placental Structure in Preterm Birth Among HIV-positive Versus HIV-negative Women in Kenya. *J Acquir Immune Defic Syndr* (2019) 80(1):94–102. doi: 10.1097/QAI.0000000000000187
19. Loukeris K, Sela R, Baergen RN. Syncytial Knots as a Reflection of Placental Maturity: Reference Values for 20 to 40 Weeks Gestational Age. *Pediatr Dev Pathol* (2010) 13:305–9. doi: 10.2350/09-08-0692-OA.1
20. Aagaard KM, Lahon A, Suter MA, Arya RP, Seferovic MD, Vogt MB, et al. Primary Human Placental Trophoblasts are Permissive for Zika Virus (ZIKV) Replication. *Sci Rep* (2017) 7:41389. doi: 10.1038/srep41389
21. Tabata T, Petitt M, Puerta-Guardo H, Michlmayr D, Wang C, Fang-Hoover J, et al. Zika Virus Targets Different Primary Human Placental Cells, Suggesting Two Routes for Vertical Transmission. *Cell Host Microbe* (2016) 20(2):155–66. doi: 10.1016/j.chom.2016.07.002
22. Rabelo K, Fernandes RCSC, Souza LJ, Souza TL, Santos FB, Nunes PCG, et al. Placental Histopathology and Clinical Presentation of Severe Congenital Zika Syndrome in a Human Immunodeficiency Virus-Exposed Uninfected Infant. *Front Immunol* (2017) 8:1704. doi: 10.3389/fimmu.2017.01704
23. Zare Mehrjardi M, Shobeirian F. The Role of the Placenta in Prenatally Acquired Zika Virus Infection. *Virus Dis* (2017) 28(3):247–9. doi: 10.1007/s13337-017-0399-z
24. Anderson VM. The Placental Barrier to Maternal HIV Infection. *Obstet Gynecol Clin North Am* (1997) 24(4):797–820. doi: 10.1016/s0889-8545(05)70345-4
25. Zanluca C, De Melo VCA, Mosimann ALP, dos Santos GIV, dos Santos CND, Luz K. First Report of Autochthonous Transmission of Zika Virus in Brazil. *Mem Inst Oswaldo Cruz* (2015) 110(4):569–72. doi: 10.1590/0074-02760150192
26. Aragão M, Holanda A, Brainer-Lima A, Petribu NCL, Castillo M, van der Linden V, et al. Nonmicrocephalic Infants With Congenital Zika Syndrome Suspected Only After Neuroimaging Evaluation Compared With Those With Microcephaly At Birth and Postnatally: How Large is the Zika Virus "Iceberg"? *AJNR Am J Neuroradiol* (2017) 38:1427–34. doi: 10.3174/ajnr.A5216
27. Ventura L, Ventura C, Lawrence L, van der Linden V, van der Linden A, Gois AL, et al. Visual Impairment in Children With Congenital Zika Syndrome. *J AAPOS* (2017) 21:295–9. doi: 10.1016/j.jaapos.2017.04.003
28. Luo H, Winkelmann ER, Fernandez-Salas I, Li L, Mayer SV, Danis-Lozano R, et al. Zika, Dengue and Yellow Fever Viruses Induce Differential Anti-Viral Immune Responses in Human Monocytic and First Trimester Trophoblast Cells. *Antiviral Res* (2018) 151:55–62. doi: 10.1016/j.antiviral.2018.01.003
29. Sheridan MA, Yunusov D, Balaraman V, Alexenko AP, Yabe S, Verjovski-Almeida S, et al. Vulnerability of Primitive Human Placental Trophoblast to Zika Virus. *Proc Natl Acad Sci* (2017) 114(9):E1587–96. doi: 10.1073/pnas.1616097114

Conflict of Interest: The authors declare that the research was conducted in the absence of any commercial or financial relationships that could be construed as a potential conflict of interest.

1. Frontiers Policies

1.1. Open Access and Copyright

All Frontiers articles from July 2012 onwards are published with open access under the CC-BY Creative Commons attribution license (the current version is CC-BY, version 4.0). This means that the author(s) retains copyright, but the content is free to download, distribute, and adapt for commercial or non-commercial purposes, given appropriate attribution to the original article.

Upon submission, the author(s) grants Frontiers a license to publish, including to display, store, copy, and reuse the content. The CC-BY Creative Commons attribution license enables anyone to use the publication freely, given appropriate attribution to the author(s) and citing Frontiers as the original publisher. The CC-BY Creative Commons attribution license does not apply to third-party materials that display a copyright notice to prohibit copying. Unless the third-party content is also subject to a CC-BY Creative Commons attribution license, or an equally permissive license, the author(s) must comply with any third-party copyright notices.

This page is available in the following languages:

Creative Commons License Deed

Attribution 4.0 International (CC BY 4.0)

This is a human-readable summary of (and not a substitute for) the license.

You are free to:

Share — copy and redistribute the material in any medium or format

Adapt — remix, transform, and build upon the material

for any purpose, even commercially.

The licensor cannot revoke these freedoms as long as you follow the license terms.

Under the following terms:

Attribution — You must give appropriate credit, provide a link to the license, and indicate if changes were made. You may do so in any reasonable manner, but not in any way that suggests the licensor endorses you or your use.

No additional restrictions — You may not apply legal terms or technological measures that legally restrict others from doing anything the license permits.

Notices:

You do not have to comply with the license for elements of the material in the public domain or where your use is permitted by an applicable exception or limitation.

No warranties are given. The license may not give you all of the permissions necessary for your intended use. For example, other rights such as publicity, privacy, or moral rights may limit how you use the material.

ANEXO 4 – Produção adicional: artigo intitulado *Downregulation of IGF 2 expression in third trimester placental tissues from Zika virus infected women in Brazil* no periódico *Journal of Infection* em setembro de 2020 e política de direitos autorais do periódico/editora.

Journal of Infection 81 (2020) 766–775

Contents lists available at ScienceDirect

Journal of Infection

journal homepage: www.elsevier.com/locate/jinf

Downregulation of *IGF2* expression in third trimester placental tissues from Zika virus infected women in Brazil

Andréia A. Suzukawa[a,1], Camila Zanluca[a,1], Natasha A.N. Jorge[b,1], Lucia de Noronha[c,1], Andrea C. Koishi[a], Caroline B.V. de Paula[c], Patrícia Z. Rebutini[c], Seigo Nagashima[c], Aruana F.F. Hansel-Frose[d], Vinícius S.C. Parreira[d], Juliano Bordignon[a], Margaret R. MacDonald[e], Charles M. Rice[e], Fabio Passetti[d,*], Claudia Nunes Duarte dos Santos[a,*]

[a] *Laboratório de Virologia Molecular, Instituto Carlos Chagas, Fundação Oswaldo Cruz, Curitiba, PR, Brazil*
[b] *Bioinformatics Group, Department of Computer Science, and Interdisciplinary Center for Bioinformatics, D-04107 Leipzig, Germany*
[c] *Laboratório de Patologia Experimental, Pontifícia Universidade Católica do Paraná, Curitiba, PR, Brazil*
[d] *Laboratório de Regulação da Expressão Gênica, Instituto Carlos Chagas, Fundação Oswaldo Cruz, Curitiba, PR, Brazil*
[e] *Laboratory of Virology and Infectious Disease, The Rockefeller University, New York, NY 10065, USA*

ARTICLE INFO

Article history:
Accepted 23 September 2020
Available online 26 September 2020

Keywords:
Zika virus
Placenta
Transcriptome
Insulin-Like Growth Factor II
Decidua

SUMMARY

Objectives: Screening for genes differentially expressed in placental tissues, aiming to identify transcriptional signatures that may be involved in ZIKV congenital pathogenesis.
Methods: Transcriptome data from placental tissues of pregnant women naturally infected with Zika virus during the third trimester were compared to those from women who tested negative for Zika infection. The findings were validated using both a cell culture model and an immunohistochemistry/morphological analysis of naturally infected placental tissues.
Results: Transcriptome analysis revealed that Zika virus infection induces downregulation of insulin-like growth factor II (*IGF2*) gene, an essential factor for fetal development. The Caco-2 cell culture model that constitutively expresses *IGF2* was used for the transcriptome validation. Asiatic and African Zika virus strains infection caused downregulated *IGF2* gene expression in Caco-2 cells, whereas other flaviviruses, such as dengue serotype 1, West Nile and wild-type yellow fever viruses, had no effect on this gene expression. Immunohistochemical assays on decidual tissues corroborated our transcriptome analysis, showing that IGF2 is reduced in the decidua of Zika virus-infected women.
Conclusions: Our results draw attention to *IGF2* modulation in uterine tissues, and this finding is expected to support future studies on strategies to ameliorate the harmful effects of Zika virus infection during pregnancy.

Introduction

Zika virus (ZIKV) is an emerging arbovirus belonging to the genus *Flavivirus*, family *Flaviviridae*, which includes other viruses relevant to public health, such as dengue (DENV), yellow fever (YFV) and West Nile (WNV) viruses. Although ZIKV infection in humans is often characterized as a self-limiting disease,[1,2] infections during pregnancy can lead to fetal malformations and neurodevelopment abnormalities.[3–5]

A major worldwide effort is underway to shed light on different aspects of ZIKV infection in humans; however, the mechanisms by which ZIKV is transmitted to intrauterine tissues, the target cell types it affects and its effects on placental tissues are not completely clear.

By the study from mice and monkeys cells and tissues and from human *ex vivo* models, significant progress has been made in the characterization of genes differentially regulated during ZIKV infection, highlighting the host response to infection during pregnancy, which mainly involves the immune and inflammatory pathways.[6–9]

* Corresponding authors.
E-mail addresses: fabio.passetti@fiocruz.br (F. Passetti), claudia.dossantos@fiocruz.br (C.N. Duarte dos Santos).
[1] AAS, CZ, NANJ, and LN contributed equally to this work.

https://doi.org/10.1016/j.jinf.2020.09.028

Although the information obtained from these studies is relevant and helps to advance knowledge on ZIKV-induced congenitally abnormal outcomes, many of these studies were performed under controlled conditions, and the overall context of a natural infection route cannot be reproduced.

Here, the transcriptome profile of placental tissues from pregnant women naturally infected with ZIKV during the third trimester of gestation were compared to placental tissues with no evidence of ZIKV infection. Despite the intrinsic genetic differences and the restricted panel of samples, we were able to identify more than a thousand differentially expressed genes in the ZIKV-positive placenta tissues. The transcriptome analysis showed a significant decrease in the gene expression of insulin-like growth factor II (*IGF2*) in the placental tissues from women with a confirmed ZIKV diagnosis.

Hormones, growth factors and nutrients in the maternal and fetal circulation regulate placental development. The insulin/insulin-like growth factor (IGF) system, which comprises the peptide hormones insulin, IGF1, IGF2, and IGF-binding proteins, is implicated in the tight regulation of fetal and placental growth.[10] In this context, IGF2 plays a fundamental role in fetal development, and its dysfunctional expression results in abnormal congenital outcomes.[11]

In recent years, substantial knowledge has been accumulated on ZIKV infection during pregnancy. Nevertheless, only a few articles using naturally infected human tissues have been published. To our knowledge, this is the first report of a placental transcriptome analysis of women infected by ZIKV at late stages of pregnancy.

In view of the severity of ZIKV infection during gestation, understanding of the host response to this infection through the analyses of gene modulation may open new avenues for Zika therapy, clinical management, and vaccine development.

Material and methods

Human samples and Ethics Approval

This study was approved by Fiocruz and the Brazilian National Ethics Committee of Human Experimentation under the number CAAE: 42481115.7.0000.5248 and was carried out in compliance with ethical principles. The waiver for written informed consent was obtained when the Molecular Virology Laboratory was identified as a Reference Center for the Diagnosis of Emerging Viruses by the Brazilian Ministry of Health.

Human placenta samples from ZIKV-infected pregnant women during the third trimester of gestation and women not infected with ZIKV (hereafter referred to as non-ZIKV) were obtained immediately after delivery. Fragments comprising both fetal and maternal tissues were kept frozen (without preservatives) for molecular purposes. Tissue sections were also formalin-fixed/paraffin embedded for further anatomopathological, morphometric and immunohistochemical analyses. ZIKV infection was confirmed either during the acute phase of disease or after delivery by molecular or immunohistochemical techniques. All the tests were performed in laboratories of the Brazilian public health network. Detailed clinical characterization of the ZIKV positive case series, including pathological and laboratory findings, had been previously described.[12] Briefly, all women included as ZIKV positive cases (LRV/16 284, LRV/16 848, LRV/16 854, LRV/16 859, LRV/16 927, and LRV/16 931) were likely infected during the 7^{th} or 8^{th} gestational month and delivered at term. No congenital disorder was observed at birth, and the placentas were either normal or showed mild pathological changes. Placentas comprised in non-ZIKV group (LRV/16 986, LRV/16 1094, LRV/16 1098, LRV/16 1121, LRV/16 1220, LRV/16 1387; LRV/18 560, and LRV/18 563) were those from patients who were either not suspected of infection or tested negative for ZIKV. All but one (LRV/16 1387) non-ZIKV placentas were delivered at term.

RNA-Seq and transcriptome data analysis

Total RNA from tissues was obtained following the manufacturer's instructions using an RNeasy kit (Qiagen, Hilden, Germany) with modifications. Briefly, 30 mg of tissue was disrupted in tubes with 5 mm metal beads under low temperature using two 2-minute cycles with 30 oscillations/minute in a TissueLyser LT (Qiagen) instrument. Tissue powder was resuspended in RTL buffer containing 10 µl/ml β-mercaptoethanol. A TRIzol reagent (Life Technologies, Rockville, MD) method was used and chloroform extraction performed prior to RNA purification using an RNeasy mini kit per the instruction manual. The quality and yield of the RNA samples were determined on a bioanalyzer platform using a total RNA nanoassay for eukaryotes (Agilent Technologies, Santa Clara, USA). Transcriptome libraries were prepared using the TruSeq Stranded Total RNA LT kit with Ribo-zero (Illumina, San Diego, USA). The 12 libraries were pooled together and sequenced in one lane of high-output 75 paired-end reads on an Illumina Next-Seq 500 sequencer.

The sequenced reads were aligned against the human genome GRCh37 sequence from Ensembl using HISAT2 version 2.1.0, retaining only the uniquely aligned reads (N:H:1 SAM flag) (parameters –dta, –fr, -q, –no-mixed, and –no-discordant). HTSeq version 0.10.0 with GENCODE (version 19) annotations of the human genome transcriptome was used to identify the expressed genes and infer the number of reads aligned to each gene (parameters: -t exon, -m intersection-nonempty, -r name, -i gene_id, and -s reverse). All statistical analyses were performed in R statistical software version 3.4.4 with DESeq2 version 1.18.1 and pheatmap version 1.0.12. The raw gene expression counts and DESeq2 were used to obtain the CPM values. Genes presenting a CPM count less than 20 in three or fewer samples were considered to be unexpressed and were removed from the analysis. We compared the normalized counts following the DESeq2 standard protocol and considered all genes presenting the $\log_2$ fold change (logFC) module $\geq$ 1.5 and an adjusted p-value $\leq$ 0.05 as differentially expressed. The differentially expressed genes (adjusted p-value $\leq$ 0.05) were used as input for the Bioconductor gage version 2.36 package.[13,14] This package selects up- and downregulated genes on which to perform 2 gene set enrichment analyses using the KEGG database. Pathways presenting the adjusted p-value $\leq$ 0.05 were considered statistically significant.

Cell culture model for transcriptome validation

Caco-2 cells (ATCC HTB-37TM *Homo sapiens* colon colorectal cells), which tested negative for mycoplasma contamination (MycoAlert® Mycoplasma Detection kit, Lonza, Basel, Switzerland), were seeded in 6-well plates at a confluency of 5.0 x 10^5 cells per well. After incubation overnight at 37°C and 5% CO_2, the cells were infected with Asian-lineage ZIKV (ZV BR 2015/15261 or ZV BR 2016/16288), which had been recently isolated from clinical specimens,[15] or with the African strain ZIKV MR766 at an MOI of 1. For comparative purposes, the Caco-2 cells were either uninfected (a mock control) or infected with a DENV-1 LRV/13400 isolate, WNV E/7229/06, wild-type YFV M17/09[16] or YFV strain used for vaccines (the 17DD strain) at the same MOI. All viruses were diluted in DMEM-F12 supplemented with 100 IU/µg/mL penicillin/streptomycin for inoculation. After 90 minutes, the inocula were removed, and the monolayers were washed three times with PBS (Lonza, Basel, Switzerland). The cells were maintained in DMEM-F12 containing 10% FBS and penicillin/streptomycin at 100

IU/µg/mL (all reagents were obtained from Thermo Fischer Scientific, Grand Island, USA). At 24, 48 and 72 h post infection (h.p.i.), the cells were harvested for RNA extraction using an RNeasy Mini kit (Qiagen) following the manufacturer's instructions. RNA was quantified using a NanoDrop system (Thermo Scientific, Waltham, Massachusetts, United States), and the concentration was normalized to 8 ng/µL in nuclease-free water.

The expression of the *IGF2* gene was assessed by real-time RT-PCR as follows: Primers and probes (Table S1) were synthesized by Integrated DNA Technologies (IDT, Coralville, USA). The *IGF2* and *RNase P* genes were assessed using a TaqMan system, while a SYBR Green assay was used to quantify endogenous SDHA and YWHAZ genes. The reactions were standardized to range from 90 to 110% efficiency. All real-time assays were performed with one-step reaction systems (Promega, Madison, Wisconsin, United States) in the QuantStudio 5 instrument (Applied Biosystem, Foster City, California, United States). The stability of endogenous genes was evaluated by the GeNorm program and resulted in an M-factor lower than 0.37 for all time points. Gene expression analysis was performed according to the double delta CT method,[17] taking individual efficiencies into account. Statistical analysis was performed in Prism software (GraphPad version 6, USA) using two-way ANOVA followed by Tukey's test. Values of $p < 0.05$ indicated significance. Real-time RT-PCR was also used to assess intracellular viral RNA, as published elsewhere (protocols are indicated in the Table S1).

Viral titration and immunofluorescence

To evaluate viable viral particles, supernatants of flavivirus-infected Caco-2 cells were titrated in ten-fold serial dilutions for a focus-forming assay using a C6/36 cell monolayer and were overlaid with a mixture of carboxymethylcellulose (1.6%), Leibovitz's L-15 medium, 0.26% tryptose and 5% FBS. After 7 days, the cells were fixed with 3% paraformaldehyde and then incubated with the anti-flavivirus monoclonal antibody 4G2 (hybridoma D1-4G2-4-15, ATCC HB-112) followed by anti-mouse IgG alkaline phosphatase-conjugated antibody (Catalog S372B - Promega, Madison, Wisconsin, United States). The reactions were developed with 5-bromo-4-chloro-3-indolyl-phosphate/nitro blue tetrazolium (BCIP/NBT) color development substrate (Promega).

Viral infection was also analyzed by indirect immunofluorescence. Cells were infected as described above. Cells were fixed with a methanol:acetone 1:1 solution 24, 48 and 72 h.p.i. The cells were then stained with 4G2 followed by goat anti-mouse IgG Alexa Fluor 488-conjugated antibody (Catalog A11001 - Life Technologies, Carlsbad, California, United States), and cell nuclei were counterstained with DAPI. Images were obtained with an Operetta high-content imaging system (PerkinElmer, Waltham, Massachusetts, United States) with a 20× objective and analyzed with Harmony High-Content Imaging and Analysis Software according to a previously established setup.[18]

Statistical analysis was performed in Prism software (GraphPad version 6, USA) using two-way ANOVA followed by Tukey's test. Values of $p < 0.05$ indicated significance.

Immunohistochemistry, semiquantitative analysis and statistics

IGF2 expression in placentas was evaluated by immunohistochemistry in all the cases, however, because of improper fixation (autolysis) or unavailability of suitable tissue sections, some samples (LRV/16 986; LRV/16 1098 and LRV/16 1094) were inappropriate for accurate analysis. Then, 4-μm histological sections from six ZIKV-positive (LRV/16 284, LRV/16 848, LRV/16 854, LRV/16 859, LRV/16 927, and LRV/16 931) and four non-ZIKV (LRV/18 560; LRV/18 563; LRV/16 1220; LRV/16 1387) samples were subjected to immunohistochemistry. Slides were subjected to deparaffinization, dehydration, and rehydration. Endogenous peroxidase was blocked with methyl alcohol and hydrogen peroxide (the first block) followed by distilled water and hydrogen peroxide (the second block). Antigen retrieval was performed using a Bio SB^{TM} ImmunoDNA Retriever. Slides were incubated overnight with the primary antibodies (anti-IGF2 rabbit polyclonal antibody, Catalog ab9574 – Abcam, Cambridge, UK) in a humid chamber from 2 to 8°C. Next, the slides were incubated with a secondary polymer (Reveal Polyvalent HRP-DAB Detection System – Spring Bioscience, Pleasanton, USA) for 25 minutes at room temperature. The reaction was developed with 3,3'-diaminobenzidine (DAB) in the presence of a hydrogen peroxide substrate for 3 minutes followed by counterstaining with Harris hematoxylin. The permanent slides were mounted in histological resin for microscopy (Entellan, Merck, Darmstadt, Germany). All immunohistochemical assays included both negative (consisting of reactions omitting the primary antibody) and positive (decidua) controls.[19,20] Images of the immunostained slides were obtained with a Zeiss Axio Scan.Z1 slide scanner (Germany), using a high-power field (HPF = 40x objective),[19,20] to generate digital Tagged Image File Format (TIFF) files.

IGF2 expression in the decidua samples was analyzed blindly using a semiquantitative technique (Allred scoring system),[21] which combines the proportion and intensity of positive immunostained cells. The proportion was calculated as the ratio of positive cells to the total number of cells and was classified as follows: 0 (0%), 1 (>0–1%), 2 (≥1%–10%), 3 (>10%–33%), 4 (>33%–66%), and 5 (>66%–100%). Intensity was classified as 0 (negative), 1+ (weak), 2+ (moderate), and 3+ (strong). The Allred score was calculated by summing the proportion and intensity scores in range from 0 to 8.[21] The mean values of the parameters for the counted fields were used for the statistical analyses. The Zika-infected and uninfected control groups were compared using t test followed by Mann-Whitney U test. Data were analyzed using GraphPad Prism (version 6). Values of $p < 0.05$ indicated significance.

Results

RNA-Seq reveals the downregulation of Insulin-like Growth Factor II (*IGF2*) and oxidative phosphorylation pathway dysregulation in naturally infected third trimester human placentas

Six samples of ZIKV-positive and non-ZIKV groups were sequenced. The raw files are available at the NCBI Sequence Read Archive (SRA) (https://www.ncbi.nlm.nih.gov/sra), under the BioProject accession number PRJNA633941.Three samples from each group were selected for differential expression analysis, as follows: LRV/16 931, LRV/16 848, and LRV/16 927 for the ZIKV-positive group, and LRV/16 1387, LRV/16 1094, and LRV/16 1220 for the non-ZIKV group. These samples showed distinct expression patterns visualized by principal component analysis (PCA) and multidimensional scaling plot (MDS) (Fig. S1 and S2; Table S2). Differential gene expression analysis showed 407 genes more expressed in the ZIKV-positive group than in the non-ZIKV group, while 603 genes were downregulated in this comparison (File S1). The hierarchical clustering analysis allowed us to visualize two groups according to ZIKV status (Fig. 1). This list was ordered by the expression measurement and manually inspected.

IGF2 was identified as differentially expressed according to the ZIKV status with the highest expression level among the downregulated nuclear genes in the ZIKV group (Table 1). RNA-Seq visual inspection showed the splice variants *IGF2-204* (ENST00000381406.8) and *IGF2-205* (ENST00000416167.7) as the two most prevalent *IGF2* transcripts. Further, we sought to determine whether genes encoding *IGF2* protein receptors (*IRS1, IRS2, IGF1R*, and *IGF2R*) or binding proteins (*IGFBP1* to *IGFBP7*, and

Table 1
Differential expression analysis according to ZIKV status of *IGF2, IGF2*-related nuclear genes, mitochondrial genes, and oxidative phosphorylation nuclear pathway genes.

	Gene Symbol	logFC	Adjusted *p*-value	DESeq2 base Mean
IGF2 and *IGF2*-related nuclear genes downregulated in ZIKV group	*IGF2*	-1.68	0.04	6,623
	IRS1	-2.46	< 0.001	107
	IRS2	-2.66	0.002	284
	IGFBP1	-4.96	0.008	1,341
	IGFBP5	-1.78	0.005	703
IGF2-related nuclear genes upregulated in ZIKV group	*IGF2BP2*	2.36	0.001	834
	IGF2BP3	1.87	0.01	475
IGF binding protein and IGF receptor genes with no differential expression	*IGFBP2*	NSS	0.30	80
	IGFBP3	NSS	0.22	923
	IGFBP4	NSS	0.10	529
	IGF1R	NSS	0.07	546
	IGF2R	-1.16 *	< 0.001	229
Mitochondrial genes more expressed in ZIKV group	*MT-CO1*	2.04	0.03	330,328
	MT-CO2	2.26	0.02	108,722
	MT-ND4	2.71	< 0.001	102,110
	MT-ATP6	2.63	0.04	76,250
	MT-CYB	2.59	0.003	74,181
	MT-ND5	2.60	< 0.001	70,563
	MT-ND1	2.68	< 0.001	51,998
	MT-ND2	3.14	< 0.001	35,307
	MT-ND4L	2.55	< 0.001	15,612
	MT-ATP8	1.99	0.02	5,204
Oxidative phosphorylation nuclear genes considered together with mitochondrial genes to determine whether pathway is dysregulated	*ATP6V0A1*	-1.57	< 0.001	177
	SDHA	-1.70	0.03	279
	NDUFB7	1.51	0.003	44
	TCIRG1	0.81	0.04	307
	ATP5F1E	1.29	0.008	82
	COX6B1	1.18	0.03	66
	COX7C	1.10	0.03	55
	ATP6V1F	1.80	0.002	60
	ATP6V1G1	1.35	0.002	163
	UQCRC2	-0.99	0.01	103
	NDUFB10	0.83	0.04	65
	ATP6V1C2	2.46	< 0.001	650
	NDUFA6	1.19	0.02	54
	NDUFA13	1.50	0.002	46

NSS: not statistically significant (adjusted p-value > 0.05); *: *IGF2R* presented relative differential expression below the threshold set in this study (|logFC| ≥ 1.5).
Abbreviations: *IRS1*, insulin receptor substrate 1; *IRS2*, insulin receptor substrate 2; *IGFBP1*, insulin like growth factor binding protein 1; *IGFBP5*, insulin like growth factor binding protein 5; *IGF2BP2*, insulin like growth factor 2 mRNA binding protein 2; *IGF2BP3*, insulin like growth factor 2 mRNA binding protein 3; *IGFBP2*, insulin like growth factor binding protein 2; *IGFBP3*, insulin like growth factor binding protein 3; *IGFBP4*, insulin like growth factor binding protein 4; *IGF1R*, insulin like growth factor 1 receptor; *IGF2R*, insulin like growth factor 2 receptor; *MT-CO1*, mitochondrially encoded cytochrome c oxidase I; *MT-CO2*, mitochondrially encoded cytochrome c oxidase II; *MT-ND4*, mitochondrially encoded NADH dehydrogenase 4; *MT-ATP6*, mitochondrially encoded ATP synthase 6; *MT-CYB*, mitochondrially encoded cytochrome b; *MT-ND5*, mitochondrially encoded NADH dehydrogenase 5; *MT-ND1*, mitochondrially encoded NADH dehydrogenase 1; *MT-ND2*, mitochondrially encoded NADH dehydrogenase 2; *MT-ND4L*, mitochondrially encoded NADH 4L dehydrogenase; *MT-ATP8*, mitochondrially encoded ATP synthase 8; *ATP6V0A1*, ATPase H+ transporting V0 subunit a1; *SDHA*, succinate dehydrogenase complex flavoprotein subunit A; *NDUFB7*, NADH,ubiquinone oxidoreductase subunit B7; *TCIRG1*, T cell immune regulator 1, ATPase H+ transporting V0 subunit a3; *ATP5F1E*, ATP synthase F1 subunit epsilon; *COX6B1*, cytochrome c oxidase subunit 6B1; *COX7C*, cytochrome c oxidase subunit 7C; *ATP6V1F*, ATPase H+ transporting V1 subunit F; *ATP6V1G1*, ATPase H+ transporting V1 subunit G1; *UQCRC2*, ubiquinol-cytochrome c reductase core protein 2; *NDUFB10*, NADH,ubiquinone oxidoreductase subunit B10; *ATP6V1C2*, ATPase H+ transporting V1 subunit C2; *NDUFA6*, NADH,ubiquinone oxidoreductase subunit A6; *NDUFA13*, NADH,ubiquinone oxidoreductase subunit A13.

IGF2BP1 to *IGF2BP3*) were differentially expressed among the samples according to ZIKV status (Table 1). Interestingly, *IRS1, IRS2, IGFBP1*, and *IGFBP5* genes were found to follow the same expression pattern as that of *IGF2*, i.e., downregulated, while *IGF2BP2* and *IGF2BP3* genes were upregulated. However, no differential expression was observed for the *IGF1R, IGF2R, IGFBP2, IGFBP3*, or *IGFBP4* genes. Considering that dysregulation of *IGF2* expression is known to cause impaired fetal development, and that other genes of the IGF system were also modulated in the transcriptome analysis, *IGF2* gene was chosen for experimental validation.

In addition to the IGF2 system genes, RNA-Seq differential expression analysis showed mitochondrial genes (*MT-CO1, MT-CO2, MT-ND4, MT-ATP6, MT-CYB, MT-ND5, MT-ND1, MT-ND2, MT-ND4L*, and *MT-ATP8*) as upregulated in the ZIKV-positive group (Table 1). Gene set enrichment analysis revealed statistically significant dysregulation of the oxidative phosphorylation pathway (*p*-value < 0.05), with most of the genes more highly expressed in the ZIKV group. The oxidative phosphorylation was the single pathway identified as statistically significant between ZIKV and non-ZIKV groups.

ZIKV infection downregulates IGF2 *in a cell line model*

To validate the transcriptome results, Caco-2 cells were infected with ZIKV, as these cells express genes in the IGF2 pathway.[22] The infection of Caco-2 cells with the African ZIKV MR766 strain resulted in decreased *IGF2* mRNA levels 48 h.p.i., while the Asian ZIKV ZV BR 2015/15261 isolate did not show a similar level of downregulation until 72 h.p.i. (Fig. 2). Intriguingly, no modulation was observed when the cells were infected with the Asian ZIKV ZV BR 2016/16288 isolate. To investigate whether other flaviviruses modulate *IGF2* expression, Caco-2 cells were infected with either DENV-1, WNV, wild-type (M17/09) YFV or the YFV 17DD vaccine strain. No significant modulation of *IGF2* expression was observed after infection by the abovementioned viruses, except for a mild (<50%) effect observed for 17DD.

To assess whether individual ZIKV fitness differences would impact the *IGF2* gene modulation results, we evaluated the time course of intracellular RNA and E protein synthesis and the secreted virus titers in Caco-2 cells (Fig. 3A-E). Compared to the Asian ZIKV strains, African ZIKV MR766 yielded higher levels of in-

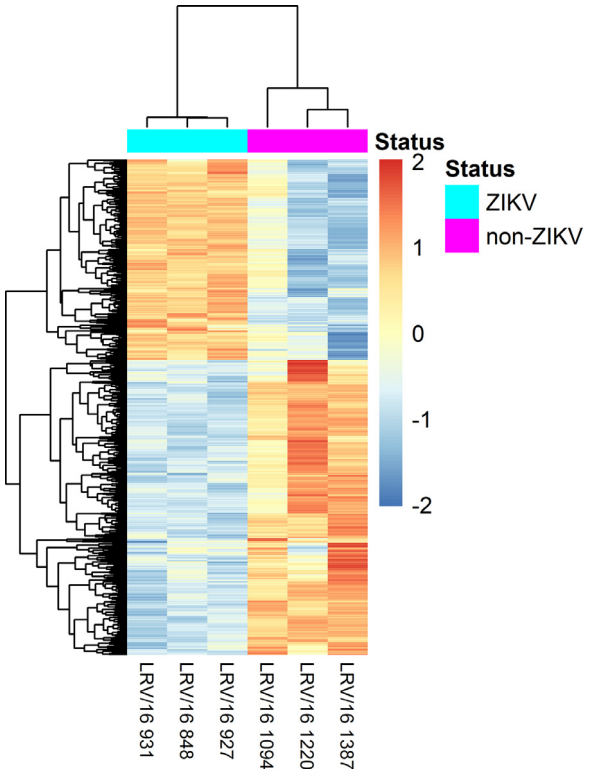

Fig. 1. Hierarchical clustering and heat map of $\log_2$-normalized CPM counts of the differentially expressed genes (adjusted p-value ≤ 0.05) of the non-ZIKV and ZIKV samples.

tracellular viral RNA at all time points analyzed (Fig. 3E). Intriguingly, ZIKV ZV BR 2016/16288 isolate infection resulted in a higher number of RNA copies than did infection with the ZIKV ZV BR 2015/15261 isolate 48 h.p.i., with both Asian ZIKV strains showing similar RNA loads 72 h.p.i (Fig. 3E). CT values obtained by real-time RT-PCR targeting viral RNA indicated that all these viruses were able to replicate successfully in this cell model (Table S3). Notably, WNV demonstrated a higher ability to favor RNA synthesis, which resulted in lower CT values, within 24 h.p.i. Similarly, higher RNA levels were obtained for wild-type YFV M17/09 24 h.p.i. than for the vaccine strain, but this difference was reduced at the following time points (Table S3).

Immunofluorescence assays corroborated previously obtained RNA results, since a higher percentage of Caco-2 cells infected by ZIKV MR766, WNV and wild-type YFV M17/09 as early as 24 h.p.i. and peaking 48 h.p.i. (Fig. 3B). WNV and YFV M17/09 sustained high infection levels through 72 h.p.i. On the other hand, the percentage of YFV 17DD-infected cells was higher at 48 h.p.i., while the percentage of DENV-1 E-infected cells increased progressively. Regarding the ZIKV isolates, although ZIKV MR766 infection resulted in a higher percentage of infected cells early, as described above, all three ZIKV isolates had reached similar percentages of infection 48 h.p.i. (Fig. 3B). Then, a decrease was observed for the ZIKV ZV BR 2015/15261 and ZIKV MR766 isolates 72 h.p.i., but not for ZIKV ZV BR 2016/16288. This effect may be related to the different degrees of cytopathic effects induced by the ZIKV ZV BR 2015/15261 and ZIKV MR766 isolates at this time point (Fig. 3A and 3C).

Differences in flavivirus replication in Caco-2 cells were also evaluated by titrating the viral particles released into supernatants over 72 hours. ZIKV MR766 presented with the highest titer levels during all the time points, and no statistical differences were observed between the Asian ZIKV isolates (Fig. 3D). At 72 h.p.i., viral titers in the C6/36 cells ranged from 10^4 ffu/mL for wild-type YFV M17/09 to 10^7 ffu/mL for ZIKV MR766 and WNV (Fig. 3D).

IGF2 peptide levels are reduced in decidual tissues naturally infected with ZIKV

Expression of IGF2 was analyzed in the fetal-maternal interface of placental tissues from six naturally ZIKV-infected pregnant women and four non-ZIKV controls. IGF2 was first assessed in the fetal portion of placentas (trophoblast villi), however, no differences were observed (data not shown). Visual inspection indicated a possible role of ZIKV to modulate IGF2 expression in the maternal portion of placentas (decidua), which was chosen for further semiquantitative analysis. Representative images of the deciduae are shown in Fig. 4A. The ratio of the number of IGF2-positive to total cells was reduced in the ZIKV-infected tissues (Fig. 4B and Table S4); these cells also showed significantly lower staining intensity than the negative control samples (Fig. 4C and Table S4). Altogether, the effect of all these parameters resulted in a lower Allred score (Fig. 4D and Table S4), which revealed broad IGF2 downregulation throughout the decidual tissues from women infected by ZIKV at the late stages of pregnancy.

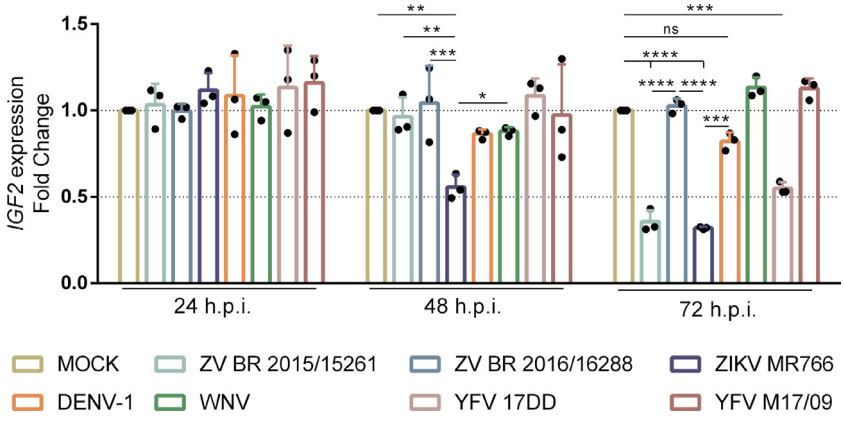

Fig. 2. ZIKV downregulates *IGF2* expression in Caco-2 cells. Cells were infected with different flaviviruses, and the gene expression was analyzed 24, 48 and 72 h.p.i. *IGF2* expression was normalized by three endogenous genes (RNase P, SDHA and YWHAZ) according to the ΔΔCT method. Data are presented as the means and standard deviation of three independent biological experiments in duplicate. Statistical analysis was performed using two-way ANOVA followed by Tukey's test. ns: not significant; * $p < 0.05$; ** $p < 0.01$; *** $p < 0.001$ and **** $p < 0.0001$.

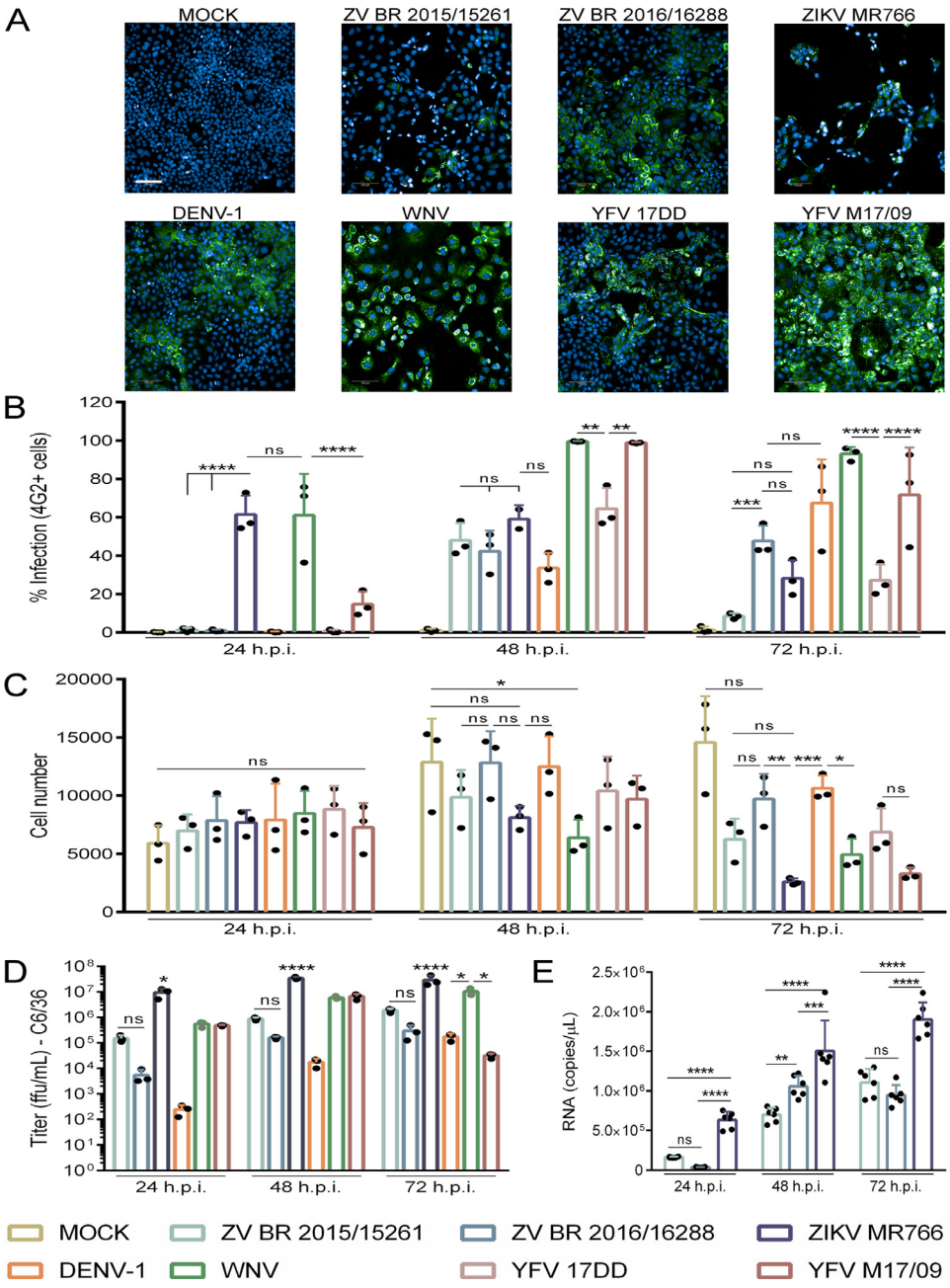

Fig. 3. Flavivirus infection in Caco-2 cells. (A) Representative immunofluorescence images of Caco-2 cells infected by different flavivirus 72 h.p.i. Scale bars: 100 µm. (B) Percentage of infected Caco-2 cells was determined according to 4G2 staining of the indicated flaviviruses 24, 48 and 72 h.p.i. Cells were counted with a high content screening imaging system (Operetta). (C) Viral infection leads to time-dependent cell death, as revealed by the progressive reduction in the Caco-2 cell population, depending on the viral isolate. Cell counting was performed by a high content screening imaging system (Operetta) according to number of nuclei stained with a DAPI fluorophore. (D) Supernatants from Caco-2 cell cultures infected with different flaviviruses were titrated 24, 48 and 72 h.p.i. on C6/36 monolayers. (E) Time course of intracellular viral RNA load in Caco-2 cells infected by different ZIKV isolates. Monolayers were washed three times with PBS before the RNA extraction. Viral RNA content was estimated by real-time RT-PCR using a commercial standard curve. The data were analyzed using two-way ANOVA followed by Tukey's multiple comparison test. The graphs are based on the means and standard deviation of three experiments in duplicate. ns: not significant; $^{*}p < 0.05$; $^{**}p < 0.01$; $^{***}p < 0.001$ and $^{****}p < 0.0001$.

Discussion

Since ZIKV emerged in Brazil, many efforts have been made to understand the mechanisms by which this virus leads to the malformation of fetuses. Detection of the ZIKV genome in amniotic fluid[23,24] and in fetal brain[25,26] indicated that ZIKV crosses the placental barrier and thus might interfere directly with fetal development.

The placenta is the key means of transferring nutrients and oxygen to the fetus and is of particular interest because dysfunctions to it are related to fetal adverse outcomes and disease predisposition.[27] We have previously described the presence of ZIKV RNA and protein in full-term placentas from mothers who were infected in the earliest stages of gestation.[12,28] The persistence of ZIKV in the placenta may have various implications that contribute to adverse fetal outcomes. In addition to this evidence, a unique study explored placental gene modulation in humans after ZIKV infection to reveal transcriptional differences in eIF2 signaling and mitochondrion and oxidative phosphorylation-related genes.[29] Notably, these data were obtained from a single case of a woman infected

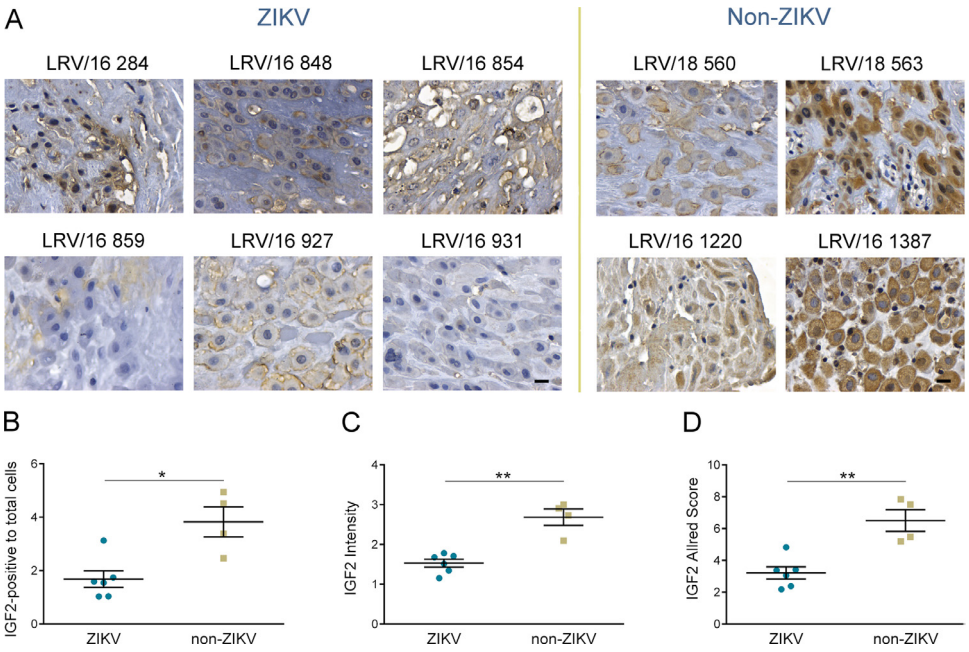

Fig. 4. Illustrative panel depicting immunohistochemical targeting IGF2 in third-trimester human deciduae is shown in (A). The tissues were blindly analyzed and scored as detailed in the Material and Methods. Scale bars: 20 μm. IGF2-positive to total cells (proportion) (B) and intensity (C) of ZIKV-positive and ZIKV-negative deciduae. These variables were combined and expressed in the Allred scoring (D). Statistical analysis was performed using the t test followed by the Mann-Whitney U test. Data represent mean ± SD. $^{*}p < 0.05$; $^{**}p < 0.01$.

during the first trimester of pregnancy, and the possibility cannot be excluded that other affected pathways were not detected during the time that elapsed between the time of infection and the delivery, when the tissues were obtained. Furthermore, individual intrinsic genetic heterogeneity must be considered.

Here, we investigated genes differentially expressed in placental tissues from naturally infected women that might disturb the delicate interplay between the mother and fetus interface. The transcriptome data obtained from the placental tissues of three women infected with ZIKV during the third trimester of gestation were compared to those from three non-ZIKV women. The rationale for using samples from women who were infected during the late stages of pregnancy was based on the objective to have the timing of virologic and immunological analyses as close as possible to the emergence of acute ZIKV infection.

In our study, the three samples in each group exhibited gene expression pattern clustering, as indicated using PCA and MDS. According to Zika status, 1010 differentially expressed genes were identified. Interestingly, *IGF2* gene was consistently downregulated in ZIKV positive samples, with expression that was -1.68-fold lower in the ZIKV-positive samples than it was in the controls (Table 1).

IGF2 is a protein hormone that participates in the insulin/insulin-like growth factor system. The IGF axis controls fetal growth during pregnancy through the combination of IGF1, IGF2, IGF receptors, insulin receptors, IGF binding proteins, and protein phosphorylation (reviewed by Forbes and Westwood[30]). During pregnancy, IGF2 is synthesized by placental and fetal tissues and, through paracrine, autocrine and endocrine effects, is involved in the regulation of both fetal and placental development.[10,11] IGF2 also regulates the proliferation and apoptosis of first-trimester extravillous cytotrophoblasts *in vitro*, and it is speculated that this mechanism could be relevant to embryo implantation[31] The expression of *IGF2* is controlled by genomic imprinting; fetal growth disorders, such as Beckwith-Wiedemann syndrome, result from dysregulation of the IGF2 balance.[32] Studies using murine models demonstrated that IGF2 is also important to adult[33] as well as fetal neurogenesis, a concept supported by the fact that knocking out the *IGF2* gene resulted in decreased fetal brain weight.[34] According to our analysis, in addition to the reduced expression of *IGF2* in the ZIKV placentas, we identified other downregulated (*IGFBP1, IGPBP5, IRS1*, and *IRS2*) as well as upregulated (*IGF2BP2* and *IGF2BP3*) genes of the IGF system, reinforcing the hypothesis that this system is dysregulated after ZIKV infection.

Evidence indicating that ZIKV may interfere with IGF pathway gene expression has been described recently by Glover and colleagues[35] that showed activation of IGF1 pathway signaling in Vero cells after ZIKV infection. Primary human astrocytes infected with either African and Asian ZIKV strains secreted less IGF2 than levels secreted by the controls.[36] However, in both studies, these findings were not further explored by the authors. Recent data from Karuppan and colleagues[37] demonstrated a significant reduction in IGF1 expression in the brains of pups from ZIKV-infected Beclin-1-deficient mouse dams. It was speculated that the downregulation of this protein potentially contributed to the smaller and underdeveloped brain of pups in the litter.

Attempts to validate our RNA-Seq results using real-time RT-PCR of the RNA extracted from nonfixed placentas were unsuccessful, likely due to the random method of placental sampling that was utilized. It is known that *IGF2* mRNA distribution varies throughout the placenta according to pregnancy gestational age.[38] Tissues were obtained at delivery time in different hospitals in that State of Paraná during a Zika outbreak in Brazil, and unfortunately, no dissection was performed before the tissues were frozen, which made it impossible to separate the maternal (decidua) from the fetal part of the placentas. This issue would potentially yield biased results. An additional limitation was reliance on the choice of an endogenous normalizer gene, since the most stable genes may vary according to fetal sex and clinical conditions.[39–41] Nevertheless, because of the abovementioned restrictions, we used a cell culture model to validate the RNA-Seq results.

Caco-2 cells were chosen for *IGF2* data validation because according to the Human Protein Atlas database,[42] Caco-2 cells shows the highest *IGF2* gene expression levels among various human

cells lines, which was essential to test the modulation of IGF2 transcription during ZIKV and other flaviviruses infection. Of note, placental-derived lineages, such as BeWo, do not express *IGF2*[42]. We found that Caco-2 cells were permissive to all the flaviviruses used in this study, as revealed by intracellular RNA (Table S3), E protein synthesis (Fig. 3B) and viral release (Fig. 3D). *IGF2* gene expression in the ZIKV-infected Caco-2 cells, as measured by real-time RT-PCR, supported the RNA-Seq data. *IGF2* was downregulated due to infection by both Asian and African ZIKV strains in a time-dependent manner. A 3-fold reduction in *IGF2* expression was found in Caco-2 cells 72 hours after ZIKV MR766 or ZIKV ZV BR 2015/15261 infection (Fig. 2). The downregulation of *IGF2* gene expression occurred earlier for ZIKV MR766 than it was for ZIKV ZV BR 2015/15261, since a reduction of nearly 50% was detected 48 h.p.i. for the African strain (Fig. 2). This result may be due to the high viral fitness of ZIKV MR766 compared to the other ZIKV low passaged recent clinical isolates, as revealed by the presence of the higher levels of intracellular viral RNA content within 24 h.p.i. (Fig. 3E), higher viral titers (Fig. 3D) and the higher percentage of infected cells observed at the same time point (Fig. 3B). Notably, ZIKV MR766 is a laboratory-adapted strain, while the Asian isolates used in this study were recently obtained from Brazilian clinical samples not extensively passaged.[15] Remarkably, differences in the ability to downregulate IGF2 between the two recently obtained low-passage clinical Asian ZIKV isolates (ZV BR 2015/15261 and ZV BR 2016/16288) were observed. This finding was intriguing since similar RNA and percentages of cells expressing E protein were observed for both isolates (Fig. 3B and 3E), although ZIKV ZV BR 2016/16288 infection was found to result in a slightly lower viral titer (Fig. 3D). Importantly, both ZIKV ZV BR 2016/16288 and ZV BR 2015/15261 were isolated from patients exhibiting similar clinical symptoms in southern Brazil in January 2016 and northeast Brazil in June 2015,[15] respectively. Studies on the effects of ZIKV on human astrocytes have also observed similar profiles among samples, with lower IGF2 release found after astrocyte infection with ZIKV MR766 or Asian PRVABC59 Puerto Rico ZIKV strains but not with the Honduras ZIKV R103451 strain.[36] The mechanisms involved in the regulation of *IGF2* gene expression by ZIKV need to be further investigated, but our results indicate the possible involvement of six amino acid differences found between the recent ZIKV clinical isolates ZV BR 2016/16288 and ZV BR 2015/15261 that map to NS1, NS2A, NS3 and NS4B proteins.[15]

IGF2 expression modulation has been described for other viruses. Dysregulation of the IGF system by human papillomavirus (HPV), hepatitis B virus (HBV) and hepatitis C virus (HCV) is associated with disease progression and cancer development. In HBV and HCV-related hepatocarcinogenesis, IGF2 expression is augmented.[43–45] HPV 16 infection downregulates IGF-binding protein 2 (IGFBP2) expression, leading to an increase in IGF1 and IGF2 signaling and consequently to increasing cell invasion and disease severity.[46]

Although the epidemiological data are still controversial,[47,48] mouse models have indicated that West Nile infection during pregnancy may result in birth defects.[49] We also sought to determine whether WNV and other flaviviruses can disturb *IGF2* gene expression. To make this determination, Caco-2 cells were infected with DENV-1, WNV and both the vaccine form and wild-type YFV. Interestingly, no significant differences in *IGF2* expression were found for DENV-1, WNV or wild-type YFV when compared to the mock-infected controls at any of the time points analyzed (Fig. 2). Apparently, the difference in results for ZIKV and the other viruses was not related solely to replication ability, since DENV-1 RNA, percentage of infected cells and viral titers were similar to those found for ZIKV ZV BR 2015/15261, while the WNV and wild-type YFV replication kinetics were comparable to those of ZIKV MR766, although ZIKV MR766 had the highest viral titers (Fig. 3A-C). In addition to ZIKV, in our cell culture model, only the YFV 17DD vaccine induced downregulation of *IGF2* (Fig. 2); this result also seems to be related to factors other than virus replication itself, since wild-type YFV presented with higher viral fitness than did 17DD YFV (Fig. 3B and Table S3). Clinical data concerning adverse events resulting from the unintentional 17DD YFV vaccination of pregnant women are not completely conclusive,[50] and other factors, such as the ability of the virus to cross the placental barrier, must be considered when analyzing the biological relevance of the results obtained from *in vitro* models.

Immunohistochemical analysis of naturally infected ZIKV decidual tissues obtained at delivery from women who had been infected at late gestation stages showed reduced IGF2 staining in both proportion and intensity (Fig. 4B and 4C). This IGF2 differential modulation seems to be more related to the deciduae than to trophoblasts, since no significant differences in IGF2 staining were observed for the trophoblasts (data not shown).

Deletion of the transcript of *IGF2* in the placentas of mice (*Igf2P0*) disturbed the ability of the placentas to adapt to protein undernutrition, which resulted in a low-weight pups.[51] Recently, protein malnutrition has been implicated in the worst fetal outcomes for mice infected with ZIKV.[52] This malnutrition and infection combination also resulted in impairment to the placental structure and in reduced body growth and neuronal development of the pups compared to the growth and development of pups born to dams that received a standard diet. Unfortunately, no information on the development of the babies born to the women participating in this study was available to investigate the relationship between nutritional status, individual IGF2 levels and pregnancy outcomes. Nevertheless, the mechanisms affecting the relationship between ZIKV infection, placental function and fetal outcomes are being gradually revealed, making it possible to understand the reasons why not every ZIKV infection during pregnancy results in congenital disease.[53] Furthermore, additional processes may also be involved in ZIKV pathogenesis, such as mitochondrial and oxidative phosphorylation gene dysregulation (Table 1). This dysregulation has been previously observed during placental transcriptome profiling[29] and may be related to an overall cellular energy imbalance induced by ZIKV infection.[54]

In summary, we conclude that ZIKV differs from other flaviviruses in downregulating *IGF2* gene expression, although further studies are necessary to investigate the mechanisms involved. We also showed that mutations in the ZIKV genome may result in differences in the biology of the viruses and, consequently, the host response. Although other factors, such as maternal nutrition or drug and alcohol consumption, may contribute to the fetal outcome of mothers infected with ZIKV during pregnancy, our findings focused to the role of placental factors, especially IGF2, that can contribute to Zika congenital syndrome in humans and can open avenues to the development of therapies to mitigate ZIKV-induced fetal injuries.

Author contributions

AAS, CZ, LN, MMD, CMR and CNDS contributed to the study design; FP, NANJ, AFFHF and VSCP performed the RNA-Seq data analysis; AAS, CZ, ACK and JB performed the cell culture experiments; CBVP performed the IHC assays; SG performed the image analysis; LN and PZR analyzed the tissue slides and performed the Allred semiquantitative analysis; AAS,CZ, FP, LN, ACK, MRM, CMR and CNDS analyzed the overall results; AAS,CZ, FP, LN, ACK, JB and CNDS wrote the manuscript.

Declaration of Competing Interest

The authors have declared that no conflict of interest exists.

Acknowledgments

The authors are grateful to Dr. Érico Tosoni Costa for kindly providing us with Caco-2 cells, Dr. Edna Teruko Kimura for donating anti-IGF2 antibody, Luana Ebbinghaus for technical support, Dr. Thiago Jacomasso for helping with the PCR gene expression data analysis and Dr. Hellen Geremias dos Santos for assistance using R. They are also grateful to Connie Zhao from the Rockefeller University Genomics Resource Center for support in sequencing and to Wagner Nagib for graphical design.

Funding

This work was supported by CNPq (Conselho Nacional de Desenvolvimento Científico e Tecnológico, Brazil) [grant number 439968/2016-0], Fiocruz (Fundação Oswaldo Cruz), and Inova Fiocruz/VPPCB [grant number VPPCB-007-FIO-18-2-19]. CNDS, LN, FP and JB received a CNPq fellowship. This study was financed in part by the Coordenação de Aperfeiçoamento de Pessoal de Nível Superior – Brasil (CAPES) [grant number 88887.124207/2016-00] and Finance Code 001 (M.Sc. scholarship to VSCP and AFFHF). The work was also supported in part through anonymous donors to a Rockefeller University Zika virus research fund.

Supplementary materials

Supplementary material associated with this article can be found, in the online version, at doi:10.1016/j.jinf.2020.09.028.

References

1. Duffy Mark R, Ho Chen Tai, Thane Hancock W, Powers Ann M, Kool Jacob L, Lanciotti Robert S. et al. Zika virus outbreak on Yap Island, Federated states of micronesia. *N Engl J Med* 2009;**360**(24):2536–43. doi:10.1056/NEJMoa0805715.
2. Zanluca Camila, De Melo Vanessa Campos Andrade, Mosimann Ana Luiza Pamplona, Dos Santos Glauco Igor Viana, dos Santos Claudia Nunes Duarte, Luz Kleber. First report of autochthonous transmission of Zika virus in Brazil. *Mem Inst Oswaldo Cruz* 2015;**110**(4):569–72. doi:10.1590/0074-02760150192.
3. Brasil P, Pereira JP, Moreira ME, MRibeiro Nogueira R, Damasceno L, Wakimoto M, et al. Zika virus infection in pregnant women in Rio de Janeiro. *N Engl J Med* 2016;**375**(24):2321–34. doi:10.1056/NEJMoa1602412.
4. Martines Roosecelis Brasil, Bhatnagar Julu, de Oliveira Ramos Ana Maria, Davi Helaine Pompeia Freire, Iglezias Silvia DAndretta, Kanamura Cristina Takami, et al. Pathology of congenital Zika syndrome in Brazil: a case series. *Lancet* 2016;**388**(10047):898–904. doi:10.1016/S0140-6736(16)30883-2.
5. Rice Marion E, Galang Romeo R, Roth Nicole M, Ellington Sascha R. Vital signs : Zika-associated birth defects and neurodevelopmental abnormalities possibly associated with congenital Zika Virus infection —. *Morb Mortal Wkly Rep, CDC* 2018;**67**(31):858–67.
6. Svetlana Khaiboullina, Timsy Uppal, Konstatin Kletenkov, St Jeor Stephen Charles, Ekaterina Garanina, Albert Rizvanov, et al. Transcriptome profiling reveals pro-inflammatory cytokines and matrix metalloproteinase activation in Zika virus infected human umbilical vein endothelial cells. *Front Pharmacol* 2019;**10**(642):1–17. doi:10.3389/fphar.2019.00642.
7. Kant Tiwari Shashi, Jason Dang, Yue Qin, Gianluigi Lichinchi, Vikas Bansal, Rana Tariq M. Zika virus infection reprograms global transcription of host cells to allow sustained infection. *Emerg Microbes Infect* 2017;**6**(4) e24-10. doi:10.1038/emi.2017.9.
8. Lima Morganna C, de Mendonça Leila, Rezende Antonio R, Carrera Raquel M, Aníbal-Silva Conceição M, Demers Matthew E, et al. The transcriptional and protein profile from human infected neuroprogenitor cells is strongly correlated to zika virus microcephaly cytokines phenotype evidencing a persistent inflammation in the CNS. *Front Immunol* 2019;**10**(1928). doi:10.3389/fimmu.2019.01928.
9. Kumar Singh Pawan, Indu Khatri, Alokkumar Jha, Pretto Carla D, Spindler Katherine R, Arumugaswami Vaithilingaraja, et al. Determination of system level alterations in host transcriptome due to Zika virus (ZIKV) Infection in retinal pigment epithelium. *Sci Rep* 2018;**8**(1):1–16. doi:10.1038/s41598-018-29329-2.
10. Ursula Hiden, Elisabeth Glitzner, Michaele Hartmann, Gernot Desoye. Insulin and the IGF system in the human placenta of normal and diabetic pregnancies. *J Anat* 2009;**215**(1):60–8. doi:10.1111/j.1469-7580.2008.01035.x.
11. Daniel Bergman, Matilda Halje, Matilda Nordin, Wilhelm Engström. Insulin-like growth factor 2 in development and disease: a mini-review. *Gerontology* 2013;**59**(3):240–9. doi:10.1159/000343995.
12. Lucia Noronha, Camila Zanluca, Marion Burger, Akemi Suzukawa Andreia, Marina Azevedo, Rebutini Patricia Z, et al. Zika virus infection at different pregnancy stages: Anatomopathological findings, target cells and viral persistence in placental tissues. *Front Microbiol* 2018;**9**(2266):1–11. doi:10.3389/fmicb.2018.02266.
13. Weijun Luo, Friedman Michael S, Kerby Shedden, Hankenson Kurt D, Woolf Peter J. GAGE: Generally applicable gene set enrichment for pathway analysis. *BMC Bioinformatics* 2009;**10**:1–17. doi:10.1186/1471-2105-10-161.
14. Weijun Luo, Cory Brouwer. Pathview: an R/Bioconductor package for pathway-based data integration and visualization. *Bioinformatics* 2013;**29**(14):1830–1. doi:10.1093/bioinformatics/btt285.
15. Maria Strottmann Daisy, Camila Zanluca, Pamplona Mosimann Ana Luiza, Koishi Andrea C, Auwerter Nathalia Cavalheiro, Faoro Helisson, et al. Genetic and biological characterization of zika virus isolates from different Brazilian regions. *Mem Inst Oswaldo Cruz* 2019;**114**(7):1–11. doi:10.1590/0074-02760190150.
16. Ricciardi Jorge Taissa, Pamplona Mosimann Ana Luiza, Lucia de Noronha, Angela Maron, Nunes Duarte dos Santos Claudia. Isolation and characterization of a Brazilian strain of yellow fever virus from an epizootic outbreak in 2009. *Acta Trop* 2017;**166**:114–20. doi:10.1016/j.actatropica.2016.09.030.
17. Livak Kenneth J, Schmittgen Thomas D. Analysis of relative gene expression data using real-time quantitative PCR and the 2-ΔΔCT method. *Methods* 2001;**25**(4):402–8. doi:10.1006/meth.2001.1262.
18. Cristine Koishi Andrea, Akemi Suzukawa Andréia, Camila Zanluca, Elena Camacho Daria, Guillermo Comach, Nunes Duarte dos Santos Claudia. Development and evaluation of a novel high-throughput image-based fluorescent neutralization test for detection of Zika virus infection. *PLoS Negl Trop Dis* 2018;**12**(3):1–15. doi:10.1371/journal.pntd.0006342.
19. Paula Percicote Ana, Lazaretti Mardegan Gabriel, Schneider Gugelmim Elizabeth, Ossamu Ioshii Sergio, Paula Kuczynski Ana, Seigo Nagashima, et al. Tissue expression of retinoic acid receptor alpha and CRABP2 in metastatic nephroblastomas. *Diagn Pathol* 2018;**13**(1):1–7. doi:10.1186/s13000-018-0686-z.
20. Adalgisa Simões Mona, Cesar Pabis Francisco, Ehrenfried de Freitas Ana Karyn, Viola de Azevedo Marina Luise, Martins Ronchi Daiane Cristine, Lucia de Noronha. Immunoexpression of GADD45β in the myocardium of newborns experiencing perinatal hypoxia. *Pathol Res Pract* 2017;**213**(3):222–6. doi:10.1016/j.prp.2016.12.011.
21. Harvey Jennet M, Clark Gary M, Kent Osborne C, Craig Allred D. Estrogen receptor status by immunohistochemistry is superior to the Ligand-Binding assay for predicting response to Adjuvant Endocrine therapy in breast cancer. *J Clin Oncol* 1999;**17**(5):1474–81.
22. Andreas Hoeflich, Yi Yang, Ulrike Kessler, Peter Heinz-Erian, Helmut Kolb, Wieland Kiess. Human colon carcinoma cells (CaCo-2) synthesize IGF-II and express IGF-I receptors and IGF-II/M6P receptors. *Mol Cell Endocrinol* 1994;**101**(1–2):141–50. doi:10.1016/0303-7207(94)90228-3.
23. Marcela Mercado, Ailes Elizabeth C, Marcela Daza, Tong Van T, Osorio Johana, Valencia Diana, et al. Zika virus detection in amniotic fluid and Zika-associated birth defects. *Am J Obstet Gynecol* 2020;**222**(6) 610.e1-610.e13. doi:10.1016/j.ajog.2020.01.009.
24. Guilherme Calvet, Aguiar Renato S, Melo Adriana SO, Sampaio Simone A, de Filippis Ivano, Fabri Allison, et al. Detection and sequencing of Zika virus from amniotic fluid of fetuses with microcephaly in Brazil: a case study. *Lancet Infect Dis* 2016;**16**(6):653–60. doi:10.1016/S1473-3099(16)00095-5.
25. Lucia Noronha, Camila Zanluca, Viola Azevedo Marina Luize, Luz Kleber Giovanni, dos Santos Claudia Nunes Duarte. Zika virus damages the human placental barrier and presents marked fetal neurotropism. *Mem Inst Oswaldo Cruz* 2016;**111**(5):287–93. doi:10.1590/0074-02760160085.
26. Brasil Martines Roosecelis, Julu Bhatnagar, Kelly Keating M, Luciana Silva-flannery, Joy Gary, Cynthia Goldsmith, et al. Evidence of Zika virus infection in brain and placental tissues from two congenitally infected newborns and two fetal losses - Brazil, 2015. *Morb Mortal Wkly Rep* 2016;**65**(6):2015–16.
27. Longtine MS, Nelson DM. Placental Dysfunction and fetal programming: the importance of placental size, shape, histopatology, and molecular composition. *Semin Reprod Medeical J* 2013;**29**(3):187–96. doi:10.1055/s-0031-1275515. Placental.
28. Rosenberg Avi Z, Yu Weiying, Ashley Hill D, Reyes Christine A, Schwartz David A. Placental pathology of zika virus: Viral infection of the placenta induces villous stromal macrophage (Hofbauer Cell) proliferation and hyperplasia. *Arch Pathol Lab Med* 2017;**141**(1):43–8. doi:10.5858/arpa.2016-0401-OA.
29. Moon Lum Fok, Vipin Narang, Susan Hue, Jie Chen, Naomi McGovern, Ravisankar Rajarethinam, et al. Immunological observations and transcriptomic analysis of trimester-specific full-term placentas from three Zika virus-infected women. *Clin Transl Immunol* 2019;**8**(11):1–15. doi:10.1002/cti2.1082.
30. Karen Forbes, Melissa Westwood. The IGF axis and placental function: a mini review. *Horm Res* 2008;**69**(3):129–37. doi:10.1159/000112585.
31. Huiyue Chen, Yating Li, Jia Shi, Weiwei Song. Role and mechanism of insulin-like growth factor 2 on the proliferation of human trophoblasts in vitro. *J Obstet Gynaecol Res* 2016;**42**(1):44–51. doi:10.1111/jog.12853.
32. Adele Murrell, Sarah Heeson, Cooper Wendy N, Douglas Eleanor, Apostolidou Sophia, Moore Gudrun E, et al. An association between variants in the IGF2 gene and Beckwith-Wiedemann syndrome: Interaction between genotype and epigenotype. *Hum Mol Genet* 2004;**13**(2):247–55. doi:10.1093/hmg/ddh013.
33. Oliver Bracko, Tatjana Singer, Stefan Aigner, Marlen Knobloch, Beate Winner, Jasodhara Ray, et al. Gene expression profiling of neural stem cells and their neuronal progeny reveals IGF2 as a regulator of adult hippocampal neurogenesis. *J Neurosci* 2012;**32**(10):3376–87. doi:10.1523/JNEUROSCI.4248-11.2012.
34. John O'Kusky, Ping Ye. Neurodevelopmental effects of insulin-like growth factor signaling. *Front Neuroendocrinol* 2012;**33**(3):230–51. doi:10.1016/j.yfrne.2012.06.002.

35. Glover Kathleen KM, Ang Gao, Ali Zahedi-Amiri, Coombs Kevin M. Vero Cell proteomic changes induced by Zika virus infection. *Proteomics* 2019;**19**(4):e1800309. doi:10.1002/pmic.201800309.
36. Raj Ojha Chet, Myosotys Rodriguez, Muthu Karuppan Mohan Kumar, Jessica Lapierre, Fatah Kashanchi, Nazira El-Hage. Toll-like receptor 3 regulates Zika virus infection and associated host inflammatory response in primary human astrocytes. *PLoS One* 2019;**14**(2):1–26. doi:10.1371/journal.pone.0208543.
37. Muthu Karuppan Mohan Kumar, Raj Ojha Chet, Myosotys Rodriguez, Jessica Lapierre, Javad Aman M, Fatah Kashanchi, et al. Reduced-Beclin1-expressing Mice Infected with Zika-R103451 and viral-associated pathology during pregnancy. *Viruses* 2020;**12**(6):608. doi:10.3390/v12060608.
38. Han V K, Bassett N, Walton J, Challis J R. The expression of insulin-like growth factor (IGF) and IGF-binding protein (IGFBP) genes in the human placenta and membranes: evidence for IGF-IGFBP interactions at the feto-maternal interface. *J Clin Endocrinol Metab* 1996;**81**(7):2680–93. doi:10.1210/jcem.81.7.8675597.
39. Drewlo S, Levytska K, Kingdom J. Revisiting the housekeeping genes of human placental development and insufficiency syndromes. *Placenta* 2012;**33**(11):952–4. doi:10.1016/j.placenta.2012.09.007.
40. Cleal JK, Day PL, Hanson MA, Lewis RM. Sex differences in the mRNA levels of housekeeping genes in human Placenta. *Placenta* 2010;**31**:556–7. doi:10.1016/j.placenta.2010.03.006.
41. Yanli Li, Huifang Lu, Yizhen Ji, Sufang Wu, Yongbin Yang. Identification of genes for normalization of real-time RT-PCR data in placental tissues from intrahepatic cholestasis of pregnancy. *Placenta* 2016;**48**:133–5. doi:10.1016/j.placenta.2016.10.017.
42. Mathias Uhlen, Cheng Zhang, Sunjae Lee, Evelina Sjöstedt, Linn Fagerberg, Gholamreza Bidkhori, et al. A pathology atlas of the human cancer transcriptome. *Science (80-)* 2017;**357**(6352):eaan2507. doi:10.1126/science.aan2507.
43. Aldona Kasprzak, Agnieszka Adamek. The insulin-like growth factor (IGF) signaling axis and hepatitis C virus-associated carcinogenesis (Review). *Int J Oncol* 2012;**41**(6):1919–31. doi:10.3892/ijo.2012.1666.
44. Lin Ha Hye, Taeho Kwon, Seon Bak In, Erikson Raymond L. Kim Bo Yeon, Yu Dae Yeul. IGF-II induced by hepatitis B virus X protein regulates EMT via SUMO mediated loss of E- cadherin in mice. *Oncotarget* 2016;**7**(35):56944–57. doi:10.18632/oncotarget.10922.
45. Yuanyuan Ji, Zhidong Wang, Haiyan Chen, Lei Zhang, Fei Zhuo, Qingqing Yang. Serum from Chronic Hepatitis B Patients promotes growth and proliferation via the IGF-II/IGF-IR/MEK/ERK Signaling Pathway in Hepatocellular Carcinoma Cells. *Cell Physiol Biochem* 2018;**47**(1):39–53. doi:10.1159/000489744.
46. Adam Pickard, McDade Simon S, McFarland Marie, McCluggage WGlenn, Wheeler Cosette M, McCance Dennis J. HPV16 Down-regulates the insulin-like growth factor binding Protein 2 to promote Epithelial Invasion in organotypic cultures. *PLoS Pathog* 2015;**11**(6):1–23. doi:10.1371/journal.ppat.1004988.
47. O'Leary Daniel R, Stephanie Kuhn, Kniss Krista L, Hinckley Alison F, Rasmussen Sonja A, John Pape W, et al. Birth outcomes following west nile virus infection of pregnant women in the United States: 2003-2004. *Pediatrics* 2006;**117**(3):2003–4. doi:10.1542/peds.2005-2024.
48. Gabriella Pridjian, Sirois Patricia A, McRae Scott, Hinckley Alison F, Rasmussen Sonja A, Kissinger Patricia, et al. Prospective study of pregnancy and newborn outcomes in mothers with West nile illness during pregnancy. *Birth Defects Res Part A - Clin Mol Teratol* 2016;**106**(8):716–23. doi:10.1002/bdra.23523.
49. Platt Derek J, Smith Amber M, Nitin Arora, Diamond Michael S, Coyne Carolyn B, Miner Jonathan J. Zika virus-related neurotropic flaviviruses infect human placental explants and cause fetal demise in mice. *Sci Transl Med* 2018;**10**(426):1–11. doi:10.1126/scitranslmed.aao7090.
50. Ruben Porudominsky, Gotuzzo Eduardo H. Yellow fever vaccine and risk of developing serious adverse events: a systematic review. *Rev Panam Salud Pública* 2018;**42**. doi:10.26633/RPSP.2018.75.
51. Sferruzzi-Perri Amanda N, Vaughan OR, Coan PM, Suciu MC, Darbyshire R, Constancia M, et al. Placental-specific Igf2 deficiency alters developmental adaptations to undernutrition in mice. *Endocrinology* 2011;**152**(8):3202–12. doi:10.1210/en.2011-0240.
52. Barbeito-Andrés J, Pezzuto P, Higa LM, Dias AA, Vasconcelos JM, Santos TMP, et al. Congenital Zika syndrome is associated with maternal protein malnutrition. *Sci Adv* 2020;**6**(2):eaaw6284. doi:10.1126/sciadv.aaw6284.
53. Bruno Hoen, Bruno Schaub, Funk Anna L, Vanessa Ardillon, Manon Boullard, André Cabié, et al. Pregnancy outcomes after ZIKV infection in French territories in the Americas. *N Engl J Med* 2018;**378**(11):985–94. doi:10.1056/NEJMoa1709481.
54. Flores Ledur Pítia, Karina Karmirian, da Silva Gouveia Pedrosa Carolina, Quintino Souza Leticia Rocha, Gabriela Assis-de-Lemos, Martino Martins Thiago, et al. Zika virus infection leads to mitochondrial failure, oxidative stress and DNA damage in human iPSC-derived astrocytes. *Sci Rep* 2020;**10**(1):1–14. doi:10.1038/s41598-020-57914-x.

Overview

In order for Elsevier to publish and disseminate research articles, we need certain publishing rights from authors, which are determined by a publishing agreement between the author and Elsevier.

For articles published open access, the authors license exclusive rights in their article to Elsevier where a CC BY-NC-ND end user license is selected, and license non-exclusive rights where a CC BY end user license is selected.

For articles published under the subscription model, the authors transfer copyright to Elsevier.

Regardless of whether they choose to publish open access or subscription with Elsevier, authors have many of the same rights under our publishing agreement, which support their need to share, disseminate and maximize the impact of their research.

For open access articles, authors will also have additional rights, depending on the Creative Commons end user license that they select. This Creative Commons license sets out the rights that readers (as well as the authors) have to re-use and share the article: please see here for more information on how articles can be re-used and shared under these licenses.

This page aims to summarise authors' rights when publishing with Elsevier; these are explained in more detail in the publishing agreement between the author and Elsevier.

Irrespective of how an article is published, Elsevier is committed to protect and defend authors' works and their reputation. We take allegations of infringement, plagiarism, ethical disputes, and fraud very seriously.

Author rights

The below table explains the rights that authors have when they publish with Elsevier, for authors who choose to publish either open access or subscription. These apply to the corresponding author and all co-authors.

Author rights in Elsevier's proprietary journals	**Published open access**	**Published subscription**
Retain patent and trademark rights	√	√

Author rights in Elsevier's proprietary journals	**Published open access**	**Published subscription**
Retain the rights to use their research data freely without any restriction	√	√
Receive proper attribution and credit for their published work	√	√
Re-use their own material in new works without permission or payment (with full acknowledgement of the original article): 1. Extend an article to book length 2. Include an article in a subsequent compilation of their own work 3. Re-use portions, excerpts, and their own figures or tables in other works.	√	√
Use and share their works for scholarly purposes (with full acknowledgement of the original article): 1. In their own classroom teaching. Electronic and physical distribution of copies is permitted 2. If an author is speaking at a conference, they can present the article and distribute copies to the attendees 3. Distribute the article, including by email, to their students and to research colleagues who they know for their personal use 4. Share and publicize the article via Share Links, which offers 50 days' free access for anyone, without signup or registration 5. Include in a thesis or dissertation (provided this is not published commercially) 6. Share copies of their article privately as part of an invitation-only work group on commercial sites with which the publisher has a hosting agreement	√	√
Publicly share the preprint on any website or repository at any time.	√	√
Publicly share the accepted manuscript on non-commercial sites	√	√ using a CC BY-NC-ND license and usually only after an embargo period (see Sharing Policy for more information)

Author rights in Elsevier's proprietary journals	Published open access	Published subscription
Publicly share the final published article	√ in line with the author's choice of end user license	×
Retain copyright	√	×